

Lyapunov Based Stable and Robust Adaptive Control Design for a Class of Space Transportation Systems

*A thesis submitted
in partial fulfillment for the award of the degree of*

Doctor of Philosophy

by

Asha P Nair



**Department of Avionics
INDIAN INSTITUTE OF SPACE SCIENCE AND
TECHNOLOGY
Thiruvananthapuram, India**

January 2023

CERTIFICATE

This is to certify that the thesis titled **Lyapunov Based Stable and Robust Adaptive Control Design for a Class of Space Transportation Systems** submitted by **Asha P Nair** to the Indian Institute of Space Science and Technology, Thiruvananthapuram, in partial fulfillment for the award of the degree of **Doctor of Philosophy**, is a bona fide record of the research work carried out by her under our supervision. The contents of this thesis, in full or in parts, have not been submitted to any other Institute or University for the award of any degree or diploma.

Dr. N. Selvagesan

Supervisor

Professor and Head,

Department of Avionics

IIST

Dr. V. R. Lalithambika

Co-Supervisor

Director (Retd)

DHSP, ISRO Headquarters

Place: Thiruvananthapuram

Date: January 2023

DECLARATION

I declare that this thesis titled **Lyapunov Based Stable and Robust Adaptive Control Design for a Class of Space Transportation Systems** submitted in partial fulfillment for the award of the degree of **Doctor of Philosophy** is a record of original work carried out by me under the supervision of **Prof. N. Selvagesan** and **Dr. V.R. Lalithambika** and has not formed the basis for the award of any degree, diploma, associateship, fellowship, or other titles in this or any other Institution or University of higher learning. In keeping with the ethical practice in reporting scientific information, due acknowledgments have been made wherever the findings of others have been cited.

Place: Thiruvananthapuram

Date: January 2023

Asha P Nair

(SC14D010)

Dedicated to My dear Achan, Amma, Rajeev and Parvathi

ACKNOWLEDGEMENTS

Completion of the work presented in this thesis and writing the thesis have been surprisingly difficult and took a long time to evolve to this present form. A long list of friends and colleagues have helped and supported me in this research.

To begin with, I would like to express my sincere gratitude to my research supervisor Prof. N Selvagesan for introducing me to the vast ocean of adaptive control, for the many online discussions which often extended upto midnight and for the encouragement and support throughout this research work. His continuous enthusiasm and hard work have been the strongest driving force behind this research. His technical and editorial advices were extremely important for the completion of this thesis work.

I have the privilege of having Dr. V. R. Lalithambika as my Guru, mentor and well wisher throughout my career. In the midst of her busy schedule, she guided me as my co-research supervisor and found time to share her valuable insights with me. I will not be able to thank her enough for shaping me with affectionate criticisms, timely advices and for helping me come out of many situations when I was feeling very low.

I would like to express the deepest appreciation to my doctoral committee chair, Dr. Deepak Mishra, HoD, Avionics Department, IIST for his constant help and encouragement. I would also like to acknowledge the members of the doctoral committee, Dr. Nandan K Sinha, Professor, IIT Madras, Dr. S. Dasguptha, Former Deputy Director, VSSC, Dr. H. Priyadarshnam, Associate Professor, IIST, Dr. N. Sabu, Professor, IIST, for their valuable comments and suggestions which helped in correcting the course of the work. I would like to thank Dr. Raju K George, Dean(R&D), IIST, for the excellent mathematics lessons which helped me understand the advanced control system literature.

I would like to acknowledge the ISRO management for giving me opportunities, associated challenges and responsibilities in developing flight control systems for various missions. I am grateful to Shri. S.Somanath, Chairman, ISRO and Dr. S. Unnikrishnan Nair, Director, VSSC, for permitting me to do the research at IIST. Also, I would like to thank Dr.S. Unnikrishnan Nair, Director, IIST, and Dr. K.S. Dasguptha, Dr. V.K Dadhwal, Dr.Sam Dayala Dev, former

directors of IIST, for providing me excellent research environment. I also would like to thank Dr.Thomas Kurian, former HoD, Avionics Department, IIST for picking me up as a doctoral student.

I salute my Gurus and seniors in the control and guidance area, starting with Dr.S.Dasguptha, Shri. M.V.Dhekane, Smt. D.S.Sheela, Shri. E. S Padmakumar, Dr.Sam K Zacharia, Dr.V.Brinda, Smt. Manju Unnikrishnan and Smt. Rani Radhakrishnan. Words are powerless to express my sincere gratitude to Dr.S.Geetha, Program Director, VSSC, for her affection, encouragement, and for patiently teaching me the art of autopilot design. I would like to thank Dr.T.Sundararajan for the structural dynamics lessons.

I would like to express my sincere gratitude to my professional colleagues and friends in the Control Design Division, Dr. Gopal Jee, Kavitha C.S., Soumya N., Kapil Kumar Sharma, Anish Antony and Anju M, who have helped me better understand and appreciate the challenging field of controls and dynamics. Special thanks to Abhijith U P for the much useful tips in Microsoft Word. I thank the reviewers of my publications, Shri. Baby Sebastian and Dr. Geethaikrishnan for their valuable comments.

I am unable to thank my family enough for their love, understanding, support and patience. I thank my parents, late Shri. K.R.Parameswaran Nair and Smt. Leelavathy Kunjamma for their wise counsel and all their sacrifices on my behalf. You are always there for me and encourage me to follow my dreams. Special thanks to my sisters for their love and support. I thank my parents-in-law and other family members for their affection and moral support.

I owe thanks to my husband, Dr. U.P Rajeev, for his continued and unflinching love, support and understanding during my pursuit of Ph.D that made the completion of the thesis possible. He helped me understand the concepts in advanced control systems and mathematics and ensured the right books and literature availability. Thank you for holding my hand and taking me along with you. I thank my daughter Parvathi for making me happy with her unconditional love and for tolerating my busy schedule. Thank you for being such a patient and empathetic person.

I thank the almighty for giving me the strength and patience to work through all these years.

ABSTRACT

A Satellite Launch Vehicle (SLV) is a dynamic system with time-varying characteristics whose model consists of highly uncertain and nonlinear parameters. During the ascent phase, the SLV experiences continuous variations in atmospheric density, Mach number and aerodynamic forces and moments. The presence of lightly damped structural and slosh modes whose frequency is closer to the control frequency, further complicates the attitude control problem. Current practice in the flight control design is to linearise the plant dynamics about various points of a nominal trajectory designed to satisfy the mission requirements. For this purpose, the plant is assumed to be frozen between the operating points. The classical gain scheduled control design works perfectly for the existing Space Transportation Systems (STS). However, these controllers cannot be applied to modern STS where the systems are highly non-linear and coupled. The flight control system for such systems has to work for a wide spectrum of flight conditions.

This thesis proposes the use of adaptive controllers for the flight control of various STS, such as structurally optimized slender launch vehicles and winged re-entry vehicles. These controllers replace the existing gain-scheduled controllers and maintain the performance of the closed-loop system in the event of failure of sub-systems and also in the presence of parametric and non-parametric uncertainties.

The initial phase of the research work focuses on dynamic modelling and ascent flight control of a highly unstable and flexible launch vehicle. Stabilising adaptive PD/PID controllers are developed in MRAC framework using standard quadratic Lyapunov function to control the time-varying rigid body dynamics during the atmospheric phase of flight. Further, Lyapunov stability and Barbalat's Lemma are applied to prove the stability of the time-varying system. These controllers are robust to parametric uncertainties and all the signals are uniformly ultimately bounded. To reduce the effect of sensor noise, a continuous form of dead zone is applied on the tracking error. The lack of robustness of these control algorithms for unstructured uncertainty is shown analytically and through simulations. A stable adaptive control design that completely avoids actuator

position and slew rate saturation is proposed using the standard quadratic Lyapunov function. Here both the control and reference inputs are adaptively adjusted.

Two adaptive control laws are proposed to improve the robustness of the adaptive controllers to non-parametric uncertainties. These controllers are developed in MRAC framework using Lyapunov functions. Time-varying reference models are used, which capture the desired behaviour of the closed-loop plant at various operating points along the nominal trajectory. Classical stability margin requirements are to be met for flight control certification. Hence, reference models are selected to satisfy these requirements. A continuous projection operator constrains the adapted parameters within the user-defined bounds in the first algorithm, which helps maintain the stability of the time-varying plant and avoids actuator saturation. The robustness of this algorithm to structured and unstructured uncertainty is proved analytically. The second algorithm uses a Barrier Lyapunov Function to constrain the trajectory tracking error and the adapted parameters within the user-defined constraint compact sets. These two algorithms require full state feedback. An extended Kalman filter is designed to estimate the plant's states from the available noisy measurements. Proposed adaptive controllers are used in the ascent phase of a highly flexible, unstable launch vehicle, and the results are compared with the existing gain scheduled controller.

In the second phase of the research work, projection and barrier Lyapunov based adaptive controllers are proposed for the descent phase flight control of a winged re-entry vehicle. A rectangular projection operator is used in the adaptive control design to simultaneously constrain the adapted gains within a maximum and minimum limit. Extensive simulation studies are conducted with non-linear actuator models, wind and extreme parametric perturbations to demonstrate the robustness of the proposed algorithms.

CONTENTS

List of Figures.....	xvii
List of Tables	xxiii
Abbreviations	xxv
Nomenclature	xxvii
INTRODUCTION	1
1.1 Classifications of Adaptive Controllers	3
1.2 Model Reference Adaptive Control.....	3
1.3 Introduction to Satellite Launch Vehicles	4
1.4 Literature Survey.....	5
1.5 Motivation of the Research	11
1.6 Research Contributions.....	12
1.7 Organisation of the Thesis	14
LYAPUNOV BASED MRAC FOR THE RIGID BODY DYNAMICS OF A SATELLITE LAUNCH VEHICLE.....	17
2.1. Introduction.....	17
2.1.1 Attitude Control System for an SLV	17
2.2. Modelling of the Rigid Body Dynamics of an SLV	18
2.3. Attitude Controller Design for the Simplified SLV Model.....	22

2.3.1 Gain Scheduled Control Law.....	22
2.3.2. Proposed Adaptive Control Design	24
2.4. Results and Discussions	29
2.4.1 Nominal Plant with a Ramp Command	32
2.4.2 Nominal Plant with a Typical Guidance Command Input.....	37
2.4.3 Perturbation Studies.....	41
2.4.4 Disturbance Rejection Studies	44
2.5. Summary.....	46
NOVEL ADAPTIVE CONTROL LAWS FOR A FLEXIBLE SATELLITE LAUNCH VEHICLE.....	49
3.1 Introduction.....	49
3.2 Model of a Flexible SLV	51
3.2.1 Slosh Dynamics	51
3.2.2 Flexibility Dynamics	54
3.3 Proposed Adaptive Controller Design	58
3.3.1 Modified Control Parameter Update Law Using Projection Operator	61
3.3.2 Modified Control Parameter Update Law using BLF.....	65
3.3.3 Stable Adaptive Controller Design in the Presence of Actuator Constraints	68
3.4 State Estimation and Noise Filtering Using EKF	71
3.5 Results and Discussions	73
3.5.1 Nominal Plant Simulated with a Ramp Command	74
3.5.2 Perturbed Plant Responses to a Ramp Command.....	77

3.5.3 Robustness Verification.....	81
3.5.4 Nominal Plant with a Typical Guidance Command	84
3.5.5 Disturbance Rejection Studies	87
3.5.6 Studies with Actuator Saturation Avoidance Algorithm	93
3.6 Summary.....	96
 ADAPTIVE CONTROL DESIGNS FOR A WINGED RE-ENTRY	
VEHICLE	99
4.1 Introduction.....	99
4.2 Modelling of an RLV in the Descent Phase	100
4.3 Adaptive Control Design	108
4.3.1 Using Rectangular Projection Operator	108
4.3.2 Using Barrier Lyapunov Functions.....	113
4.4 Results and Discussions	113
4.4.1 Studies with Nominal RLV Plant	114
4.4.2 Studies with Perturbed RLV Plant.....	118
4.4.3 Disturbance Rejection Studies	129
4.5 Summary.....	132
 CONCLUSIONS AND FUTURE SCOPE.....	
133	
5.1 Future Scope.....	134
 BIBLIOGRAPHY	
137	
 APPENDIX A	
147	

A.1 Mathematical Preliminaries Required to Derive the Control Laws in Chapter 3	147
A.2 Uniform Ultimate Stability.....	151
A.3 Projection Operator	153
A.4 Barrier Lyapunov Based Control Design	159
A.5 Derivation of the Adaptive PID Control Law for the Simplified SLV Plant 163	
A.6 Derivation of the Inequalities Given in Chapters 3 and 4.....	165
LIST OF PUBLICATIONS BASED ON THESIS.....	169

List of Figures

Figure 1. 1 Feedback Control Structure for a Plant with Uncertainty	2
Figure 1. 2 MRAC Structure	4
Figure 1. 3 Comprehensive Flow Diagram that Explains the Proposed Work	15
Figure 2. 1 Block Diagram of NGC Subsystem	18
Figure 2. 2 Short Period Model of the SLV in Pitch Plane	20
Figure 2. 3 Plant Characteristics	30
Figure 2. 4 Variation of the Control Parameters for the Rigid Body Model	31
Figure 2. 5 Variation of the Aero Parameters for the Rigid Body Model	32
Figure 2. 6 Simulation Setup	33
Figure 2. 7 Tracking Performance of the Controllers for a Ramp Command	33
Figure 2. 8 Tracking Error of the Controllers for a Ramp Command	34
Figure 2. 9 Initial Capture of Tracking Errors by the Controllers for a Ramp Command	34
Figure 2. 10 Noise Generated for Simulation Study	35
Figure 2. 11 Attitude Rate of the SLV while Tracking the Ramp Command	36
Figure 2. 12 Control Deflections for Ramp Tracking	36
Figure 2. 13 Attitude Tracking for a Typical Guidance Command	38
Figure 2. 14 Tracking Errors of Different Controllers for a Typical Guidance Command	38
Figure 2. 15 Attitude Rates for a Typical Guidance Command Tracking	39

Figure 2. 16 Control Responses of Different Controllers for a Typical Guidance	
Command Tracking	40
Figure 2. 17 Perturbed Plant Parameters	41
Figure 2. 18 Tracking Performance of Controllers for a Perturbed Plant	42
Figure 2. 19 Tracking Error for a Perturbed Plant	42
Figure 2. 20 Control Responses of Different Controllers for a Perturbed Plant	43
Figure 2. 21 Angle of Attack Build up due to Synthetic Wind Disturbance	44
Figure 2. 22 Attitude Error Build up due to Injected Wind	45
Figure 3. 1 Interaction Between Flight Control System and the Structural	
Dynamics	49
Figure 3. 2 Slosh Pendulum in Pitch Plane	52
Figure 3. 3 Flexible SLV in Pitch Plane	54
Figure 3. 4 Slosh Parameter Variations	74
Figure 3. 5 Attitude Tracking by Different Controllers with Ramp Command	75
Figure 3. 6 Attitude Tracking Error of Different Controllers with Ramp	
Command	75
Figure 3. 7 Control Responses of Different Controllers for Ramp Command	76
Figure 3. 8 Attitude Rate for Ramp Command Tracking	77
Figure 3. 9 Attitude Rate Estimated using EKF	77
Figure 3. 10 Perturbed Plant Parameters – Rigid Body	78
Figure 3. 11 Attitude Tracking of Perturbed Plant for Ramp Command	79
Figure 3. 12 Attitude Tracking Error of Perturbed Plant for Ramp Command	79
Figure 3. 13 Control Responses of Perturbed Plant for Ramp Command	80
Figure 3. 14 Attitude Rate of Perturbed Plant for Ramp Command	80

Figure 3. 15 Plant Parameter Perturbation Tolerable by Different Controllers	82
Figure 3. 16 Tracking of Ramp Commands by Different Controllers for the Plant Parameters Perturbed to the Limit	82
Figure 3. 17 Control Response of Different Controllers for the Plant Parameters Perturbed to the Limit	83
Figure 3. 18 Attitude Rate of Different Controllers for the Plant Parameters Perturbed to the Limit	83
Figure 3. 19 Attitude Tracking by Different Controllers for Nominal Plant with Typical Open Loop Guidance Command	85
Figure 3. 20 Attitude Tracking Error by Different Controllers for Nominal Plant with Typical Open Loop Guidance Command	85
Figure 3. 21 Control Response for Typical Open Loop Guidance Command by Different Controllers for Nominal Plant	86
Figure 3. 22 Attitude Rate for Typical Open Loop Guidance Command by Different Controllers for Nominal Plant	86
Figure 3. 23 Comparison of Wind Disturbance Rejection Capability of Different Controllers for Perturbed Plant	88
Figure 3. 24 Attitude Tracking and Wind Disturbance Rejection for Typical Guidance Command by Different Controllers for Perturbed Plant	89
Figure 3. 25 Attitude Tracking Error for Typical Guidance Command by Different Controllers for Perturbed Plant with a Wind Disturbance	89
Figure 3. 26 Control Response for Typical Guidance Command by Different Controllers for Perturbed Plant with a Wind Disturbance	90

Figure 3. 27 Control Response by Different Controllers: Fig.3.26 Zoomed from 35 s to 80 s	90
Figure 3. 28 Attitude Rate Response for Typical Guidance Command by Different Controllers for Perturbed Plant with a Wind Disturbance	91
Figure 3. 29 Slosh Pendulum Angles in Response to Typical Guidance Commands for Perturbed Plant with Wind Disturbance	91
Figure 3. 30 Slosh Pendulum Angles for Perturbed Plant: Fig 3.29 Zoomed from 35 s to 80 s	92
Figure 3. 31 Bending Mode Generalised coordinate in Response to Typical Guidance Commands for Perturbed Plant with Wind Disturbance	92
Figure 3. 32 Control Output of the Stable Adaptive Controller that Avoids Actuator Saturation	93
Figure 3. 33 Control Output of the Stable Adaptive Controller that Avoids Actuator Saturation – Fig 3.32 Zoomed from 50 s to 70 s	94
Figure 3. 34 Attitude Rate Response of the Stable Adaptive controller that Avoids Actuator Saturation–Zoomed from 50 s to 70 s	95
Figure 3. 35 Slosh Pendulum Angles –Zoomed from 50 s to 70 s	95
Figure 3. 36 Bending Mode Generalized coordinates –Zoomed	96
Figure 4. 1 RLV Co-ordinate System	101
Figure 4. 2 Pictorial Representation of Rectangular Projection Operator	110
Figure 4. 3 Longitudinal Plane Responses for Nominal Case	116
Figure 4. 4 Lateral Plane Responses for Nominal Case	116
Figure 4. 5 Bank Angle Tracking Error for the Nominal Case	117
Figure 4. 6 Control Demand in Roll/Yaw/Pitch Planes for the Nominal Case	117

Figure 4. 7 Control Deflection of Various Effectors for the Nominal Case	118
Figure 4. 8 Longitudinal Plane Responses for Perturbed Case 2	120
Figure 4. 9 Lateral Plane Responses for Perturbed Case 2	121
Figure 4. 10 Control Demands in Roll/Yaw/Pitch Channels for Perturbed	121
Figure 4. 11 Control Deflections of Effectors for Perturbed Case 2	122
Figure 4. 12 Longitudinal Plane Responses for Case 3	123
Figure 4. 13 Control Demands in Roll/Yaw/Pitch Channels for Case 3	123
Figure 4. 14 Longitudinal Plane Responses for Case 4	124
Figure 4. 15 Lateral Plane Responses for Case 4	125
Figure 4. 16 Control Demands in Roll/Yaw/Pitch Channels for Case 4	125
Figure 4. 17 Longitudinal Plane Responses for Case 5	126
Figure 4. 18 Lateral Plane Responses for Case 5	127
Figure 4. 19 Control Demands in Roll/Yaw/Pitch Channels for Case 5	127
Figure 4. 20 Longitudinal Plane Responses with Wind Gust	129
Figure 4. 21 Control Demands in Roll/Yaw/Pitch Channels with Wind Gust	130
Figure 4. 22 Control Deflections of Effectors with Wind Gust	130
Figure 4. 23 Lateral Plane Responses with Wind Gust	131
Figure 4. 24 Bank Angle Tracking with Wind Gusts Applied	131
Figure A.3. 1 Gradient Vector on the Boundary of a Convex Set	153
Figure A.3. 2 The Projection Operator	155

List of Tables

Table 2. 1	Comparison of the Performance of Different Schemes with Typical Guidance Commands for Nominal Plant	40
Table 2. 2	Comparison of the Performance of Different Control Schemes with Typical Guidance Commands under Plant Parameter Perturbation	43
Table 2. 3	Comparison of the Wind Disturbance Rejection of Different Control Schemes	45
Table 3. 1	Performance Evaluation of Different Adaptive Controllers for a Ramp Command	81
Table 3. 2	Comparison of the Performance of Different Controllers for Typical Guidance Commands	87
Table 4. 1	Plant Parameter Perturbations for Different Cases	119
Table 4. 2	Performance Evaluation of Various Controllers During Approach and Landing Phase of RLV	128

Abbreviations

AoA	Angle of Attack
BLF	Barrier Lyapunov Function
CG	Center of Gravity
CLG	Closed Loop Guidance
DoF	Degrees of Freedom
EKF	Extended Kalman Filter
FAT	Function Approximation Techniques
MIMO	Multi-Input-Multi-Output
MRAC	Model Reference Adaptive Control
NGC	Navigation, Guidance and Control
NN	Neural Network
PD	Proportional-Derivative
PID	Proportional-Integral-Derivative
RLV	Reusable Launch Vehicles
SLV	Satellite Launch Vehicles
STS	Space Transportation Systems
TAEM	Terminal Area Energy Management
UUB	Uniformly Ultimately Bounded

Nomenclature

A_x, A_y, A_z	Body Accelerations in X, Y, Z Directions
D	Aerodynamic Drag Force
EI	Bending Stiffness
F_x, F_y, F_z	Components of Forces in X, Y, Z Directions
\vec{g}	Gravity Vector
I	Moment of Inertia
K_A	Forward Path Gain
K_I	Integrator Gain
K_R	Rate Feedback Gain
K_α	Angle of Attack Feedback Gain
K_θ	Attitude Feedback Gain
l	Length Parameter along Vehicle Longitudinal Axis
L, M, N	Moments about the Body Axes
l_c	Control Moment Arm
L_{pk}	Length of the Slosh Pendulum
l_{pk}	Distance Between the Hinge Point of the Slosh Pendulum from the CG of the Vehicle
L_α	Aerodynamic Load per Unit Angle of Attack
l_α	Aerodynamic Moment Arm
m	Mass of the SLV
M_i	Generalised Mass of the i^{th} Bending Mode
m_{pk}	Sloshing Mass
P, Q, R	Components of the Angular Velocity of the Body Frame about X, Y, Z axes
P_0, Q_0, R_0	Steady State Values of P, Q, R

p, q, r	Perturbation Values of P, Q, R
$q_i(t)$	Generalised Coordinate of the i^{th} Natural Vibration Mode
$Q_i(t)$	Generalised Force of the i^{th} Bending Mode
s	Laplace Variable
t	Time
T_c	Control Thrust
T_s	Un-gimballed Thrust
U, V, W	Inertial Velocity of the Body Frame in X, Y, Z Directions
U_0, V_0, W_0	Steady State Values of U, V, W
u, v, w	Perturbation Values of U, V, W
u_c	Reference Command to be Followed
V	Total Velocity of the Vehicle
V_T	True Airspeed
V_w	Velocity of Wind in the Lateral Direction
\dot{z}	Normal Velocity of the Vehicle along the body axis Z_b
α	Angle of Attack
γ	Flight Path Angle
δ	Control Deflection Angle
δ_{ail}	Aileron Deflection
δ_e	Elevator Deflection
δ_{rud}	Rudder Deflection
ζ_m	Damping of the Second Order Reference Model
ζ_k	Damping of the Slosh Pendulum
θ, ψ, φ	Attitude Angles (angle at which body frame to be rotated to align with inertial frame)
ξ	Deflection due to Bending
$\varphi_i(l)$	Shape of i^{th} Natural Vibration Mode
ω	Angular Velocity of the Body Frame

ω_k	Slosh Pendulum Frequency
ω_m	Natural Frequency of the Second Order Reference Model
\mathcal{R}	Set of Real Numbers

Chapter 1

Introduction

Adaptive controllers are ideal for dealing with complex systems with unpredictable parameter variations and uncertainties and maintaining consistent system performance. These controllers will adjust themselves to the changing environments. The plant's output carries information about its current state and the change in its parameters. Hence adaptive controller is designed with a feedback structure and adjustable controller parameters which vary with respect to the change in plant parameters.

Adaptive controllers were proposed for flight control in the early 1950s as an option to enhance the performance of the autopilot design for fighter aircraft [1][2][3]. Such aircraft dynamics are time-varying and nonlinear and operate over a wide range of speeds and altitudes. These dynamics can be linearized about the operating point specified by the aircraft's velocity and altitude. The controllers need to be designed for each operating point for large stability margins. The controller parameters are scheduled with respect to parameters whose variations correlate well with the change in plant behavior. This procedure is time-consuming and the controller's performance at all the points along the trajectory is not guaranteed. This emphasizes the need for adaptive controllers that can handle non-linear time varying characteristics of the aircraft.

All formal control designs are based on the mathematical model of a physical system [4]. Before starting the control design, a model that captures the plant's behavior in the desired domain of operation is to be developed. A plant model may be developed using the laws of physics [4][5][6] and also using identification methods by processing the input and output of the plant [3]. Such a model may be complicated and may not be helpful for control design. A simplified model is to be developed for control design purposes using certain approximations and assumptions. Usually, in the classical control design, sufficient margins are built so that the controller's performance is satisfactory for the actual plant and

stability is maintained; however, performance is gracefully degraded in the presence of uncertainties. Hence, the main criteria for any flight control system design is to embed robustness properties so that closed-loop stability and tracking performance are achieved even with uncertainties. Fig. 1.1 shows the control structure of a plant with uncertainty.

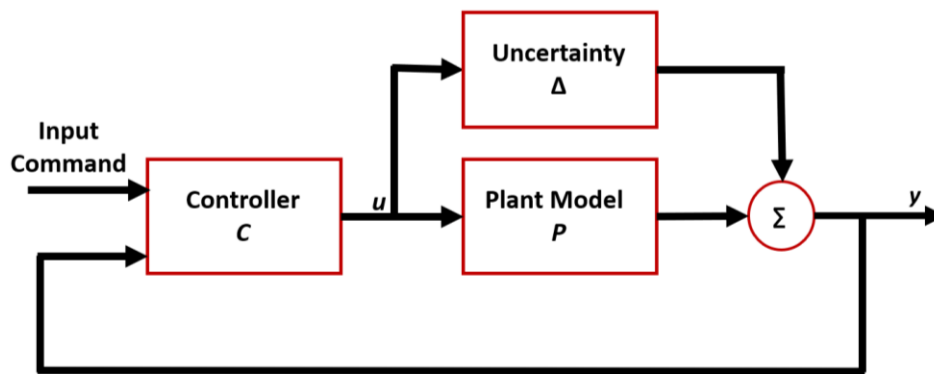


Figure 1. 1 Feedback Control Structure for a Plant with Uncertainty

There are two ways of handling the uncertainties in the plant model. The first is robust control, which can regulate the plant with bounded uncertainties. These controllers are designed to work for a set of plants (can be linear or non-linear), assuming a worst-case condition. Hence the robust controllers are more conservative and there will be performance limitations for the nominal plant. Such controllers may use excessive control actions to control the plant. The second option is adaptive control, which helps to enhance the applicability domains of a robust control system. The adaptive controllers use some kind of online estimate of the controller and plant parameters and are more suitable for time-varying plants. They produce control input to anticipate or overcome the undesirable deviations from the desired closed-loop behaviour. However, designing a stable adaptive controller is challenging as the controller and plant parameters continuously vary with time.

Various researchers propose many methods to design stable adaptive controllers for time-varying plants [1][2] and are still not sufficiently robust to bounded uncertainties. Hence, a combination of robust and adaptive controllers is

the best option for maintaining closed-loop stability, enforcing robustness to uncertainties and ensuring the desired performance in unanticipated events.

1.1 Classifications of Adaptive Controllers

An adaptive controller is formed by combining an online parameter estimator and control law for a known plant. Adaptive controllers are classified as indirect adaptive control or explicit adaptive control and direct adaptive control or implicit adaptive control based on how the estimator and the controller are combined. In indirect adaptive control, the plant parameters are estimated online and are used to compute the controller parameters. In direct adaptive control law, the plant model is parametrized in terms of controller parameters that are directly estimated online without estimating plant parameters. This cannot be used for non-minimum phase plants, whereas the indirect method can be used for both minimum and non-minimum phase plants.

1.2 Model Reference Adaptive Control

Model Reference Adaptive Control [1] popularly known as MRAC is derived from the model following problem. Here the desired plant behaviour is captured by a reference model. The controller parameters are adjusted online by an adaptation mechanism that operates based on the error between the plant output and the output of the reference model. The adaptation mechanism (also known as adaptation law, update law or adjustment mechanism) will adjust the controller parameters in such a way that this error is converged to zero with time. The design of the adaptation law is crucial for the stability properties of the adaptive controller. The adaptation law introduces a multiplicative nonlinearity to the plant, making the closed loop plant nonlinear and time-varying. This makes the analysis of the stability and robustness of the adaptive controllers more challenging [7]. Some of the methods used for the design of adaptive law [2] are (i) Sensitivity methods (MIT rule) (ii) Positivity and Lyapunov Design (iii) Gradient method and least-squares methods. The general MRAC block diagram is given in Fig. 1.2.

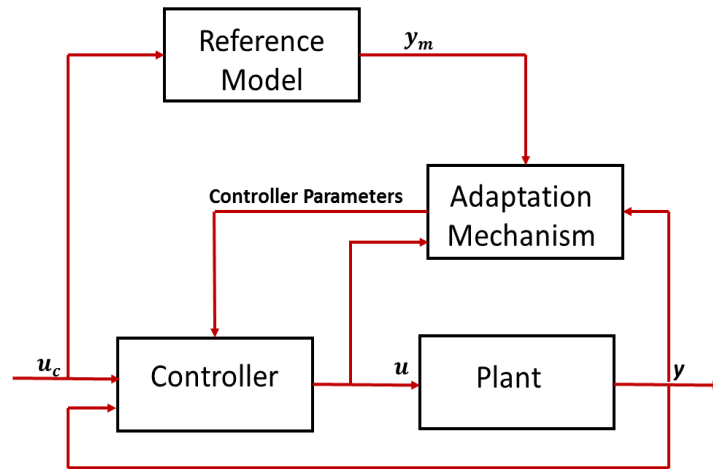


Figure 1. 2 MRAC Structure

1.3 Introduction to Satellite Launch Vehicles

Satellite Launch Vehicles (SLV) are generally aerodynamically unstable, highly flexible and have time-varying dynamics. The basic approach to stability and control analysis for aerospace vehicles like aircraft and launch vehicles are the same. But, large variation of vehicle mass due to the expulsion of fuel and staging of rockets makes the problem complex for launch vehicles. Stabilizing the conditionally stable, lightly damped structural modes of a slender launch vehicle or missile and avoiding control-structure interaction is a very challenging problem. The attitude control design problem is further complicated by the presence of liquid propelled stages which introduces moments due to sloshing of the liquid propellant and the gimballed engines used for controlling the vehicle. On the other hand, winged re-entry vehicles and crew re-entry modules have to undergo a wide spectrum of flight conditions. The flight control system has to cater to various abort mission scenarios due to partial or total failure of sub-systems and under actuation due to failure.

Accurate models are to be developed for flight control system design to ensure satisfactory performance. At the same time, a hi-fidelity model will be highly non-linear and coupled with time-varying parameters. It is challenging to

design controllers for such plant models. Hence a simplified model is derived, which captures the behavior of the plant reasonably well and then the controller is designed. Various interactions between different dynamics for complex systems are difficult to capture using a simplified model. The controller parameters should be allowed to vary to cater to the time-varying nature of the plant and also be able to cater to the uncertainties due to modelling inadequacy. Adaptive controllers are ideal for handling such scenarios.

1.4 Literature Survey

Many adaptive controllers, when applied to high-risk aerospace applications, are infeasible due to the rigorous flight certification environment [8]. These control techniques are not suitable for controlling conditionally stable dynamics like structural flexibility. Metrics of performance and robustness of adaptive controllers are difficult to reconcile with the classical control system performance and robustness requirements specified using gain margin and phase margin. Hence an adaptive controller augmented with an existing well-designed classical controller is proposed. L1 output feedback adaptive controller is proposed in [9] for the Ares launch vehicle, whose first flexible mode frequency is close to the rigid body frequency. It consists of a state predictor and a control law defined via the output of a low-pass filter.

The adaptive controllers can be constructed to “learn.” Learning refers to remembering or recognizing specific patterns and then act on some prior knowledge. Several learning controllers based on neural networks, fuzzy logic etc., are available in the literature. A direct adaptive fuzzy controller is designed in [10] to control the pitch dynamics of a launch vehicle. The adaptation law is designed using Lyapunov theorem, which ensures asymptotic stability of the closed-loop system. An adaptive controller in MRAC framework is designed for an expendable launch vehicle [11] in which several basis functions are used to represent various uncertainties in the system dynamics. A reference model is obtained using feedback linearization. This avoids the use of several reference models and a single reference model which is suitable for all operating points is used. Choice of appropriate basis

functions is another criticality. Several basis functions may be required to represent the uncertainties when the plant contains other modes like slosh and flexibility.

An adaptive attitude and vibration control law is designed in MRAC framework for the Ares crew launch vehicle [12]. The control law uses an output feedback neural network adaptive element which augments an existing gain scheduled decoupled linear control law to enhance the controller's performance in the presence of a wider class of uncertainties. The major concern here is the stability of the resulting closed-loop system, which is demonstrated through a Lyapunov-like stability analysis where all the signals are shown to be Uniformly Ultimately Bounded (UUB). An integrated guidance and control design for autonomous launch vehicles using direct model reference adaptive control is presented in [13]. It consists of an inner loop controller, a dynamic inversion based controller, made robust using an adaptive neural network based controller. The outer guidance loop is also based on adaptive control, which adapts to the force perturbations. Pseudo control hedging is used in the inner loop to enable adaptation during control saturation and in the outer loop to prevent adaptation to inner loop dynamics. It may not be able to ensure stability and the performance of the adaptive neural network based controller for a condition that is outside the training set.

The major challenge in the flight control system design is to build the capacity to handle underactuated dynamics. Launch vehicle systems have inherent underactuated dynamics like slosh and flexibility. Aircraft and RLV vehicles become underactuated when some fault occurs in the actuators. Since adaptive controllers adjust to various environments, they are considered an ideal choice to control underactuated systems. Stability and tracking performance of an SLV is ensured in [14] in the event of an actuator fault by designing an adaptive control in MRAC and combining it with the control allocation algorithm. An improved weighting algorithm and an anti-saturation controller are developed to compensate for the saturation error. A multi-variable adaptive control method that uses an observer is presented in [15] for a wing-damaged aircraft. Two different adaptive control approaches are presented in [16] to solve aerodynamic surface failure during formation flight. A reconfigurable control system for re-entry vehicles based on an

adaptive control strategy combined with a control allocation approach is presented in [17].

An adaptive notch filter design and a PID controller are proposed to stabilize the flexible modes for an SLV in [18]. This controller can be implemented for real-time applications. Here, the notch filter parameters are adjusted adaptively to handle the time-varying nature of the flexibility data and the uncertainties. But the parameters of the PID are fixed, which are insufficient to handle the time-varying rigid body parameters. An attitude controller is designed for a flexible launch vehicle in MRAC framework [19]. This paper assumes that the vehicle is symmetric in pitch and yaw planes with negligible flexibility effect. The yaw plane rigid body dynamics is identified and its closed-loop model is used as a reference for the pitch plane. This assumption will not work for clustered launch vehicles.

Robust identification of the dominant flexible mode frequencies is done and closed-loop notch filtering at these frequencies is employed in [20]. In [21], a linear control design methodology is presented for a launch vehicle autopilot using a multi-objective method based on the Youla parameterization and the optimization under constraints described by linear matrix inequalities. These controllers are scheduled, which guarantees the closed-loop stability. A systematic approach to robustness analysis of a classical controller for a flexible launch vehicle with multi-linear uncertainties, having multiple minimum phase margin and gain margin points is described [22]. An adaptive controller is designed to stabilise the aeroservoelastic mode of a hypersonic air-breathing vehicle [23]. In this case, the first three flexible modes are stabilised using an adaptive notch filter. Its performance is compared with a phase stabilised controller, where stabilisation is achieved by properly placing the sensor. A nonlinear feedback control law is developed for the ascent vehicle [24] that stabilises the equilibrium point by suppressing lateral motion due to pitching and sloshing. Here slosh is modelled as a pendulum. A nonlinear dynamic inversion based control law is developed in [25] to stabilise the ascent vehicle which is modelled as a multi-body-vehicle with slosh modelled as a pendulum. This is a critically under-actuated system.

In [3], three modifications are suggested to improve the robustness of the adaptive control algorithms (i) deadzone (ii) e-modification and (iii) sigma-modification. A Lipschitz-continuous version of the projection operator is proposed in [26][27][28]. This modification enables the adaptive control law to achieve more robustness to both parametric and non-parametric uncertainties. Here the adaptation law is continuously modified such that the negative definiteness of the Lyapunov function time derivative is ensured and at the same time, the adaptive gains are uniformly bounded in time. A projection-like modification of the adaptation law is proposed in [29] and an extended version of this method is presented in [3]. The projection based control law tolerates fast adaptation and enforces uniform boundedness to adapted parameters.

Another method to get robust adaptive controllers is using Barrier Lyapunov Functions (BLF), which constrains tracking error and the adapted parameters within the limit. BLF is used along with backstepping controllers and learning controllers to achieve this. A backstepping controller is designed with BLF [30] to constrain the states to an allowable boundary that satisfies the stability conditions. Asymptotic tracking is achieved without violating the constraints and all the closed-loop signals remain bounded. An adaptive servo controller is designed in [31] with both position and velocity constraints using BLF.

A method to constrain both tracking error and adaptive gains of an adaptive controller is given in [32]. An adaptive finite-time tracking problem is solved for a hypersonic flight vehicle with state constraints using backstepping control and BLF [33]. As required by the backstepping algorithm, a sliding mode differentiator is used to estimate the virtual control laws' derivatives. A reinforcement learning controller using two Radial Basis Function (RBF) neural networks is proposed in [34] to control the longitudinal dynamics of a hypersonic air-breathing vehicle with variable geometry inlet. Here the tracking performance and state constraints are guaranteed by a BLF.

MRAC for a Multi-Input-Multi-Output (MIMO) system with quadratic Lyapunov function is formulated in [3]. A robust adaptive non-affine control is designed in [35], combining the sliding mode method, fuzzy logic systems and

adaptive control techniques. Compound adaptive fuzzy H-infinity control is presented in [36] to solve the attitude control problem of RLV in the presence of parameter uncertainties and external disturbances. A robust adaptive backstepping controller is designed in [37] during the re-entry phase of RLV. A saturating adaptive control law is developed in [38] for a MIMO uncertain aeroelastic system with constraints on control surface deflections. An adaptive fault-tolerant controller is developed in [39] based on H_∞ and RBF. An output feedback adaptive controller which augments a baseline controller with a Luenberger observer is designed for a MIMO system [40]. This approach uses a closed loop reference model and Linear Matrix Inequality technique.

An adaptive predictor-corrector guidance law is proposed in [41] for the approach and landing phase of an RLV. An integrated guidance and control scheme is developed for RLV [42] in which the outer loop guidance law is obtained using adaptive Gauss pseudospectral method (GPM) and attitude control law is developed based on a multi-variable smooth second order sliding mode control and disturbance observer. An adaptive-gain fast super-twisting algorithm is proposed in [43] for the finite-time fault-tolerant attitude control problem of the RLV without any knowledge of the bounds of uncertainties and actuator faults. Super twisting sliding mode control scheme is a modified second order sliding mode control scheme that does not require the information of any derivative of the sliding variable. The direct MRAC method is used to develop a multiple model adaptive control scheme in [44] and is applied to a linear multivariable plant.

A new adaptive control framework is presented in [45], in which the update law is modified to achieve a faster learning rate. Higher adaptation gain causes high-frequency oscillations and is filtered out in the update law ensuring UUB for the parameters. A higher-order direct MRAC is presented in [46]. Here the conventional Lyapunov based parameter update law is augmented by an observer type parameter predictor dynamics. A novel adaptive robust fault-tolerant control is proposed in [47] for a linear MIMO system with unmatched uncertainties. Additive functions are designed to compensate for the un-matched uncertainty. An

adaptive feedback linearization-based disturbance rejection scheme is developed in [48] for a multi-variable nonlinear system with unmatched input disturbances.

Adaptive control laws based on Lyapunov methods are not adequately robust to parameter uncertainties and bounded disturbances. To enhance the robustness, various modifications are suggested in literature. Also, BLF are more used whenever there are constraints on the states and outputs. An adaptive backstepping design based on BLF is proposed in [49] which is applied to a system transformed to strict-feedback structure. A time-varying BLF method is integrated with backstepping technique to constrain the states is proposed in [50], which is independent of the initial state and ensures constraint satisfaction even during the transient phase. Various adaptive control methods using BLF are given in [51][52][53] to constrain the states of a hypersonic flight vehicle.

An adaptive Neural Network (NN) based output feedback optimal controller is designed in [54] in the backstepping framework for a class of nonlinear systems in strict-feedback form which have unknown internal dynamics. Some of the states of the system are not measurable and estimated using an adaptive NN. Another NN approximates the internal dynamics of the system. Barrier optimal cost functions combined with the actor–critic architecture have been employed to construct virtual and actual optimal controllers. This control strategy guarantees that the system states are confined within specified compact sets. For strict-feedback nonlinear systems with stochastic disturbance, an adaptive NN based optimal controller in backstepping framework is designed [55] based on identifier–critic–actor architecture for the reinforcement learning algorithm. Novel BLF are defined for various sub-systems to constrain the system states.

Recently, a new set of robust adaptive control strategies based on Function Approximation Techniques (FAT) have been proposed in literature. Here the uncertainties (both parametric and non-parametric) are represented using orthogonal basis functions such as Fourier series expansion, Bessel functions, Legendre polynomials, etc. In [56], a novel FAT based robust adaptive impedance controller is proposed for an electrically driven robot. Here the uncertainty is approximated by Fourier series expansion and the Fourier series coefficients are

adaptively adjusted based on Lyapunov stability. This algorithm has the advantage that the number of regressor matrices are reduced and is very simple to implement for robots with large number of joints. A Szász–Mirakyan operator is used in [57] as universal approximator for both parametric uncertainty and un-modelled dynamics. The polynomial coefficients are tuned adaptively based on Lyapunov stability. The effectiveness of the algorithm is demonstrated for the chaotic synchronization of two Duffing–Holmes oscillators.

1.5 Motivation of the Research

In order to improve the payload capability, modern Space Transportation Systems (STS) are adopting highly optimized slender and long structures. This results in lightly damped, very low frequency bending modes which are difficult to control. The attitude control design problem is further complicated by the presence of liquid propelled stages which introduces moments due to sloshing of the liquid propellant and the gimballed engines used for controlling the vehicle. SLV dynamics is modelled using a set of nonlinear, time-varying differential equations whose parameters are highly uncertain [4][5][6]. Non-linear control problems arising in the digital autopilot design of present-day space transportation systems are mostly handled by time-slice approach in which a sequence of linear systems approximates the non-linear system. The controllers designed for the linear systems are scheduled as a function of one or more independent parameters [4][5][6]. Though this approach provides viable practical designs, its applicability is limited for complex systems with a high degree of coupling, dominant nonlinearities and increased degrees of freedom due to structural flexibility.

For the last several decades, there has been an increasing interest in the design and development of Re-usable Launch Vehicles (RLV) which can be engaged for multiple missions. This is undoubtedly the best solution to achieve lower cost, higher reliability and on-demand access to space. Such vehicles require a reliable navigation, guidance and control system which is robust under all conditions. Re-usable vehicles such as space shuttle mostly use classical control tools for the flight control system design, resulting in gain scheduling. The design

task is to be performed for several operating points which is cumbersome and become in-effective when flight envelope becomes large or when unforeseen changes occur in the dynamics.

The nonlinearities present in such systems can be effectively handled by designing nonlinear controllers which are free from approximations due to linearization. But large parametric variations can be handled only by building novel adaptation mechanisms in the flight control system. For RLV missions which carry humans to outer space, flight control designs should be able to work like a nominal mission in the event of a subsystem failure. Various abort missions are to be designed for expendable launch vehicles which carry humans in re-entry modules. Currently, these missions are executed by generating large number of abort trajectories anticipating various failures on ground itself and then designing the flight controller for these trajectories using the classical gain scheduling method. These trajectories and flight control parameters are stored onboard. This is a very time-consuming process and huge effort is required for flight control system design. This can be reduced by designing algorithms that can cater to a wide spectrum of flight conditions without retuning the controller parameters.

Moreover, to handle the loss of the degrees of freedom in the presence of partial failure or degradation of the control effectors, the controller should be capable of controlling under-actuated systems. This feature also helps to cater to the extra degrees of freedom resulting from large flexible modes and fuel sloshing. This dissertation will focus on the development of stable adaptive controllers in MRAC framework for aerospace applications like SLV and RLV.

1.6 Research Contributions

As stated earlier in this dissertation, the main focus is on developing adaptive control laws for high-risk aerospace systems. Though the academic community has been emphasizing the use of advanced control techniques such as adaptive controllers for SLV and missile systems, the industrial practice is to go for legacy classical control designs. This is mostly because of the flight certification

requirements and the concerns raised regarding the stability of the adaptive controllers. Moreover, many adaptive control techniques are unsuitable for conditionally stable systems like the flexibility dynamics of a launch vehicle.

Our attempt is to develop implementable, stable adaptive controllers for advanced STS. Two applications are selected for this purpose (i) Atmospheric phase autopilot design for a highly flexible launch vehicle whose stabilization is difficult due to high aero dynamic disturbance moments and lightly damped low frequency structural modes and (ii) design of autopilot for a reusable launch vehicle during the autonomous landing phase. The research contributions of the thesis are summarized as follows:

- (i) Adaptive controller design for the atmospheric phase of an aerodynamically unstable SLV plant
 - a. Lyapunov methods are utilized to design adaptive PD/PID controllers in MRAC framework to replace the existing gain scheduled PD/PID controllers. Standard quadratic Lyapunov function is used for controller design.
 - b. Stability of the time-varying closed-loop system, the convergence of the tracking error to zero and the boundedness of all the signals are analytically proved using Barbalat's Lemma.
 - c. Extensive simulation studies are carried out to demonstrate the tracking performance and robustness of the proposed controllers to parametric uncertainties and wind disturbances.
- (ii) Novel adaptive control schemes to ensure robustness to non-parametric uncertainties
 - a. A continuous form of projection operator and barrier Lyapunov functions are used to update the parameters of the MRAC. These controllers use full state information for feedback.
 - b. Slosh and flexibility dynamics are introduced in the existing rigid body SLV model and states of those dynamics are estimated using extended Kalman filter from available noisy measurements.

- c. Robustness of the proposed algorithms to parametric uncertainties, unmodelled dynamics etc. is proved analytically and are demonstrated through simulations.
 - d. An adaptive control scheme is developed to ensure the stability of the system in the presence of actuator position and slew rate constraints. This scheme gives theoretically justifiable and verifiable conditions for stable adaptive controller design and avoids actuator saturation by modifying control input and reference model dynamics.
- (iii) The modified adaptive control laws are extended to control a MIMO system: re-entry vehicle dynamics during the approach and landing phase of an RLV.
- a. A rectangular projection operator is used to simultaneously constrain both the upper and lower bounds of the adapted parameters so that both gain margin and gain reduction margin constraints are met.
 - b. Stability and robustness of the controllers are demonstrated through extensive simulation studies.

Fig. 1.3 show the summary of the proposed work in the form of a flow diagram.

1.7 Organisation of the Thesis

Modelling and control of the rigid body dynamics of an SLV is described in chapter 2. Various assumptions to get a simplified model which can be used for the controller design are described. A quadratic Lyapunov function based MRAC design is done on this model and the results are compared with existing classical control design.

In order to increase the robustness of this controller to non-parametric uncertainties and bounded disturbances, two modifications are proposed in the update law (adaptation mechanism). The derivation of these update laws is presented in chapter 3.

The robustness of these laws is demonstrated for an SLV with underactuated dynamics like slosh and flexibility. A full state feedback structure is provided for the controller. Since all the states are unavailable and the measurements are noisy, an Extended Kalman Filter (EKF) is also proposed. The development of the SLV model is also described in this chapter.

Chapter 4 describes the modelling of the rotational dynamics of an RLV during the descent phase. RLV is simulated with various adaptive controllers and performance is compared. Conclusions and future scope of the research is given in chapter 5.

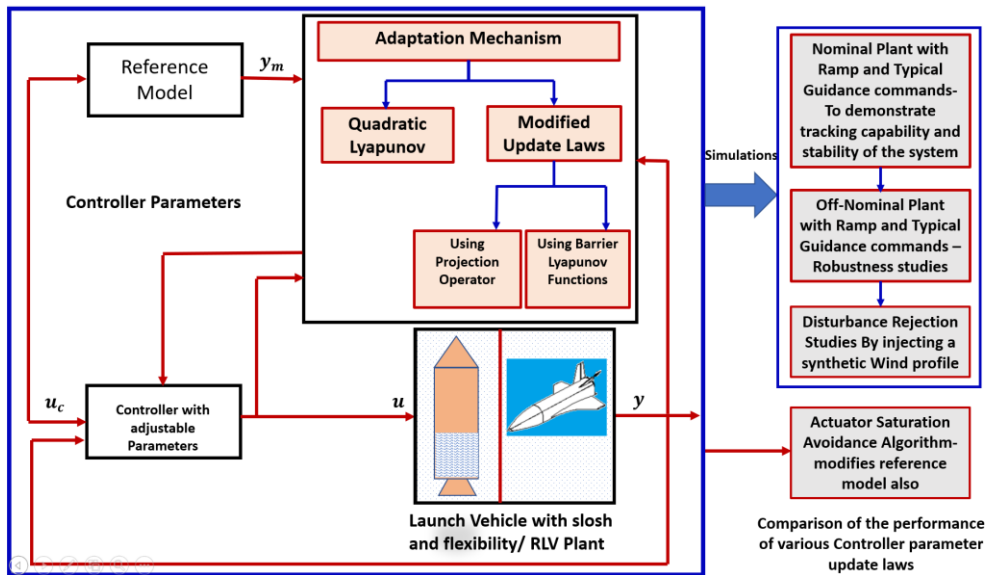


Figure 1. 3 Comprehensive Flow Diagram that Explains the Proposed Work

Chapter 2

Lyapunov Based MRAC for the Rigid Body Dynamics of a Satellite Launch Vehicle

2.1. Introduction

As discussed in chapter 1, SLV dynamics is nonlinear, time-varying and unstable. The instability is caused by the aerodynamics in which the center of pressure is ahead of the center of gravity in most launch vehicles. The aerodynamic forces and moments depend on the angle of attack, which is the angle between the vehicle's longitudinal axis and the velocity vector. For an aerodynamically unstable vehicle, due to wind, if the angle of attack builds up, the aerodynamic moment will try to further increase the angle of attack. Hence the function of the controller is to stabilize the vehicle during the atmospheric phase and to reduce the angle of attack. The attitude controller has to track the guidance commands with minimum error.

In this chapter, the rigid body equations for an SLV are derived and is reduced to a simplified transfer function model. Further, this is converted to a second order state-space model. Adaptive PD/PID controllers are developed in MRAC framework using standard quadratic Lyapunov function for the time-varying launch vehicle plant in the atmospheric phase. It is proved using Lyapunov stability and Barbalat's Lemma that the time-varying system is robust to parametric uncertainties and all the signals are UUB. The performance of the designed controllers is compared with existing gain scheduled PD/PID controllers.

2.1.1 Attitude Control System for an SLV

Attitude control system (also called 'autopilot') is the inner loop of the Navigation, Guidance and Control (NGC) sub-system of a launch vehicle. It controls the rotational dynamics (motion about the Centre of Gravity) of the launch vehicle. The block diagram of the NGC system is given in Fig. 2.1.

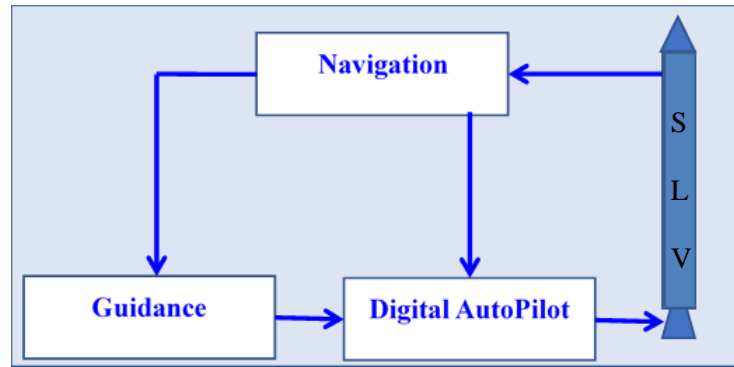


Figure 2. 1 Block Diagram of NGC Subsystem

Navigation gives the current position, velocity and the attitude of the launch vehicle with respect to an inertial frame and also the body rate information. Navigation derives this information from accelerometer and gyroscopes mounted on the body of the SLV. The Guidance system controls the translational dynamics (motion of the CG) of the launch vehicle. It receives the position and velocity information with respect to an inertial frame from navigation. The objective of the guidance is to steer the space vehicle optimally to the designated terminal conditions satisfying the constraints imposed by the environment, mission and space vehicle subsystems. Typically, guidance is formulated as a constrained non-linear optimal control problem with split boundary conditions. The guidance system computes the optimum acceleration profile to control the trajectory of the space vehicle. The propulsion system controls the acceleration magnitude (in the case of engines with throttling capability) and the acceleration direction is controlled by digital autopilot by changing the attitude. Hence the primary function of the attitude control system is to follow the guidance commands while maintaining the stability and integrity of the launch vehicle. It achieves this by using the vehicle's present attitude and body rate. This dissertation focuses on the design and development of attitude control systems for STS.

2.2. Modelling of the Rigid Body Dynamics of an SLV

The oscillations about the CG of the vehicle have a comparatively short period and are called short-period oscillations. The short period dynamics of the SLV is derived for analysis and design of the attitude control system [4][5]. A pre-

requisite for this model development is a nominal reference trajectory obtained from a trajectory optimiser, generated after considering various constraints and maximising the payload. The vehicle is assumed to be moving along this nominal trajectory with slight deviations. Another assumption is that the time-varying parameters are assumed to be frozen at the linearisation point over a short period of time. In this way, powerful linear analysis techniques can be used for the analysis and design of attitude control system.

Short period equations are derived in the body axis system (a right-handed coordinate system $X_b Y_b Z_b$) whose origin is coinciding with the CG of the vehicle. Here X_b axis is defined along the longitudinal axis of the vehicle, $X_b Z_b$ is the pitch plane and $X_b Y_b$ is the yaw plane. Since the launch vehicles are axi-symmetric, attitude control design can be performed plane wise. Fig. 2.2 shows the geometry of the SLV in pitch plane. Here Z_b is the lateral axis. In this plane, there are two translational Degrees of freedom (DoF). Y_b axis points towards us, out of the plane of paper. Rotation about Y_b axis is the third DoF. Rotation is achieved by deflecting the thrust vector T_c by an angle δ . Since the translational motion along the X_b axis will not be much affected by the control deflection δ , this can be neglected.

Hence there are only one translational DoF and one rotational DoF. This produces two rigid body equations (i) force equation and (ii) moment equation. Force equation defines the relation between lateral acceleration (\ddot{z}) / drift and the forces acting and moment equation gives the relation between angular acceleration ($\ddot{\theta}$) and moments acting on the vehicle. These relationships are defined using Newtons laws which are applied on an inertial frame and then translated to body frame. Various forces and moments acting on the vehicle are aerodynamic forces (with modification by the bent shape of the vehicle due to flexibility) and thrust (again modified by the bent shape of the vehicle). For the present study, effects due to flexibility are not considered and vehicle is assumed as a pure rigid body.

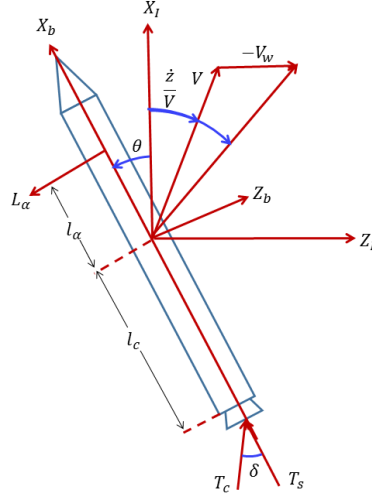


Figure 2.2 Short Period Model of the SLV in Pitch Plane

Referring to Fig. 2.2, we can write the force equation as

$$\ddot{z} = -\frac{T_T - D}{m}\theta - \frac{L_\alpha}{m}\alpha + \frac{T_c}{m}\delta \quad (2.1)$$

where, total thrust $T_T = T_c + T_s$, is the sum of control thrust (T_c) and the un-gimballed thrust (T_s). D is the aerodynamic drag force which will be acting opposite to the direction of velocity. Mass of the vehicle is defined by m . θ is the attitude angle (angle at which body frame to be rotated to align with inertial frame) and α is the angle of attack of the vehicle (angle between velocity vector and longitudinal axis). L_α is the aerodynamic load per unit angle of attack acting at the center of pressure location. δ is the control deflection angle. It is assumed that all these angles are small. It is also assumed that the variation of the flight path angle γ is negligible compared to α and θ . The force equation can be re-written in terms of the drift angle ($\frac{\dot{z}}{V}$) as

$$\frac{\dot{z}}{V} = -\frac{(T_T - D)}{mV}\theta - \frac{L_\alpha}{mV}\alpha + \frac{T_c}{mV}\delta \quad (2.2)$$

where, z is the inertial Z axis drift position of the center of mass and \dot{z} is the inertial drift velocity. Moment equation can be written as

$$\ddot{\theta} = \mu_\alpha\alpha + \mu_c\delta \quad (2.3)$$

where,

$\mu_\alpha = \frac{L_\alpha l_\alpha}{I}$, $\mu_c = \frac{T_c l_c}{I}$, l_α (aerodynamic moment arm) is the distance from center of gravity of the vehicle to the center of pressure location and l_c (control moment arm) is the distance from the center of gravity to the engine gimbal point. I is the moment of inertia. The effective angle of attack (α) can be written as

$$\alpha = \theta + \frac{\dot{z}}{V} + \alpha_w \quad (2.4)$$

where, α_w is the wind induced angle of attack which can be defined as $\alpha_w = \frac{-V_w}{V}$, V_w is the velocity of the wind in the lateral direction and V is the total velocity of the vehicle. During the control design phase, wind disturbances are not considered. Hence the angle of attack can be written as $\alpha = \theta + \frac{\dot{z}}{V}$. For a launch vehicle, the total velocity of the vehicle (V) is very much higher than the lateral drift velocity. Hence, in order to get a simplified transfer function model for the rigid body of the SLV, the term $\frac{\dot{z}}{V}$ is neglected. Hence it is assumed that $\alpha = \theta$. Substituting this in the moment equation (2.3) we get

$$\ddot{\theta} = \mu_\alpha \theta + \mu_c \delta \quad (2.5)$$

Taking the Laplace transform on both sides and neglecting the initial conditions

$$s^2 \cdot \theta(s) = \mu_\alpha \cdot \theta(s) + \mu_c \cdot \delta(s) \quad (2.6)$$

where, s is the Laplace variable. The transfer function can be written as

$$\frac{\theta(s)}{\delta(s)} = \frac{\mu_c}{s^2 - \mu_\alpha} \quad (2.7)$$

Remark 1: This simplified transfer function has two roots $s = \pm\sqrt{\mu_\alpha}$. If μ_α is positive, then this transfer function will have one pole on the right half side of the complex plane which indicates the instability of the plant. Most of the SLV's have positive μ_α and are aerodynamically unstable.

Remark 2: Parameters of the plant (μ_α and μ_c) vary with respect to time. These are derived from the following time dependant parameters. Thrust of the vehicle varies with time; Mass and inertial properties (CG location and the moment of inertia) of the vehicle are continuously varying as the propellant is getting depleted;

Aerodynamic force is dependent on the aerodynamic characteristics of the vehicle and the dynamic pressure which in turn depends on the velocity and altitude of the vehicle.

The state-space representation of the simplified transfer function model of the rigid body dynamics of the SLV can be written as

$$\begin{aligned} \dot{x}_p &= A_p x_p + B_p u \\ y_p &= C_p x_p + D_p u \end{aligned} \quad (2.8)$$

where, $A_p = \begin{bmatrix} 0 & 1 \\ \mu_\alpha & 0 \end{bmatrix}$, $B_p = \begin{pmatrix} 0 \\ \mu_c \end{pmatrix}$, $C_p = \begin{bmatrix} 1 & 0 \\ 0 & 1 \end{bmatrix}$, $D_p = \begin{pmatrix} 0 \\ 0 \end{pmatrix}$

2.3. Attitude Controller Design for the Simplified SLV Model

The function of the attitude controller is to track the guidance command stabilising the vehicle suppressing various high frequency oscillations due to other dynamics. The launch vehicle achieves this by deflecting the thrust vector or using additional thrusters that provide control moments to rotate the vehicle so that the vehicle follows the desired trajectory commanded by the guidance system. Since the plant is time-varying, time-varying controller gains are required.

2.3.1 Gain Scheduled Control Law

During the atmospheric phase, the load acting on the vehicle is mostly due to the aerodynamic and control forces. The load should be less than the limit specified by the structural designers to maintain structural integrity. By reducing the angle of attack, the load acting on the vehicle will be minimized (aerodynamic load is a function of the dynamic pressure and angle of attack). In general, ‘load relief’ is achieved by two methods. The first is a passive method in which the attitude steering angles will be ‘biased’ to the wind measured before launch. In this case, the attitude controller (autopilot) has to track the steering commands closely

to avoid the angle of attack build-up. Here the structure of the attitude controller is of the form

$$\delta = K_A * (K_\theta(u_c - \theta) - K_R * \dot{\theta}) \quad (2.9)$$

where, u_c is the guidance command to be followed, K_A is the forward path gain, K_R is the rate feedback gain, K_θ is the attitude feedback path gain which is equal to 1 for this control law. This control law uses two feedbacks (θ and $\dot{\theta}$). Forward path gain decides the bandwidth of the system and rate path gain is used to stabilise the plant. These gains are scheduled with respect to time and stored onboard.

In order to reduce the tracking error and counteract the slowly varying disturbances, an integrator also can be included in the control law.

$$\delta = K_A * (K_\theta(u_c - \theta) - K_R * \dot{\theta} + K_I * \int (u_c - \theta)) \quad (2.10)$$

where, K_I is the integrator gain which is also a scheduled parameter.

The second method to achieve load relief is the active load relief scheme in which the autopilot will use lateral acceleration feedback, body rate, and attitude angle feedback. There are two active load relief control concepts introduced by Hoelkner [58] in 1959. They are “drift-minimum” and “load-minimum” control principles. These laws help to reduce the angle of attack and load. Control law will be in the form

$$\delta = K_A(-K_R\dot{\theta} + K_\theta(u_c - \theta) - K_\alpha\alpha) \quad (2.11)$$

where, θ attitude angle, $\dot{\theta}$ attitude rate and α is the angle of attack. K_α is the α feedback gain scheduled with respect to time. Here the tracking performance is compromised to get reduction in load and the attitude gain K_θ can be less than one. For an aerodynamically unstable vehicle, to get load relief, α feedback is required. For pure attitude tracking control law, α feedback is not applied and $K_\theta=1$ gives good tracking capability. Load relief control law will not be designed in this work. The launch vehicle considered for this study uses only attitude and rate feedback and uses Day-of-the launch wind biased steering for load reduction.

2.3.2. Proposed Adaptive Control Design

The current practice in the SLV autopilot design is to linearise the plant about the operating point, design the controller for each operating point and then schedule the control gains with respect to an auxiliary variable that correlate well with the changes in the plant parameters [7][59]. In this section, two Lyapunov based adaptive controllers are designed in MRAC framework to replace the existing gain-scheduled controller.

2.3.2.1 Adaptive PD Controller Design

In this section, a Lyapunov based MRAC is developed for the simplified SLV plant. A standard quadratic Lyapunov function is used for the design. Consider the plant defined in (2.8) and is re-written as

$$\dot{x} = Ax + Bu \quad (2.12)$$

where, $x \in \mathcal{R}^2$, $A \in \mathcal{R}^{2 \times 2}$, $B \in \mathcal{R}^{2 \times 1}$ and (A, B) is controllable. It is a second order model with full state measurements available for feedback. A second order model whose characteristics are defined based on the desired characteristics of the closed loop system is chosen as the reference model.

$$\begin{aligned} \dot{x}_m &= A_m x_m + B_m u_c \\ y_m &= C_m x_m + D_m u_c \end{aligned} \quad (2.13)$$

where, x_m is the state of the reference model, A_m is a Hurwitz matrix and u_c is the bounded reference signal to be tracked. The state trajectory of the plant $x(t)$ should follow the reference state trajectory $x_m(t)$. The closed loop plant should behave similar to a second order dynamics with 3.5 rad/s bandwidth and 0.7 damping. Hence the natural frequency ω_m is equal to 3.5 rad/s and ζ_m is equal to 0.7. Hence A_m , B_m , C_m and D_m can be defined as $A_m = \begin{pmatrix} 0 & 1 \\ -\omega_m^2 & -2\zeta_m\omega_m \end{pmatrix}$, $B_m = \begin{bmatrix} 0 \\ \omega_m^2 \end{bmatrix}$, $C_m = \begin{pmatrix} 1 & 0 \\ 0 & 1 \end{pmatrix}$ and $D_m = \begin{bmatrix} 0 \\ 0 \end{bmatrix}$.

If the plant matrices A and B are known accurately, the following control law can be defined, which helps in tracking the reference signal and stabilising the plant:

$$u = -K^{*T}x + L^*u_c \quad (2.14)$$

where, K^* is the state feedback gain matrix and L^* is the feedforward gain.

Remark 3: Since a second order SLV plant is considered here with states θ and $\dot{\theta}$, this control law can be written in the form of a PD control law $u = -K^*(1) \cdot \theta - K^*(2) \cdot \dot{\theta} + L^*u_c = L^*(u_c - \frac{K^*(1)}{L^*}\theta - \frac{K^*(2)}{L^*}\dot{\theta})$.

The closed loop system can be written as

$$\dot{x} = (A - BK^{*T})x + BL^*u_c \quad (2.15)$$

Applying the model matching condition

$$A - BK^{*T} = A_m, BL^* = B_m \quad (2.16)$$

If K^* and L^* are chosen to satisfy the matching condition, then the transfer matrix of the closed loop system is the same as that of the reference model and $x(t) \rightarrow x_m(t)$ exponentially for any bounded reference input. But sometimes K^* and L^* may not exist, indicating that the control structure needs to be modified to satisfy the matching conditions. Since the plant matrix A and B are known with uncertainty, the control law in (2.14) cannot be implemented. Hence the estimates of K^* and L^* is used to implement the control law. These estimates, defined as $K(t)$ and $L(t)$ has to be generated by an adaptation law. The adaptation law is derived using a quadratic Lyapunov function defined in terms of the tracking error between the trajectories ($e = x(t) - x_m(t)$) and the deviations of the gains from the ideal gains which satisfy the matching conditions ($\tilde{K} \triangleq K - K^*$, $\tilde{L} \triangleq L - L^*$). The tracking error dynamics can be obtained from

$$\dot{e} = \dot{x} - \dot{x}_m \quad (2.17)$$

Let's add and subtract the desired term $-B(K^{*T}x - L^*u_c)$ from the plant given in (2.12).

$$\begin{aligned}
\dot{x} &= Ax + Bu - B(K^{*T}x - L^*u_c) + B(K^{*T}x - L^*u_c) \\
&= (A - BK^{*T})x + BL^*u_c + B(u + K^{*T}x - L^*u_c) \\
&= A_mx + B_mu_c + B(-K^T x + Lu_c + K^{*T}x - L^*u_c)
\end{aligned} \tag{2.18}$$

Subtracting \dot{x}_m from (2.18) the error dynamics is obtained

$$\dot{e} = A_m e + B(-\tilde{K}^T x + \tilde{L}u_c) \tag{2.19}$$

A quadratic Lyapunov function in terms of e , \tilde{K} and \tilde{L} is defined as follows:

$$V(e, \tilde{K}, \tilde{L}) = e^T P e + \text{tr}(\tilde{K}^T \Gamma^{-1} \tilde{K} + \tilde{L} \Gamma^{-1} \tilde{L}) \tag{2.20}$$

where, P satisfies the algebraic Lyapunov equation

$$PA_m + A_m^T P = -Q, \quad Q = Q^T > 0 \tag{2.21}$$

Control parameter update law can be found out from the derivative of the Lyapunov function in such a way that this ensures the negative definiteness of the derivative of the Lyapunov function. Derivative of the Lyapunov function evaluated along the trajectories of (2.19) is

$$\begin{aligned}
\dot{V}(e, \tilde{K}, \tilde{L}) &= \dot{e}^T P e + e^T P \dot{e} + \text{trace}(\dot{\tilde{K}}^T \Gamma^{-1} \tilde{K} + \tilde{K}^T \Gamma^{-1} \dot{\tilde{K}} + \\
&\quad \dot{\tilde{L}} \Gamma^{-1} \tilde{L} + \tilde{L} \Gamma^{-1} \dot{\tilde{L}}) \\
&= (A_m e + B(-\tilde{K}^T x + \tilde{L}u_c))^T P e \\
&\quad + e^T P (A_m e + B(-\tilde{K}^T x + \tilde{L}u_c)) \\
&\quad + 2 \text{trace}(\tilde{K}^T \Gamma^{-1} \dot{\tilde{K}} + \tilde{L} \Gamma^{-1} \dot{\tilde{L}}) \\
&= e^T (A_m^T P + P A_m) e + (-\tilde{K}^T x + \tilde{L}u_c)^T B^T P e \\
&\quad + e^T P B (-\tilde{K}^T x + \tilde{L}u_c) + 2 \text{trace}(\tilde{K}^T \Gamma^{-1} \dot{\tilde{K}} \\
&\quad + \tilde{L} \Gamma^{-1} \dot{\tilde{L}}) \\
&= e^T (-Q) e + 2e^T P B (-\tilde{K}^T x) + 2 \text{trace}(\tilde{K}^T \Gamma^{-1} \dot{\tilde{K}}) \\
&\quad + 2e^T P B \tilde{L} u_c + 2 \text{trace}(\tilde{L} \Gamma^{-1} \dot{\tilde{L}})
\end{aligned} \tag{2.22}$$

Using the vector trace identity, for any two co-dimensional vectors a and b , the trace identity relation is $a^T b = \text{tr}(ba^T)$,

$$\begin{aligned}\underbrace{e^T PB}_{a^T} \underbrace{(-\tilde{K}^T x)}_b &= \text{trace}(\underbrace{(-\tilde{K}^T x)}_b \underbrace{e^T PB}_{a^T}) \\ \underbrace{e^T PB}_{a^T} \underbrace{(\tilde{L}u_c)}_b &= \text{trace}(\underbrace{(\tilde{L}u_c)}_b \underbrace{e^T PB}_{a^T})\end{aligned}\quad (2.23)$$

Substituting (2.23) in (2.22) we get

$$\begin{aligned}\dot{V}(e, \tilde{K}, \tilde{L}) &= e^T(-Q)e + 2\text{trace}(-\tilde{K}^T x e^T PB + \tilde{K}^T \Gamma^{-1} \dot{\tilde{K}}) \\ &\quad + 2\text{trace}(\tilde{L}u_c e^T PB + \tilde{L} \Gamma^{-1} \dot{\tilde{L}})\end{aligned}\quad (2.24)$$

In order to make $\dot{V}(e, \tilde{K}, \tilde{L}) = e^T(-Q)e$ (negative semi-definite), all the terms inside trace have to be made zero.

$$-\tilde{K}^T x e^T PB + \tilde{K}^T \Gamma^{-1} \dot{\tilde{K}} = 0 \quad (2.25)$$

$$\tilde{K}^T \Gamma^{-1} \dot{\tilde{K}} = \tilde{K}^T x e^T PB \quad (2.26)$$

Pre-multiplying both sides of (2.26) by $\Gamma \tilde{K}^{T^{-1}}$, we get

$$\dot{\tilde{K}} = \Gamma x e^T PB \quad (2.27)$$

Since $\dot{\tilde{K}} = \dot{K} - \dot{K}^* = \dot{K}$ ($\dot{K}^* = 0$), we get the update law for K

$$\dot{K} = \Gamma x e^T PB \quad (2.28)$$

Similarly

$$\tilde{L}u_c e^T PB + \tilde{L} \Gamma^{-1} \dot{\tilde{L}} = 0 \quad (2.29)$$

Pre-multiplying both terms of (2.29) by $(\Gamma \tilde{L}^{-1})$, we get

$$\dot{\tilde{L}} = \dot{L} = -\Gamma u_c e^T PB \quad (2.30)$$

Equations (2.28) and (2.30) are the controller gain update laws which ensure the negative semi-definiteness of the derivative of Lyapunov function. The resulting

closed loop system is a nonautonomous system of the form $\dot{x} = f(t, x), x(t_0) = x_0, f(t, 0) = 0$. In order to prove that the tracking error tends to zero and the adapted controller parameters $K(t)$ remain bounded in time, the same Lyapunov function can be used and then Barbalat's Lemma can be applied. Derivative of the Lyapunov function is

$$\begin{aligned}\dot{V}(e, \tilde{K}) &= \dot{e}^T P e + e^T P \dot{e} + 2 \text{trace} \left(\tilde{K}^T \Gamma^{-1} \dot{\tilde{K}} \right) \\ &\quad + 2(-\tilde{K}x)^T B_m^T P e \\ &= -e^T Q e \leq 0\end{aligned}\tag{2.31}$$

The inequality presented here infers global stability and uniform boundedness of $e(t)$, $K(t)$ and $L(t)$. This in turn ensures the boundedness of $\dot{e}(t)$ and the second time derivative of the Lyapunov function $\ddot{V}(e, \tilde{K}, \tilde{L}) = -2e^T Q \dot{e}$. Therefore, $\dot{V}(e, \tilde{K}, \tilde{L})$ is continuous in t . Since $V(e, \tilde{K}, \tilde{L}) \geq 0$ and $\dot{V}(e, \tilde{K}, \tilde{L}) \leq 0$, the Lyapunov function is having a limit. By applying the Barbalat's Lemma : If a scalar function $f: R \rightarrow R$ is twice continuously differentiable on $[0, \infty)$ and has a finite limit, $\lim_{t \rightarrow \infty} f(t) < \infty$, and its second derivative is bounded, then $\lim_{t \rightarrow \infty} \dot{f}(t) = 0$, $\lim_{t \rightarrow \infty} [e^T(t) P e(t)] = \lim_{t \rightarrow \infty} [\dot{V}(t), K(t), L(t)] = 0$, and consequently $\lim_{t \rightarrow \infty} \|e(t)\| = 0$; . This ensures global convergence of the tracking error to the origin and the other parameters remain bounded.

2.3.2.2 Adaptive PID Controller Design

In order to improve the tracking performance and disturbance rejection capability to steady or slowly varying disturbances, an integrator is added to the error path. Here also control design is attempted with full state feedback. The integrator state (x_I) is augmented to the original plant defined in (2.12). Integrator dynamics can be written as

$$\dot{x}_I = x(1) - u_c\tag{2.32}$$

Control structure is

$$u = K_1^T x\tag{2.33}$$

Here feedforward control is not required as integrator is added in the system. The augmented plant with integral state is

$$\begin{bmatrix} \dot{x} \\ \dot{x}_I \end{bmatrix} = \begin{bmatrix} A & 0 \\ 1 & 0 \end{bmatrix} \begin{bmatrix} x \\ x_I \end{bmatrix} + \begin{bmatrix} B \\ 0 \end{bmatrix} u + \begin{bmatrix} 0 \\ -1 \end{bmatrix} u_c \quad (2.34)$$

The control law with integrator can be written as

$$u = K_1^T x_p + K_I x_I \quad (2.35)$$

Here also a standard quadratic Lyapunov function in terms of tracking error and gains is chosen.

$$V(e, \tilde{K}) = e^T P e + \text{trace}(\tilde{K}^T \Gamma^{-1} \tilde{K}) \quad (2.36)$$

Following the same procedure described in sub-section 2.3.2.1, the control parameter update law can be obtained as

$$\begin{bmatrix} \dot{K} \\ \dot{K}_I \end{bmatrix} = -\Gamma \begin{bmatrix} x \\ x_I \end{bmatrix} e^T P B \quad (2.37)$$

The detailed steps to obtain the controller parameter update law is given in Appendix-A.5. This control law ensures global convergence of tracking error to the origin and all other parameters remain bounded.

2.4. Results and Discussions

A simplified rigid body model given in (2.7) is used for the simulation studies. The first 100 s of the trajectory of a highly unstable SLV is simulated. The plant parameters are varying with respect to time. The variation of plant parameters during the atmospheric phase of flight is given in Fig. 2.3. The control moment coefficient μ_c appearing in the numerator of (2.7) is dependent on the thrust variations and the inertia variations of the SLV.

The parameter μ_α is the aerodynamic disturbance moment coefficient. This represents the aerodynamic stability/instability of the SLV. Positive μ_α shows the

aerodynamic instability. The parameter μ_α depends on the aerodynamic characteristics of the vehicle, inertial properties and also on the dynamic pressure $Q = \frac{1}{2}\rho V^2$ where, ρ is the atmospheric density which depends on the altitude and temperature and V is the velocity of the vehicle. Peaking of μ_α occurs from 45 s to 65 s where the dynamic pressure is high. This is called ‘high-Q’ region. For all aerospace vehicles, the aerodynamic characteristics are highly uncertain and vary significantly around transonic Mach numbers (0.8 to 1.2). For the SLV considered in this study, the transonic and high Q regimes coincided around 45 s. A jump in μ_α can be seen from 35 s to 45 s which is the transonic region. μ_c also comes down from 25 s to 50 s. This is because of the reduction in thrust to reduce the dynamic pressure. Variation of the control parameters is shown in Fig. 2.4 and aero parameters are shown in Fig. 2.5.

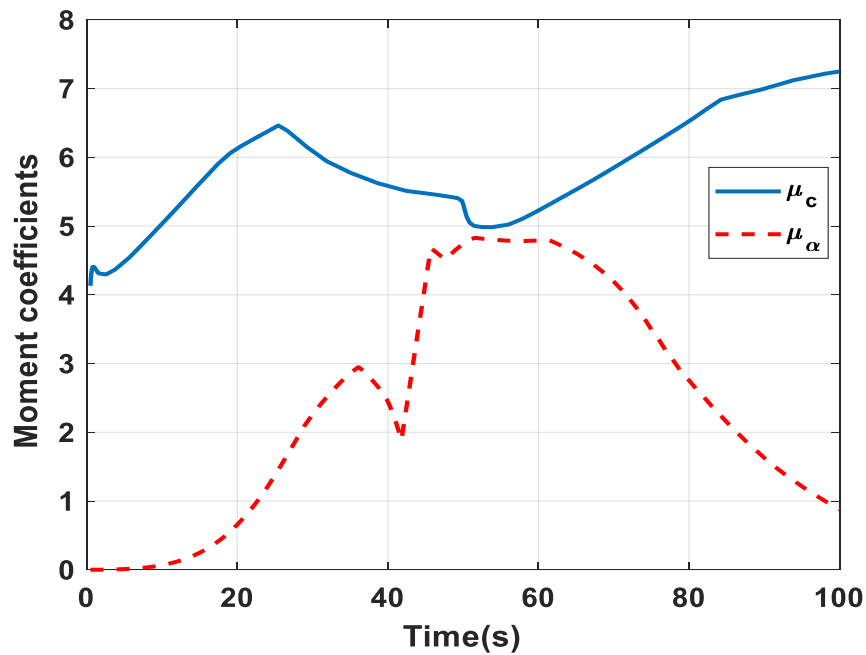


Figure 2. 3 Plant Characteristics

The plant is simulated for a duration of 100 s with Gaussian white noise introduced in the rate sensor output for full scale. During the design of the controllers, actuator dynamics is not considered. But a second order actuator model with a deflection limit of 8 deg, slew rate limit of 10 deg/s and angular acceleration limit of 1000 deg/s² is simulated.

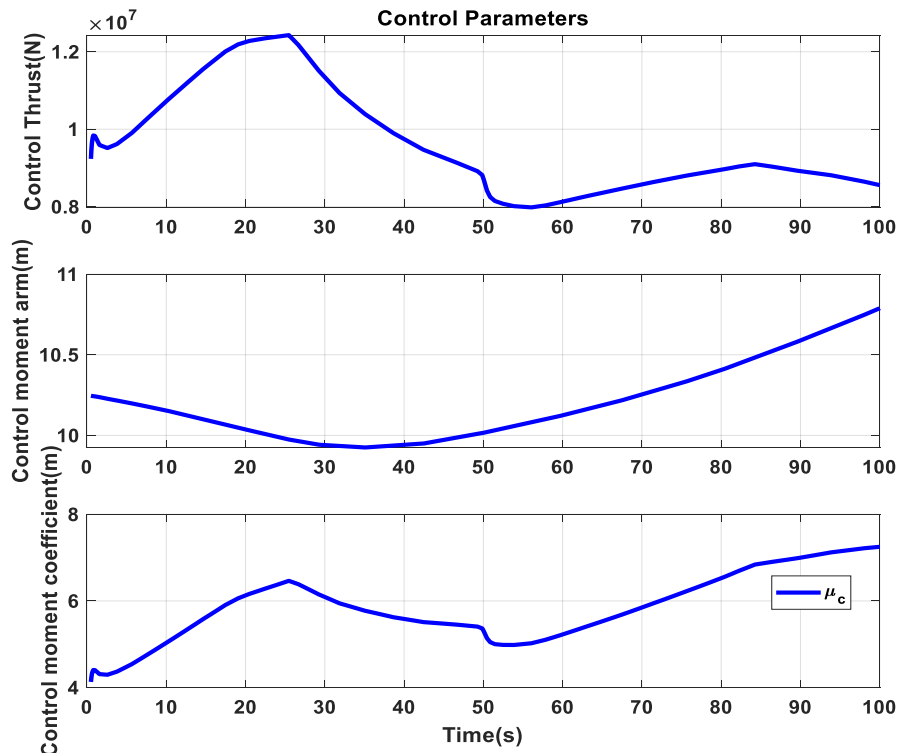


Figure 2.4 Variation of the Control Parameters for the Rigid Body Model

The purpose of the feedback control is to stabilise the plant dynamics and make it follow a desired attitude command during the atmospheric phase generated by the open loop guidance system. Four different types of controllers are designed in Section 2.3. They are

- (i) Gain Scheduled PD controller
- (ii) Gain Scheduled PID controller
- (iii) Adaptive PD controller and
- (iv) Adaptive PID controller

The plant is simulated with these controllers in loop and their performances are compared in terms of stability, robustness, tracking performance and disturbance rejection.

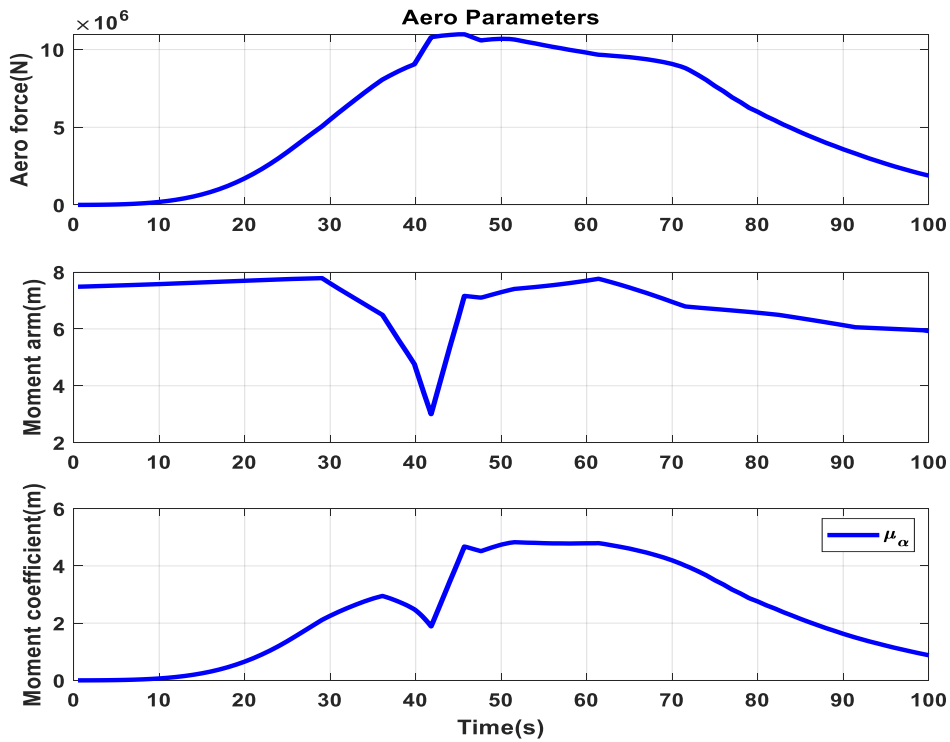


Figure 2.5 Variation of the Aero Parameters for the Rigid Body Model

Two different types of reference signals are given to the plant to demonstrate the tracking capability (i) a ramp input and (ii) a typical guidance command. In order to demonstrate the robustness, plant parameters are perturbed to the specified limit and the performance of the controllers are assessed. The disturbance rejection capability of the controllers is demonstrated by injecting a synthetic wind profile with shear and gust. Simulation set up is shown in Fig. 2.6.

2.4.1 Nominal Plant with a Ramp Command

Tracking performance of different controllers are tested by inputting a ramp command to the closed loop plant. During the atmospheric phase, the steering commands are usually biased to the wind. In the presence of a wind shear, a ramp command is likely to come for a short duration. The tracking performance of the controllers and corresponding tracking error for a ramp command are shown in Fig. 2.7 and Fig. 2.8.

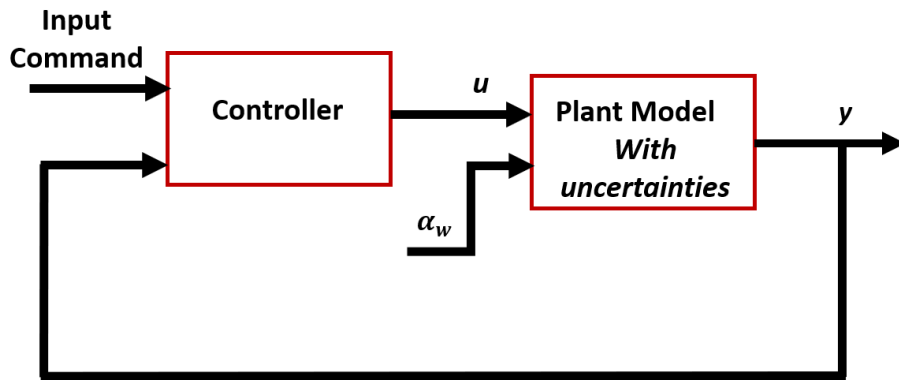


Figure 2. 6 Simulation Setup

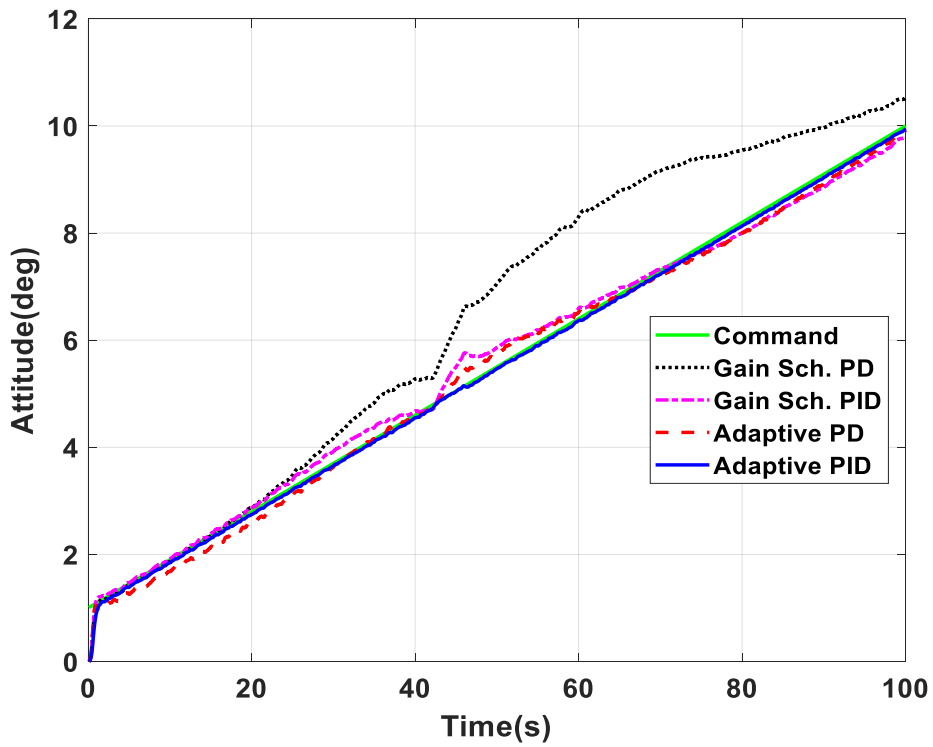


Figure 2. 7 Tracking Performance of the Controllers for a Ramp Command

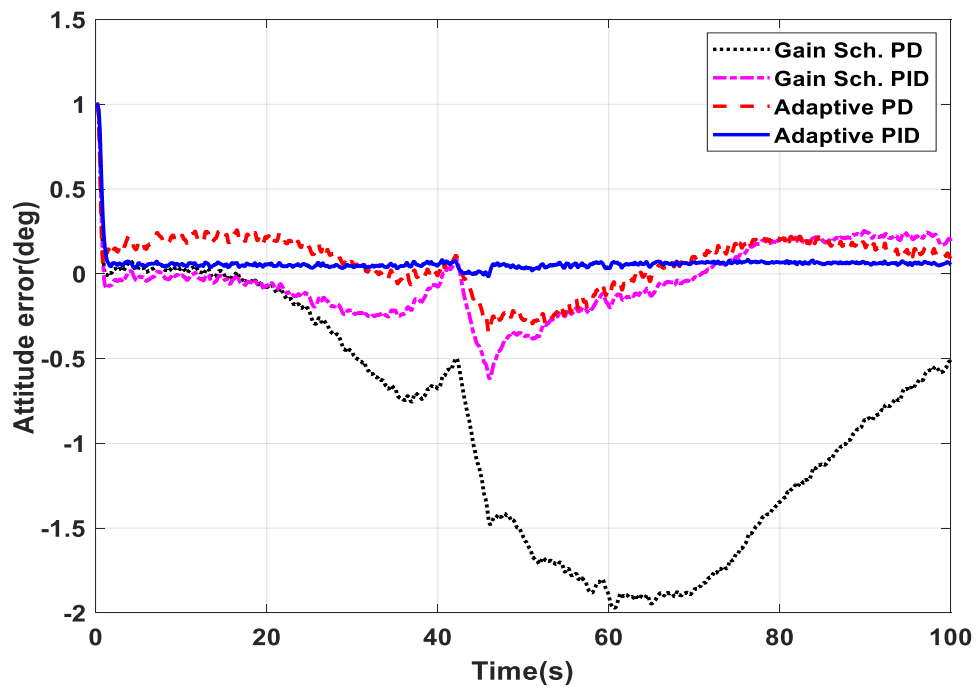


Figure 2. 8 Tracking Error of the Controllers for a Ramp Command

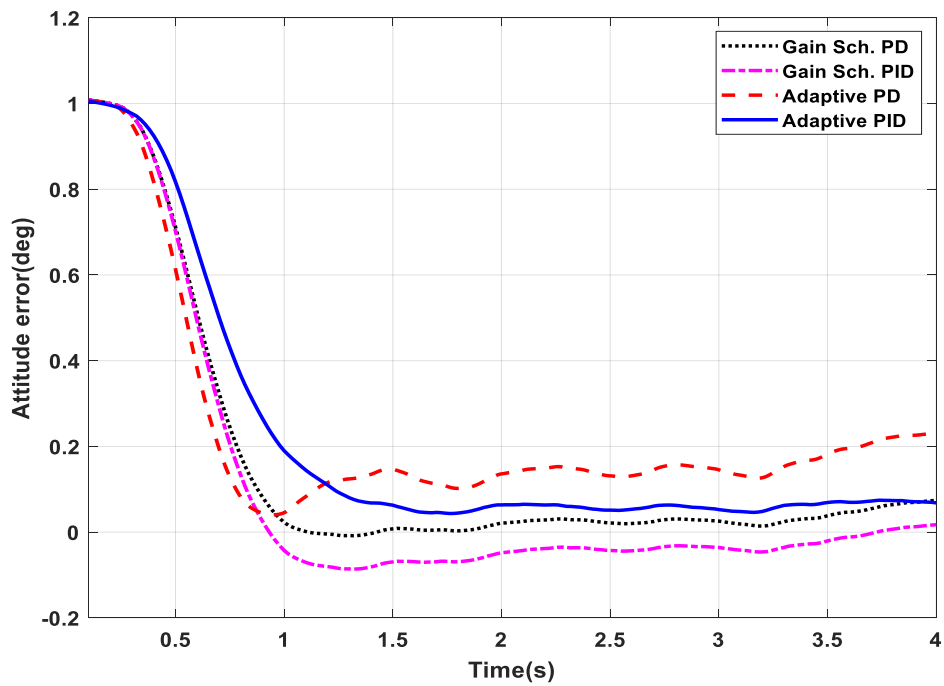


Figure 2. 9 Initial Capture of Tracking Errors by the Controllers for a Ramp Command

From Fig. 2.8, it can be seen that the gain-scheduled PD controller has the maximum tracking error ($\sim 2\text{deg}$) during the high-Q regime. Both gain-scheduled PID and adaptive PD have almost same performance however with lesser tracking error for adaptive PD. The adaptive PID controller produces better tracking performance (less error) than adaptive PD and gain scheduled PD/PID controllers. However, it is noted from Fig. 2.9 that the time taken to capture the initial conditions is slightly more in the case of adaptive PID controller, which improves the tracking performance as time progresses. During transonic regime (from 35 s to 45 s) where the aerodynamic parameters are changing drastically (refer Fig. 2.5), adaptive PID gives near zero tracking error compared to other controllers.

Gaussian white noise is added at the sensor output and the noisy rate is used for feedback. Fig. 2.10 shows the noise used to perform the simulations. Fig. 2.11 shows the attitude rate of the SLV after the sensor. It is observed that adaptive PD controller is showing less noise suppression. Initial rate during the capture is also high for adaptive PD. This can be reduced by reducing the bandwidth of the reference model used in the adaptive PD design.

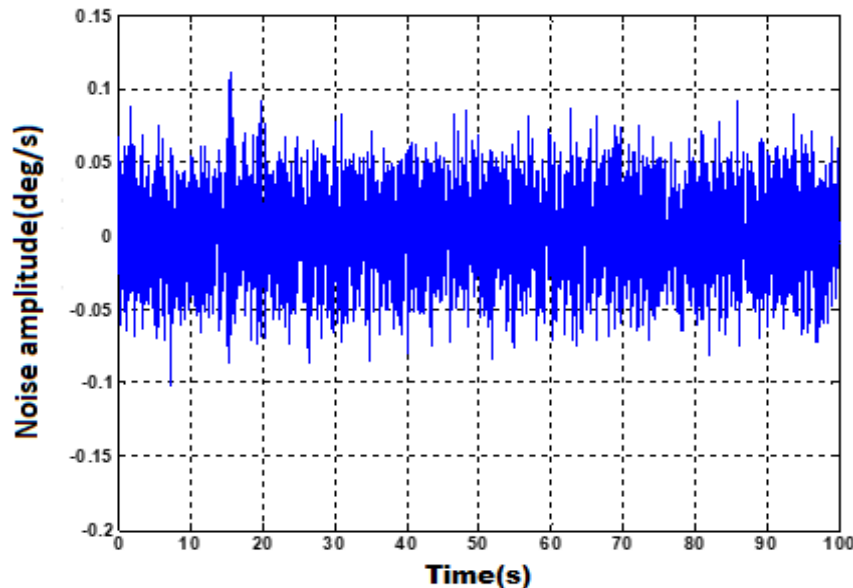


Figure 2. 10 Noise Generated for Simulation Study

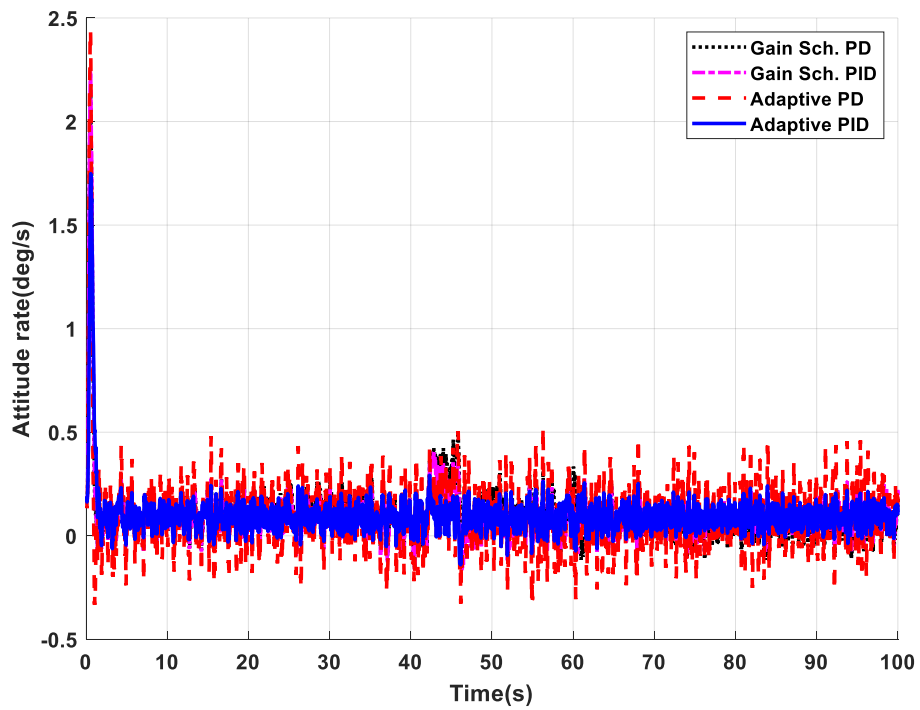


Figure 2. 11 Attitude Rate of the SLV while Tracking the Ramp Command

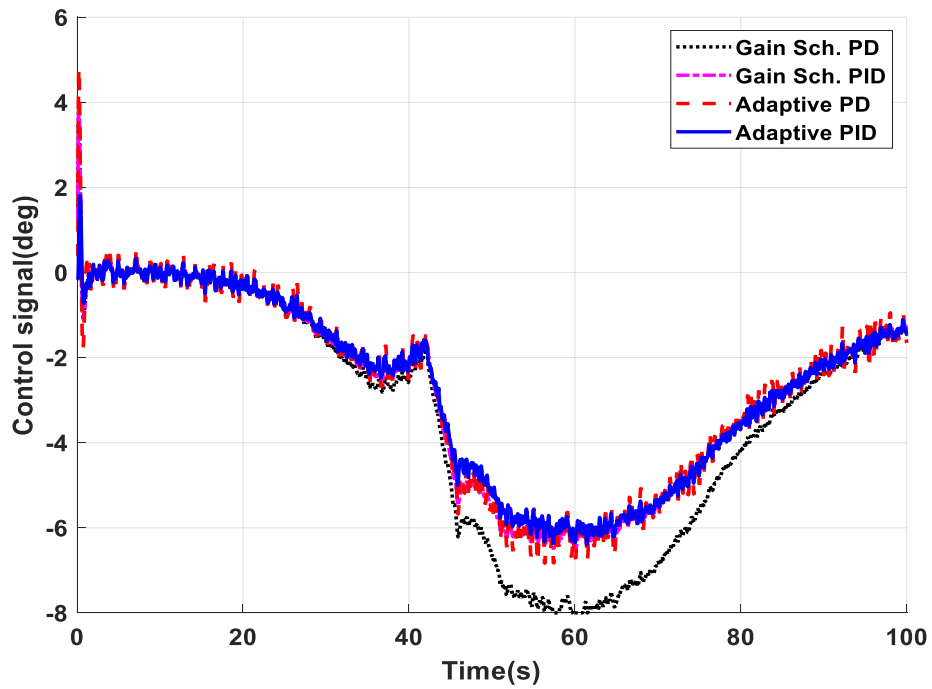


Figure 2. 12 Control Deflections for Ramp Tracking

Fig. 2.12 shows the control deflections of various controllers for ramp command tracking. Since the initial condition capture is slow for adaptive PID, initial control demand is less. Adaptive PD controller demands maximum control during capture followed by gain scheduled controllers. During high dynamic pressure regime, gain scheduled PD controller demands full gimbal deflection while adaptive PID demands the least deflection. Gain scheduled PD saturates for a short duration during high Q. In general, adaptive controllers are noisier compared to gain scheduled controllers.

2.4.2 Nominal Plant with a Typical Guidance Command Input

During the atmospheric phase of flight, most important function of the control system is to reduce the aerodynamic load acting on the vehicle. As explained in sub-section 2.3.1, there are two types of load relief systems: Passive (wind biased steering) and active load relief (using additional feedback which senses the angle of attack build up or lateral acceleration due to aerodynamic forces). This SLV uses ‘Day-of-the-launch’ wind biased steering to achieve load reduction. Here, open loop guidance commands are generated which are biased to the wind measured prior to launch on the same day. Depending on the measured wind, the steering can give aggressive commands which may excite high frequency dynamics. In this section, a typical open loop guidance command is applied to the closed loop plant and results are compared for various controllers.

Fig. 2.13 shows the attitude tracking performance of various controllers. Initially, the guidance commands are zero because the vehicle has to vertically go up till it clears the launch tower. Around 10 s, the gravity turn maneuver starts to reduce the angle of attack. Vehicle experiences a step like command at this point. During the maneuvers, the adaptive PID controller responds slowly, but improves the tracking in increasing timescale and provides a near zero tracking error during the steady phase.

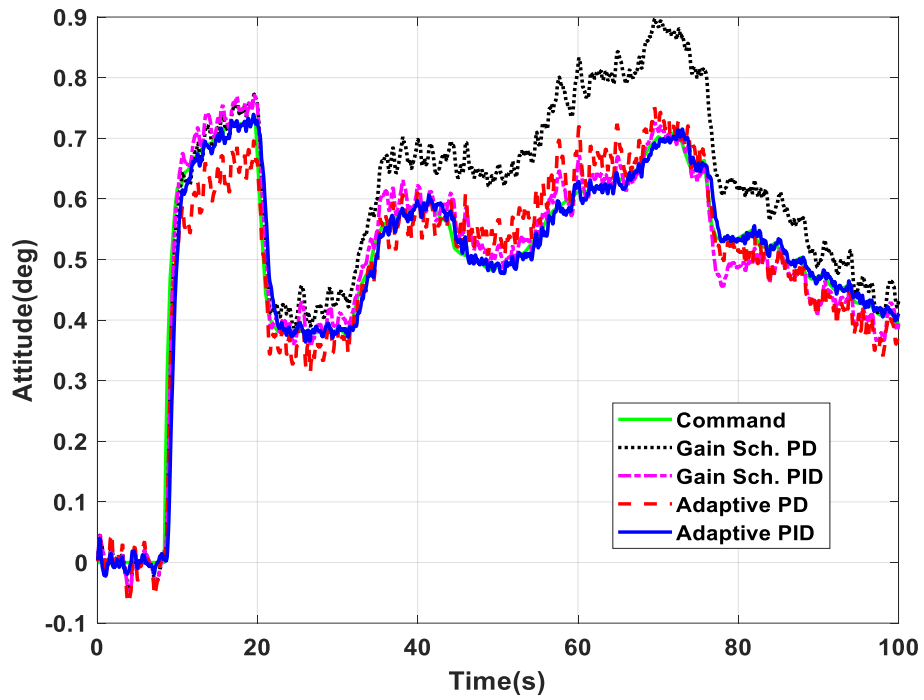


Figure 2. 13 Attitude Tracking for a Typical Guidance Command

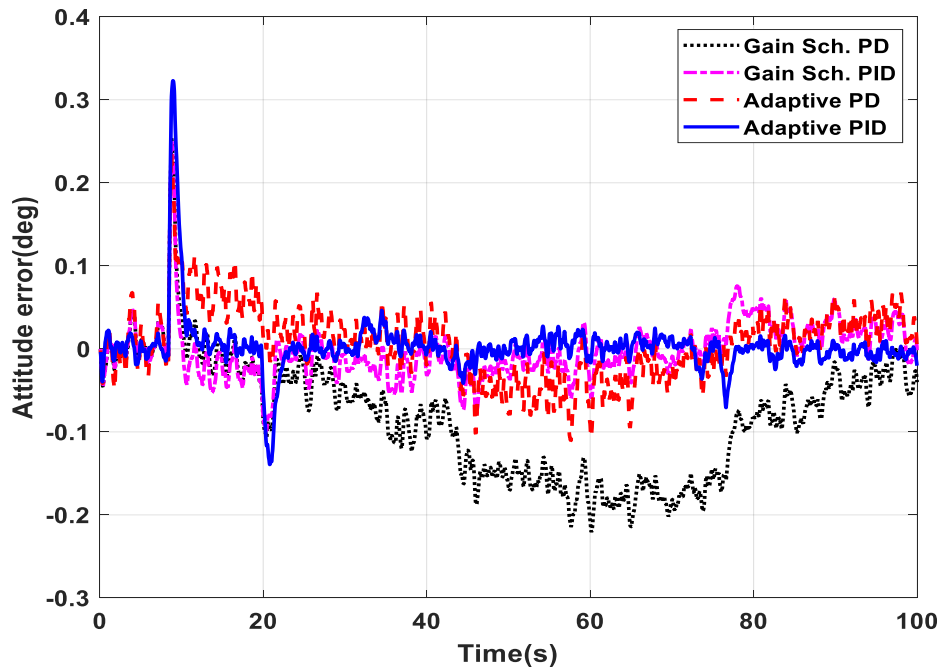


Figure 2. 14 Tracking Errors of Different Controllers for a Typical Guidance Command

Fig. 2.14 shows the tracking error. It can be seen that, during the transients, adaptive PID shows slightly higher tracking error compared to the other three controllers however, steady state tracking error is near zero. Fig. 2.15 shows the rate of the SLV. As in earlier simulations with ramp input, rates are noisy for adaptive controllers. Control demands are shown in Fig. 2.16. Adaptive controller outputs are noisy compared to gain scheduled controllers.

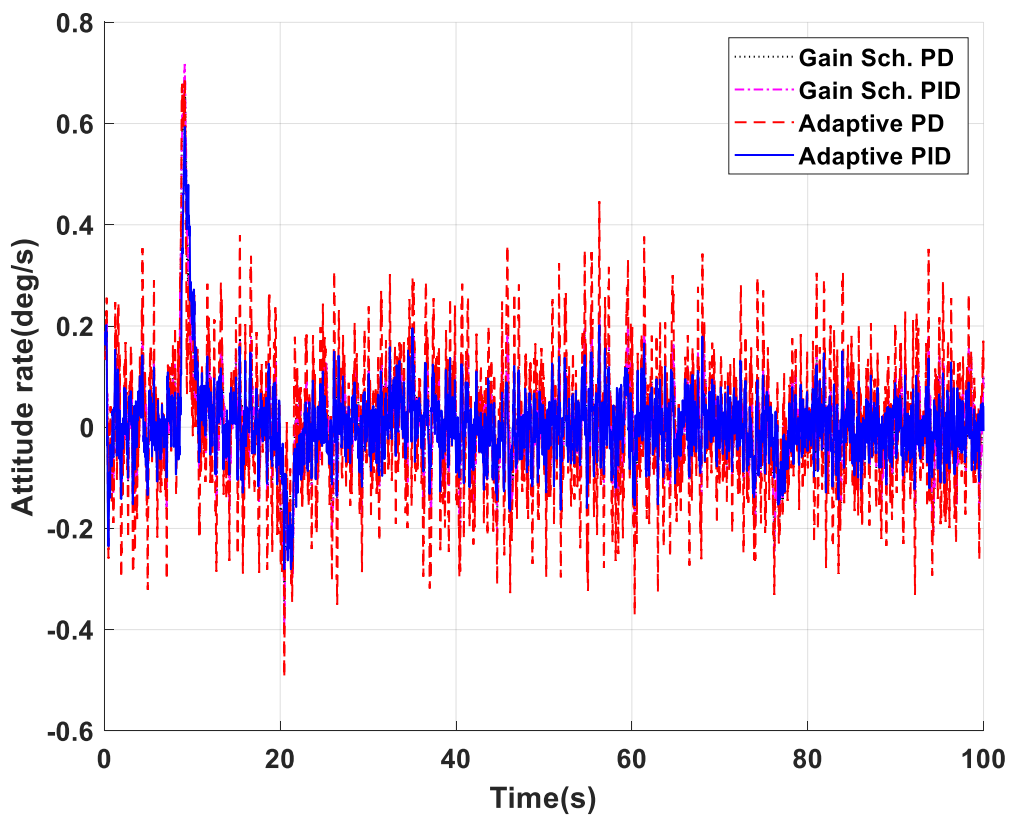


Figure 2. 15 Attitude Rates for a Typical Guidance Command Tracking

A comparison of the performances of different controllers for a typical guidance command is consolidated and given in Table 2.1.

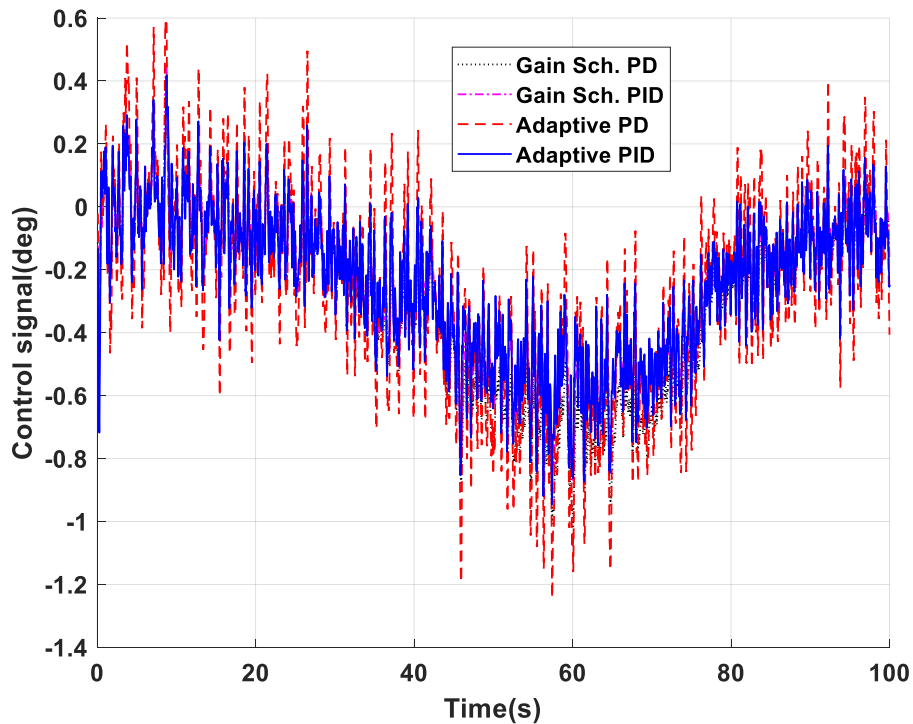


Figure 2. 16 Control Responses of Different Controllers for a Typical Guidance Command Tracking

Table 2. 1 Comparison of the Performance of Different Control Schemes with Typical Guidance Commands for Nominal Plant

Scheme	Maximum Control Demand (deg)	Control effort (deg)	Integral Absolute Error (degrees)
Gain Scheduled PD Controller	1.0 deg during high disturbance	17.2571	1.1811
Gain Scheduled PID controller	0.8733 deg during high disturbance	13.9822	0.1950
Adaptive PD Controller	1.2 deg during high disturbance	15.6068	0.2134
Adaptive PID Controller	1.15 deg during high disturbance	13.5636	0.0562

Gain scheduled PD control scheme gives the maximum tracking error, Integral of absolute error and control effort. Performance of gain scheduled PID and adaptive PD are much closer, and adaptive PID gives the best tracking performance with the least control effort.

2.4.3 Perturbation Studies

Aerodynamic parameters are highly uncertain during the transonic regime of flight. There will be uncertainties in the launch vehicle's thrust values and inertial properties. Hence to demonstrate the robustness of the control schemes, plant is simulated with perturbed parameters. For all launch vehicles, bounds on the perturbations will be available and the controller has to stabilize the vehicle and perform satisfactorily within these bounds. The bounds used for this SLV are $\pm 10\%$ in thrust and 15% in mass and inertia. Aerodynamic coefficient perturbations vary with Mach number. Variation of perturbed μ_c and μ_α is shown in Fig. 2.17. There are sudden variations in the aerodynamic parameters between 40 to 50 s when the vehicle is in the transonic regime. These jumps will be reflected in the body rates and enter the control loop through feedback. The control commands also will respond to these jumps.

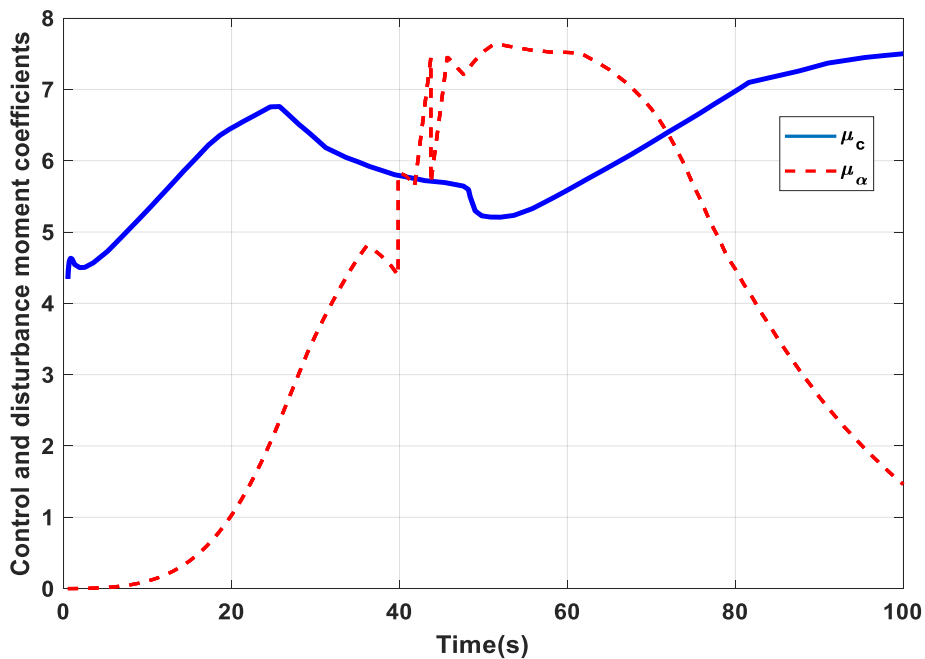


Figure 2. 17 Perturbed Plant Parameters

Fig. 2.18 shows the tracking performance of various controllers under parameter perturbation. Adaptive PID controller follows the open loop guidance command with very little tracking error as shown in Fig. 2.19. The proposed adaptive PID controller offers a near nominal tracking performance with a slight

increase in the control deflections, as shown in Fig. 2.20. Tracking performance of gain scheduled PID and adaptive PD controllers are very close. As in the nominal case, adaptive control commands are noisy compared to gain scheduled controllers. Hence proper noise filtering should be provided for the output signals before using them in adaptive control.

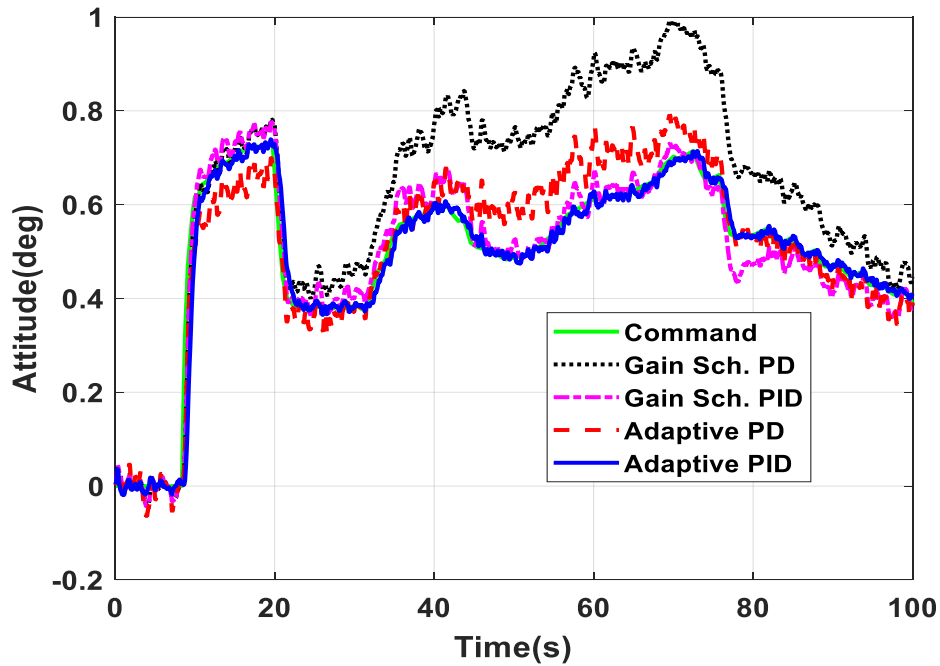


Figure 2. 18 Tracking Performance of Controllers for a Perturbed Plant

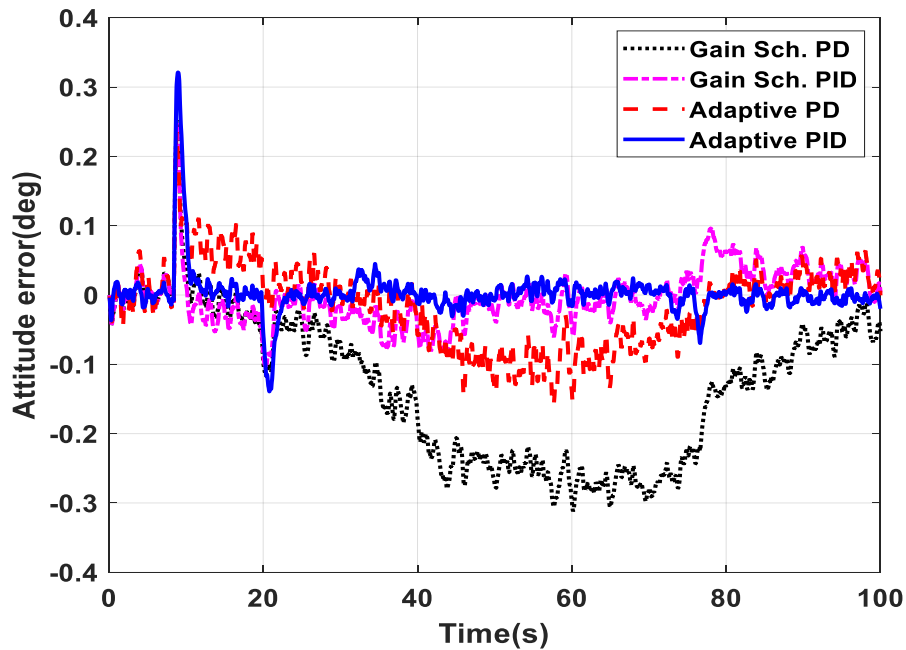


Figure 2. 19 Tracking Error for a Perturbed Plant

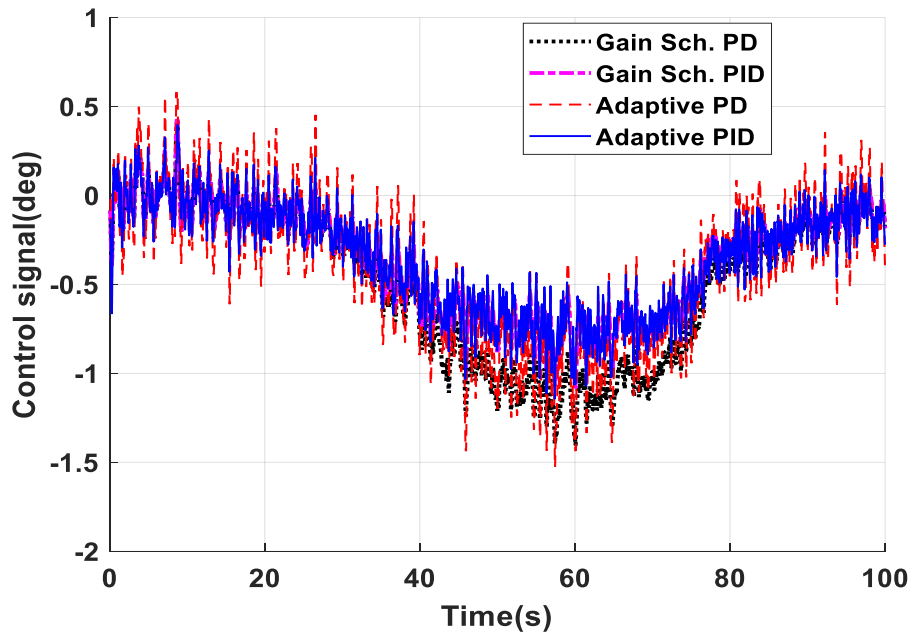


Figure 2.20 Control Responses of Different Controllers for a Perturbed Plant

Table 2.2 compares performance in terms of tracking error and control demand for different controllers with a typical guidance command for the plant under parameter perturbations. It is observed that the adaptive PID control works with near zero tracking error and requires slightly increased control demand for the perturbed system compared to the nominal system discussed in section 2.4.2.

Table 2.2 Comparison of the Performance of Different Control Schemes with Typical Guidance Commands under Plant Parameter Perturbation

Scheme	Maximum Control Demand (deg)	Control effort (deg)	Integral Absolute Error (degrees)
Gain Scheduled PD Controller	0.4 deg for initial capture 1.404 deg during high disturbance	41.93	2.8574
Gain Scheduled PID controller	0.4 deg for initial capture 1.0722 deg during high disturbance	23.31	0.2783
Adaptive PD Controller	0.46 deg for initial capture 1.528 deg during high disturbance	30.89	0.3589
Adaptive PID Controller	1.24 deg for initial capture 1.33 deg during high disturbance	23.7558	0.0558

2.4.4 Disturbance Rejection Studies

During the atmospheric phase of flight, a launch vehicle experiences severe disturbances such as wind shear and gust. The rigid body model given in (2.2) to (2.4) is simulated to study SLV's wind disturbance rejection capability. Controllers are designed using the simplified transfer function model. A synthetic wind profile with wind shears and a gust is injected into the closed-loop plant keeping the command zero. During the atmospheric phase of flight, the angle of attack (AoA) should be kept minimum to reduce the aerodynamic loads acting on the vehicle, which is a function of the dynamic pressure and the angle of attack.

Fig. 2.21 gives the AoA build up due to the injected wind. All controllers show the same AoA build up however adaptive PID giving slightly lower AoA with reduced tracking error. For this vehicle AoA is smaller than the injected wind. The adaptive PID controller's initial response is somewhat higher than other controllers. Fig. 2.22 gives the attitude error build-up due to injected wind. It can be seen that, adaptive PID gives the slightest error build-up compared to the other three controllers.

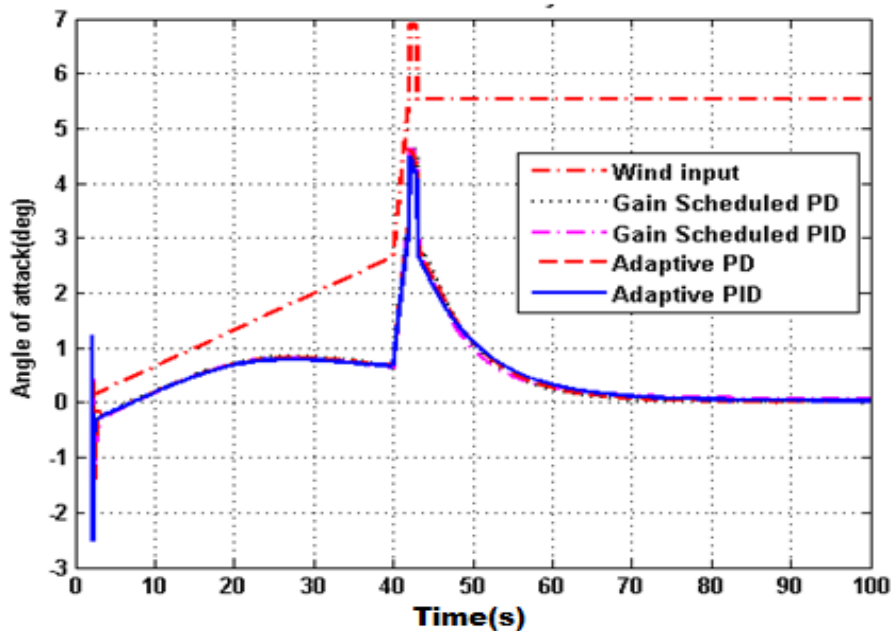


Figure 2. 21 Angle of Attack Build up due to Synthetic Wind Disturbance

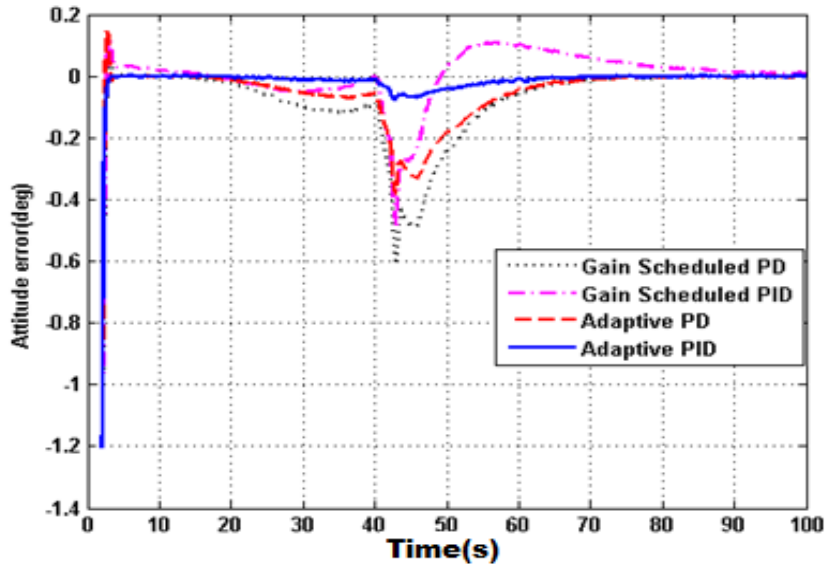


Figure 2. 22 Attitude Error Build up due to Injected Wind

The wind disturbance rejection capability of different controllers is shown in Table 2.3. It is evident that adaptive PID controller provides the least angle of attack build-up and almost zero integral of absolute error compared with gain scheduled controller and adaptive PD controller. However, it requires more control demand during initial capture.

Table 2. 3 Comparison of the Wind Disturbance Rejection of Different Control Schemes

Scheme	Angle of Attack (deg)	Tracking Error (deg)	Maximum Control Demand (deg)	Integral Absolute Error (deg)
Gain Scheduled PD Controller	4.663	0.6103	4.04 deg for initial capture 2.36 deg during wind gust	2.2879
Gain Scheduled PID controller	4.631	0.4802	4.066 deg for initial capture 2.34 deg during wind gust	1.0804
Adaptive PD Controller	4.602	0.3804	5.82 deg for initial capture 2.20 deg during wind gust	0.8710
Adaptive PID Controller	4.49	0.078	8 deg for initial capture 2.142 deg during wind gust	0.1427

2.5. Summary

Lyapunov based Adaptive PD/PID controllers are developed in MRAC framework for a highly unstable SLV plant. Only rigid body dynamics of the plant is considered for this work. It is demonstrated that adaptive controllers can replace existing gain scheduled controllers that use classical control design techniques.

A rigid body model of the SLV plant is developed and then a simplified transfer function model is derived by making certain assumptions. A gain-scheduled PD controller and a PID controller is developed for the atmospheric phase of an aerodynamically unstable plant. The function of the controller is to stabilise the plant and follow a guidance command. These controllers are replaced by adaptive PD and PID controllers. Since the plant and controller parameters are changing with respect to time, the stability of the closed-loop system is to be ensured. To achieve stabilising adaptive controllers, Lyapunov methods are utilised. Stability of the time-varying closed-loop system, the convergence of the tracking error to zero and the boundedness of all the signals are analytically proved using Barbalat's Lemma. These controllers can be extended to MIMO dynamical systems also.

Extensive simulation studies are carried out to demonstrate the tracking performance of the proposed adaptive controllers. It is seen that both adaptive controllers are showing superior tracking performance with a ramp input compared to gain scheduled classical controllers. Simulations are repeated with a typical guidance command. Here also, the adaptive PID controller is giving a near zero tracking error. In order to demonstrate the robustness of the controllers to parametric uncertainties, perturbation studies are conducted. The adaptive PID controller gives a near nominal performance in the presence of parametric uncertainties with slightly increased control deflection. The disturbance rejection capability of the controllers are demonstrated by injecting a synthetic wind profile.

Simulations are carried out with Gaussian white noise injected at the rate output. It is observed that the adaptive controllers are noisier compared to gain scheduled controllers and the controller parameters are drifting from the ideal value.

Hence proper noise filtering should be done before feeding back the sensed signals to the adaptive controllers.

The controller developments are done for a simplified rigid body model neglecting higher dynamics like slosh and flexibility whose stabilisation is the most challenging task in SLV flight control system design. These dynamics also will be considered in the controller design in the next chapter.

Chapter 3

Novel Adaptive Control Laws For A Flexible Satellite Launch Vehicle

3.1 Introduction

A launch vehicle is essentially a long slender beam with a large length to diameter ratio. Hence it is structurally very flexible. The flight control system designed for SLV uses signals from sensors mounted along the vehicle to stabilize the vehicle and track the guidance commands. These sensors pick up local elastic vibrations also along with the rigid body motions. To achieve attitude control, the SLV's use thrust vector control which deflect the nozzle to generate control forces. The forces and moments generated in this way are governed both in magnitude and direction on the sensor outputs which are fed back. Under some adverse conditions, the closed-loop control can reinforce the amplitude of structural vibration, leading to structural failure [4][5]. This is called control-structure interaction and this is illustrated in Fig. 3.1. Stabilisation of the structural modes is the most challenging task in autopilot design for SLV's.

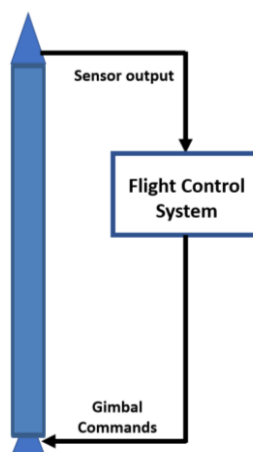


Figure 3. 1 Interaction Between Flight Control System and the Structural Dynamics

Preliminary structural analysis is conducted by assuming SLV as a free-free beam. For launch vehicles with more strapons and clustered engines, sophisticated finite element analysis will be required to generate the vibration frequencies and mode shape data. There will be a large number of lightly damped vibrational modes for a free-free beam. In general, the first few modes will be of importance for flight control system design. High frequency modes will be usually attenuated by the low-pass nature of the autopilot system. The first bending mode frequency will be closer to the rigid body frequency and the control actions of the autopilot will excite this mode and may destabilise the vehicle dynamics if not properly compensated. Some of the higher modes are also significant and can cause control- structure interaction unless modelled and compensated properly.

Presently the control-structure interaction problem arising in the flight control system is handled in two ways (i) phase stabilisation and (ii) gain stabilisation. In phase stabilisation, the phase of the sensor feedback signal is modified so that the control actively damps out the structural oscillations. For this, accurate phase of the sensor outputs is required, which in turn depends on the accuracy of the bending mode's mode shape/frequency information. Usually, the mode shape and frequency data will be more accurate for the first, low-frequency bending mode. Hence this mode is phase stabilised. Gain stabilisation is used for higher mode stabilisation in which the control system will not be allowed to pump in energy at the resonant structural frequencies by filtering or attenuating the signals. A review of the various stabilisation techniques is given in [60]. Detailed modelling and stability analysis of longitudinal and lateral structural vibrations are also given. Effect of wind on the flexible launch vehicle and trajectory planning during atmospheric phase is also described.

Conventional roll off and/or notch filters are used for the stabilisation of unstably interacting bending modes [61][62]. Some launch vehicles use body rate feedbacks from more than one rate gyros placed at different locations along the length of the vehicle. The outputs from these rate sensors are blended and used in the control law so that the control signal damps out the oscillations. The blending ratios are designed to achieve the phase stabilisation of the low-frequency bending

mode. Sometimes, rate blending is used to reduce the magnitude of the bending mode signal in the rate fed back so that gain stabilisation is achieved. Usage of non-minimum phase structural filters is shown to be very effective and robust in flexible mode stabilisation [5][63][64].

Since the parameters of the flexible body model change with time and are highly uncertain, several advanced control techniques are also proposed for flexible mode stabilisation. These techniques avoid the use of gain scheduling and complex compensator switching algorithms. Designing classical controllers that ensure stability and robustness at all flight regimes is time-consuming and requires huge effort. Adaptive control techniques are more suitable for such time-varying systems. In this chapter we extend the Lyapunov based MRAC design for the stabilisation of under actuated dynamics such as slosh and flexibility. Though this controller has sufficient robustness to parametric uncertainties, it lacks robustness to non-parametric uncertainties.

3.2 Model of a Flexible SLV

Effect of flexible mode vibrations on attitude control system of an SLV is explained in section 3.1. The attitude control design problem is further complicated by the presence of liquid stages, which introduces moments due to sloshing of the liquid propellant and the gimballed engines used for controlling the vehicle.

3.2.1 Slosh Dynamics

Rigid body models for an SLV were developed in section 2.2. Mathematical equations depicting the slosh dynamics are derived in this section. Slosh refers to the movement of liquid in a partially filled tank. External torques and resonant modes can excite the fuel and amplify slosh behaviour causing rapid energy dissipation. This unpredicted coupled resonance between the vehicle and its onboard fuel could threaten a mission. Launch vehicles have an enormous percentage of their initial weight as fuel. Consequently, the dynamic forces resulting from the motions of these large liquid masses could be substantial, even

beyond the capabilities of the control system to counteract them or the structure to resist them. The dynamic effects of the sloshing can be closely approximated by replacing the liquid mass with a rigid mass and a series of pendulums whose size and location along the longitudinal axis of the vehicle depend on the vehicles mass, size and geometry of the tank, liquid fill level and also on the liquid properties. But if the tank wall is flexible, the interaction between the liquid free surface motions and the elastic motion of the tank wall can become significant. But the analysis for the case of a coupled elastic tank and liquid propellant is complex. Hence the bending modes are computed in terms of normal coordinates after removing the sloshing pendulums and swivellable rocket engines. The slosh modes are computed assuming rigid vehicle. In this way, the slosh and flexible dynamics are artificially de-coupled. The coupling will be introduced through the forcing function while writing the equations of motion. A detailed theoretical procedure for generating these parameters is presented in [65].

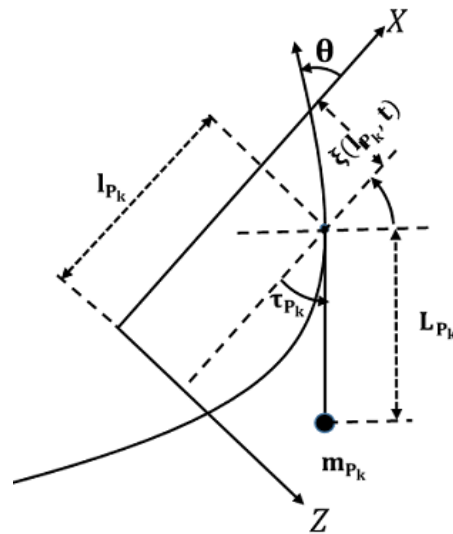


Figure 3. 2 Slosh Pendulum in Pitch Plane

One or more slosh modes are associated with each tank and each mode (k) can be visualised as a pendulum attached to a flexible tank as shown in Fig. 3.2. Each pendulum has the following parameters: mass (m_{pk}), frequency (ω_k), damping (ζ_k), length of the pendulum (L_{pk}), hinge point of the pendulum with

respect to the CG of the vehicle (l_{pk}). Pendulum length (equivalently frequency) depend on the longitudinal acceleration of the vehicle.

The forces on the slosh pendulum originate from the lateral and rotational acceleration of the vehicle. It is assumed that forces due to structural flexibility is not affecting slosh as their frequencies are separated. Also, it is assumed that the sloshing pendulum angles are small and is represented by a second order dynamics. Velocity of the k^{th} sloshing pendulum relative to inertial space is given by

$$\mu_{pk} = \mu + \frac{d\rho_{pk}}{dt} = \mu + \frac{\partial\rho_{pk}}{\partial t} + \omega \times \rho_{pk} \quad (3.1)$$

where $\mu = U\hat{i} + W\hat{k}$ is the inertial velocity of body frame, $\omega = Q\hat{j}$ is the angular velocity of body frame in pitch plane and $\hat{i}, \hat{j}, \hat{k}$ are the unit vectors in X, Y, Z directions in body frame. The radius vector from the pendulum to the origin of the body axis system (ρ_{pk}) which can be written as

$$\rho_{pk} = (l_{pk} - L_{pk} \cos(\tau_{pk}))\hat{i} + (L_{pk} \sin(\tau_{pk}))\hat{k} \quad (3.2)$$

The effect of flexibility is neglected while writing this equation. Substituting this in (3.1) we get,

$$\begin{aligned} \mu_{pk} = [U + L_{pk}\dot{\tau}_{pk} \sin(\tau_{pk}) + QL_{pk} \sin(\tau_{pk})]\hat{i} + [W \\ + L_{pk}\dot{\tau}_{pk} \cos(\tau_{pk}) - Q(l_{pk} - L_{pk} \cos(\tau_{pk}))]\hat{k} \end{aligned} \quad (3.3)$$

where, τ_{pk} is the pendulum angle. The Kinetic Energy (KE) is $\frac{1}{2}m_{pk}\mu_{pk}^2$. Since the system is in free fall, there is no potential energy; hence, the total energy is L=KE. The equation of motion can be expressed in Lagrangian form as

$\frac{d}{dt} \left(\frac{\partial L}{\partial \dot{\tau}_{pk}} \right) - \frac{\partial L}{\partial \tau_{pk}} = 0$. Assuming τ_{pk} and $\dot{\tau}_{pk}$ as small quantities we get

$$\ddot{\tau}_{pk} + \frac{\dot{U}}{L_{pk}} \tau_{pk} = -\frac{1}{L_{pk}} [\dot{W} - UQ - \dot{Q}(l_{pk} - L_{pk})] \quad (3.4)$$

where, $\frac{\dot{U}}{L_{pk}} = \omega_{pk}^2$, $W = W_0 + w$, $U = U_0 + u$, $Q = Q_0 + q$

Here, U_0, W_0, Q_0 are the steady state values of U, W, Q and u, w, q are the perturbation values and $\dot{U}_0, \dot{W}_0, \dot{Q}_0$ are zero. After subtracting the steady components, the perturbed equation in pitch plane can be written as

$$\ddot{\tau}_{pk} + \omega_{pk}^2 \tau_{pk} = \frac{1}{L_{pk}} [U_0 \dot{\theta} - \dot{w} + \ddot{\theta}(l_{pk} - L_{pk})] \quad (3.5)$$

3.2.2 Flexibility Dynamics

The launch vehicle in ascent flight can be considered as a free-free beam. The schematic diagram of the flexible SLV in the pitch plane is given in Fig. 3.3.

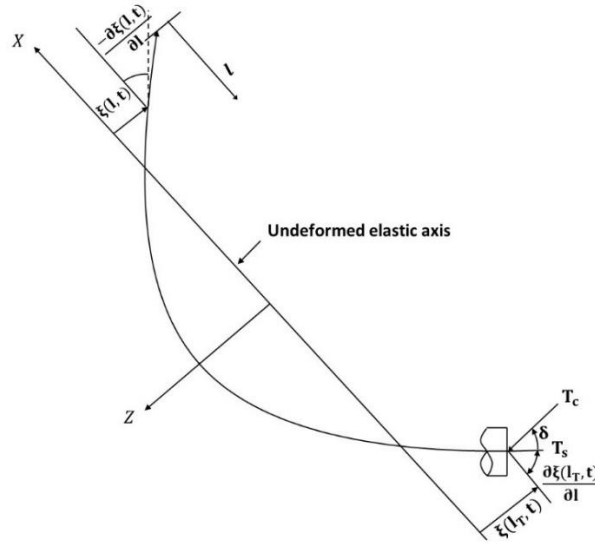


Figure 3.3 Flexible SLV in Pitch Plane

The forced vibration of a free-free beam model can be expressed mathematically by Euler-Bernoulli beam model. Detailed derivations for the Euler-Bernoulli model and forced vibrations of nonuniform beam can be found in [4][5][66]. Neglecting shear and rotational inertia,

$$m(l) \frac{\partial^2 \xi(l, t)}{\partial t^2} + \frac{\partial^2}{\partial l^2} \left[EI(l) \frac{\partial^2 \xi(l, t)}{\partial l^2} \right] = T(t) \delta \quad (3.6)$$

where, m is mass per unit length, EI is the bending stiffness and ξ is beam deflection. In the case of free vibration, right hand side of (3.6) will be zero. For free-free case, the bending moment $\frac{\partial^3 \xi}{\partial l^3}$ and shear $\frac{\partial^2 \xi}{\partial l^2}$ is zero at the ends of the beam, boundary conditions can be written as

$$\begin{aligned}\frac{\partial^2 \xi(0, t)}{\partial l^2} &= \frac{\partial^2 \xi(L, t)}{\partial l^2} = 0 \\ \frac{\partial^3 \xi(0, t)}{\partial l^3} &= \frac{\partial^3 \xi(L, t)}{\partial l^3} = 0\end{aligned}\quad (3.7)$$

Assume that the solution to (3.6) can be written as

$$\xi(l, t) = q_i(t)\varphi_i(l) \quad (3.8)$$

where, $\varphi_i(l)$ represents the shape of i^{th} natural vibration mode and $q_i(t)$ is the modal coordinate (normal coordinate or generalised coordinate) of this mode. Substituting (3.8) in (3.6) we get

$$-\frac{1}{q_i(t)} \frac{d^2 q_i(t)}{dt^2} = \frac{d^2}{dl^2} \left[EI(l) \frac{d^2 \varphi_i(l)}{dl^2} \right] \quad (3.9)$$

The term on the left side is a function of time only and that on the right side is a function of length. This can be true only if they are equal to some constant, say ω^2 where ω is the vibration frequency. Thus, the partial differential equation in (3.6) can be written as two ordinary differential equations.

$$\frac{d^2 q_i(t)}{dt^2} + \omega^2 q_i(t) = 0 \quad (3.10)$$

$$\frac{d^2}{dl^2} \left[EI(l) \frac{d^2 \varphi_i(l)}{dl^2} \right] - \omega^2 m(l) \varphi_i(l) = 0 \quad (3.11)$$

Numerical methods are used to get the solutions of (3.10) and (3.11) to get the frequencies and mode shapes of various modes to get the complete solution which can be written as

$$\xi(l, t) = \sum_{i=1}^{\infty} q_i(t) \varphi_i(l) \quad (3.12)$$

We have

$$\frac{\partial \xi(l, t)}{\partial l} = - \sum_{i=1}^{\infty} q_i(t) \sigma_i(l) \quad (3.13)$$

where, $\sigma_i(l) = \frac{\partial \varphi_i(l)}{\partial l}$ is called the normalised mode slope of the i^{th} bending mode.

The generalised coordinate satisfies

$$\ddot{q}_i + 2\zeta_i \omega_i \dot{q}_i + \omega_i^2 q_i = \frac{Q_i(t)}{M_i} \quad (3.14)$$

ζ_i is the damping ratio, $Q_i(t)$ is the generalised force and M_i is the generalised mass of the i^{th} bending mode which are defined as

$$Q_i(t) = \int_0^L \sum F \varphi_i(l) dl \quad (3.15)$$

$$M_i = \int_0^L m(\varphi_i(l))^2 dl$$

The model of the flexible SLV with slosh dynamics can now be written. Assuming $\alpha \approx \theta$,

$$\ddot{\theta} = \mu_\alpha \theta - \mu_p \tau_p - \frac{T_c(l_c \sigma_{lt} + \varphi_{lt})}{I} q + \mu_c \delta$$

$$\dot{\tau}_p = \frac{\left(\frac{L_\alpha}{m_0} + (l_p - L_p) \mu_\alpha\right) \theta}{L_p}$$

$$- \left(\frac{1}{L_p}\right) \left(\left(1 + \frac{m_p}{m_0}\right) \dot{u}_0 + (l_p - L_p) \mu_p \right) \tau_p$$

$$- 2\zeta_p \omega_p \dot{\tau}_p \quad (3.16)$$

$$+ \left(\frac{1}{L_p}\right) \left(\frac{T_c \sigma_{lt}}{m_0} - \frac{(l_p - L_p) T_c (l_c \sigma_{lt} + \varphi_{lt})}{I} \right) q$$

$$- \left(\frac{1}{L_p}\right) \left(\frac{T_c}{m_0} - (l_p - L_p) \mu_c \right) \delta$$

$$\ddot{q} = (-\omega^2 + T_c \sigma_{lt} \varphi_{lt} / M) q - 2\xi_q \omega \dot{q} - (T_c \varphi / M) \delta$$

where, $\mu_\alpha = \frac{L_\alpha l_\alpha}{I}$, $\mu_c = \frac{T_c l_c}{I}$, $\mu_p = \frac{m_p l_p \dot{u}_0}{I}$. Here the moment of inertia (I), thrust (T_c), control moment arm (l_c), aerodynamic force (L_α) and moment arm (l_α) are time varying and hence the parameters μ_c , μ_α and μ_p are time varying. Flexibility parameters also vary with time. The dynamical equations (3.16) can be presented in state space form as

$$\begin{aligned} \dot{x}_p &= A_p x_p + B_p u \\ Y_p &= C_p x_p + D_p u \end{aligned} \quad (3.17)$$

x_p are the states θ , $\dot{\theta}$, τ_p , $\dot{\tau}_p$, q , \dot{q} and u is the control input (δ).

$$A_p = \begin{bmatrix} A_{p11} & A_{p12} & A_{p13} & A_{p14} & A_{p15} & A_{p16} \\ A_{p21} & A_{p22} & A_{p23} & A_{p24} & A_{p25} & A_{p26} \\ A_{p31} & A_{p32} & A_{p33} & A_{p34} & A_{p35} & A_{p36} \\ A_{p41} & A_{p42} & A_{p43} & A_{p44} & A_{p45} & A_{p46} \\ A_{p51} & A_{p52} & A_{p53} & A_{p54} & A_{p55} & A_{p56} \\ A_{p61} & A_{p62} & A_{p63} & A_{p64} & A_{p65} & A_{p66} \end{bmatrix}$$

where, $A_{p12} = 1$, $A_{p21} = \mu_\alpha$, $A_{p23} = -\mu_p$, $A_{p25} = -\frac{T_c(l_c \sigma_{lt} + \varphi_{lt})}{I}$, $A_{p34} = 1$,

$$A_{p41} = \frac{\left(\frac{L_\alpha}{m_0} + (l_p - L_p) \mu_\alpha\right)}{L_p}, A_{p43} = -\left(\frac{1}{L_p}\right) \left(\left(1 + \frac{m_p}{m_0}\right) \dot{u}_0 + (l_p - L_p) \mu_p \right),$$

$$A_{p44} = -2\xi_p \omega_p, A_{p45} = \left(\frac{1}{L_p}\right) \left(\frac{T_c \sigma_{lt}}{m_0} - \frac{(l_p - L_p) T_c (l_c \sigma_{lt} + \varphi_{lt})}{I} \right), A_{p56} = 1,$$

$$A_{p65} = (-\omega^2 + T_c \sigma_{lt} \varphi_{lt} / M), A_{p66} = -2\xi_q \omega$$

where, φ_{lt} and σ_{lt} is the mode shape and slope at the thrust acting location.

All other A_{pij} are zeros.

$$B_p = [B_{p1} \quad B_{p2} \quad B_{p3} \quad B_{p4} \quad B_{p5} \quad B_{p6}]^T$$

$$B_{p2} = \mu_c, B_{p4} = \left(\frac{T_c}{m_0} - (l_p - L_p) \mu_c\right), B_{p6} = -(T_c \varphi_{lt} / M)$$

All other B_{pi} are zeros

$$C_p = \begin{bmatrix} 1 & 0 & 0 & 0 & \sigma_{pos} & 0 \\ 0 & 1 & 0 & 0 & 0 & \sigma_r \end{bmatrix}$$

$$D_p = \begin{bmatrix} 0 \\ 0 \end{bmatrix}$$

where, σ_{pos} is the mode slope of the first bending mode at the position sensor location and σ_r is the slope at the rate sensor location.

3.3 Proposed Adaptive Controller Design

A Lyapunov based MRAC is developed in chapter 2 for the rigid body dynamics of an SLV using a quadratic Lyapunov function. It is proven that the stability of the system and convergence of the tracking error to zero using Barbalat's Lemma. Also, the robustness of the controller for parametric uncertainty is demonstrated using extensive simulation studies. To solve the state feedback output regulation problem for a generic class of MIMO uncertain dynamical systems, a generalized MIMO plant model with matched nonlinear uncertainty and bounded environmental disturbance is presented below.

$$\begin{aligned}\dot{x} &= Ax + B\Lambda(u + \theta^T \Phi(x)) + B_m u_c + \xi(t) \\ y_p &= Cx\end{aligned}\tag{3.18}$$

where, $\xi(t) \in R^n$ is a uniformly bounded time-dependent disturbance such that $\|\xi(t)\| \leq \xi_{max}$. The upper bound $\xi_{max} \geq 0$ is known. $\Lambda \in R^{m \times m}$ is a diagonal positive-definite matrix which is used to simulate the control failures and increase in control gain and $\theta \in R^{N \times m}$. $x \in R^n$ is the system state vector and $u \in R^m$ is the control input. u_c is the command to be tracked. The pair $(A, B\Lambda)$ is controllable. $\theta^T \Phi(x) \in R^m$ is the linear-in-parameter state-dependent matched uncertainty, $\theta \in R^{N \times m}$ is the matrix of unknown constant parameters, $\Phi(x) \in R^N$ is the known N-dimensional regressor vector whose components are locally Lipschitz-continuous functions of x . Also $B \in R^{N \times m}$ is known and $A \in R^{n \times n}$ is unknown. The control goal is to force the system regulated output $y_p \in R^{m \times 1}$ to track any bounded time-varying reference signal $u_c \in R^{m \times 1}$, with bounded errors and in the presence of constant parametric uncertainties A, Λ, θ and bounded uncertainty $\xi(t)$. We shall also require that the rest of the signals in the corresponding closed-loop system remain uniformly bounded in time. The MRAC system is designed to enable tracking of the reference model output. The model is as follows

$$\begin{aligned}\dot{x}_m &= A_m x_m + B_m u_C \\ y_m &= C_m x_m\end{aligned}\tag{3.19}$$

To derive the control law, it is assumed that there exists a gain matrix K_x which satisfies the matching condition. Given a reference Hurwitz matrix A_m and an unknown positive diagonal matrix Λ , there exists a constant unknown matrix $K_x \in R^{n \times m}$ such that $A_m = A + B\Lambda K_x^T$. Using this we can write the open-loop extended system dynamics in the form

$$\dot{x} = A_m x + B\Lambda \left(u - K_x^T x + \theta^T \Phi(x) \right) + B_m u_C + \xi(t)\tag{3.18A}$$

Absorbing the uncertain $K_x^T x$ in the uncertainty $\theta^T \Phi(x)$, we can write the generic open loop plant as

$$\dot{x} = A_m x + B\Lambda \left(u + \theta^T \Phi(x) \right) + B_m u_C + \xi(t)\tag{3.18B}$$

A full state feedback control law is chosen to make the system output follow the reference output in the presence of system parametric uncertainties while maintaining all other signals uniformly bounded. The control law is

$$u = \hat{\theta}^T \Phi(x)\tag{3.20}$$

where, $\hat{\theta} \in R^{N \times m}$ are the adaptive parameters to be found out. Substituting (3.20) in (3.18B), we get

$$\begin{aligned}\dot{x} &= A_m x + B\Lambda \left(-((\hat{\theta}^T - \theta^T) \Phi(x)) \right) + B_m u_C + \xi(t) \\ &= A_m x - B\Lambda \Delta \theta^T \Phi(x) + B_m u_C + \xi(t)\end{aligned}\tag{3.21}$$

where, $\Delta \theta = \hat{\theta} - \theta$ is the parameter estimation error. Let the tracking error be defined as

$$e = x - x_m\tag{3.22}$$

The tracking error dynamics can be written as

$$\dot{e} = A_m e - B\Lambda \Delta \theta^T \Phi(x) + \xi(t)\tag{3.23}$$

The quadratic Lyapunov function chosen is

$$V(e, \Delta\theta) = e^T P e + \text{trace}(\Delta\theta^T \Gamma^{-1} \Delta\theta \Lambda) \quad (3.24)$$

where, Γ is positive and are the constant adaptation rates. P is a positive-definite matrix and is the solution of the algebraic Lyapunov equation. Differentiating V along the trajectories of (3.23) and using (2.22), we get

$$\begin{aligned} \dot{V}(e, \Delta\theta) = & -e^T Q e + 2\text{trace}(\Delta\theta^T \{\Gamma^{-1} \dot{\hat{\theta}} - \Phi(x) e^T P B\} \Lambda) \\ & + 2e^T P \xi(t) \end{aligned} \quad (3.25)$$

The adaptive law chosen was to make $\dot{V}(e, \Delta\theta)$ negative semi-definite, that is

$$\dot{\hat{\theta}} = \Gamma \Phi(x) e^T P B \quad (3.26)$$

This adaptation law will make [82][83]

$$\begin{aligned} \dot{V}(e, \Delta\theta) = & -e^T Q e + 2e^T P \xi(t) \\ \leq & -\lambda_{\min}(Q) \|e\|^2 + 2\|e\| \lambda_{\max}(P) \xi_{\max} \end{aligned} \quad (3.27)$$

Hence, $\dot{V}(e, \Delta\theta) < 0$ outside of the set E_0 which is defined as

$$E_0 = \{(e, \Delta\theta): \|e\| \leq 2 \frac{\lambda_{\max}(P)}{\lambda_{\min}(Q)} \xi_{\max} = e_0\} \quad (3.28)$$

Derivation of these inequalities is given in Appendix A.6

Theorem 3.1:

Lyapunov-like theorem to show the uniform boundedness and ultimate boundedness [3][67][68]. Consider the system

$$\dot{x} = f(t, x) \quad (3.29)$$

where, $f: [0, \infty) \times D \rightarrow R^n$ is piecewise continuous in t and locally Lipschitz in x , $D \subset R^n$ is a domain that contains the origin. Let $V: [0, \infty) \times D \rightarrow R$ be a continuously differentiable function such that

$$\begin{aligned}\alpha_1(\|x\|) &\leq V(t, x) \leq \alpha_2(\|x\|) \\ \frac{\partial V}{\partial t} + \frac{\partial V}{\partial x} f(t, x) &\leq -W_3(x) \quad \forall \|x\| \geq \mu > 0\end{aligned}\tag{3.30}$$

$\forall t \geq 0$ and $\forall x \in D$, where α_1, α_2 are class \mathcal{K} functions and $W_3(x)$ is a continuous positive definite function. Take $r > 0$ such that $B_r \subset D$ and suppose that $\mu < \alpha_2^{-1}(\alpha_1(r))$. Then, there exists a class \mathcal{KL} function β and for every initial state $x(t_0)$, satisfying $\|x(t_0)\| \leq \alpha_2^{-1}(\alpha_1(r))$, there is $T \geq 0$ (dependent on $x(t_0)$ and μ) such that the solution of (3.29) satisfies

$$\begin{aligned}\|x(t)\| &\leq \beta(\|x(t_0)\|, t - t_0), \quad \forall t_0 \leq t \leq t_0 + T \\ \|x(t)\| &\leq \alpha_1^{-1}(\alpha_2(\mu)), \quad \forall t \geq t_0 + T\end{aligned}\tag{3.31}$$

If $D = R^n$ and α_1 belongs to class \mathcal{K}_∞ and (3.31) hold for any initial state $x(t_0)$, with no restriction on how large μ is.

According to the theorem 3.1, trajectories of $e(t)$ defined by the dynamics (3.23) enter a compact set $(\Omega_0 \supset E_0) \subset R^n$ in finite time and will remain there for all future time. However, Ω_0 is not compact in the $(e, \Delta\theta)$ space and is unbounded since the parameter estimation errors are not restricted. Hence, inside Ω_0 , \dot{V} can become positive and the parameter estimation errors $(\Delta\theta)$ builds up even though the tracking error norm remains at finite at all times. This phenomenon is known as parameter drift; hence, the adaptive control law defined in (3.26) is not robust to bounded disturbances and unmodelled dynamics.

Many design modifications are proposed in the literature to make the adaptation law robust to bounded disturbances. In this chapter, we propose to use projection operators and BLF to make the MRAC robust to both parametric and non-parametric uncertainties.

3.3.1 Modified Control Parameter Update Law Using Projection Operator

Let the plant model be defined by (3.18) and the reference model by (3.19). Let the Lyapunov function be as in (3.24) and its time derivative be (3.25). The design task is to choose $\hat{\theta}$ such that the trace term in (3.25) became nonpositive while the adapted parameters $\hat{\theta}$ remained uniformly bounded functions of time. Let

$f(x): R^n \rightarrow R$ be a differentiable convex function, select a constant $\delta > 0$ and consider the subset $\Omega_\delta = \{\theta \in R^n | f(\theta) \leq \delta\} \subset R^n$, Ω_δ is a convex set. Projection operator [3] is defined as

$$\begin{aligned} & Proj(\theta, y) \\ &= \begin{cases} y - \frac{\Gamma \nabla f(\theta) (\nabla f(\theta))^T}{\|\nabla f(\theta)\|_\Gamma^2} y f, & \text{if } f(\theta) \geq 0 \wedge y^T \nabla f(\theta) > 0 \\ y, & \text{if not} \end{cases} \end{aligned} \quad (3.32)$$

where, $\Gamma \in R^{n \times n}$ is any constant symmetric positive definite matrix and $\|\nabla f(\theta)\|_\Gamma^2 = \nabla f^T \Gamma \nabla f$ is the weighted Euclidean squared norm of ∇f . In order to derive the adaptive control law, we make use of the important convex property of the projection operator given in Lemma 3.1.

Lemma 3.1: For any symmetric positive-definite matrix $\Gamma \in R^{n \times n}$,

$$(\theta - \theta^*)^T (\Gamma^{-1} Proj(\theta, \Gamma y) - y) \leq 0 \quad (3.33)$$

Proof of Lemma 3.1 is given in Appendix A.3. Another result which is of conceptual importance is stated in Lemma 3.2. This is also used in the development of the adaptive controllers.

Lemma 3.2: Let $f(\theta)$ be a convex continuously differentiable map from $R^n \rightarrow R$. Using the projection operator given in (3.32), consider the n -dimensional dynamics

$$\dot{\theta} = Proj(\theta, y) \quad (3.34)$$

where, $\theta \in R^n$ is the system state and $y \in R^n$ is a time-varying piecewise continuous vector. Then starting from any initial condition $\theta(0) = \theta_0$ within the set

$$\Omega_0 = \{\theta \in R^n | f(\theta) \leq 0\} \quad (3.35)$$

the system trajectory $\theta(t)$ will remain in the set

$$\Omega_1 = \{\theta \in R^n | f(\theta) \leq 1\} \quad (3.36)$$

for all $t \geq 0$

Proof of Lemma 3.2 is given in Appendix A.3.

The trace term in (3.25) can be written as

$$\begin{aligned} & \text{trace}(\Delta\theta^T \{\Gamma^{-1}\dot{\hat{\theta}} - \Phi(x)e^T PB\}\Lambda) \\ &= \sum_{i=0}^n (\hat{\theta} - \theta)^T_i \{\Gamma^{-1}\dot{\hat{\theta}} - \Phi(x)e^T PB\}\lambda_j \end{aligned} \quad (3.37)$$

Selecting the adaptation law as

$$\dot{\hat{\theta}} = \text{Proj}(\hat{\theta}, \Gamma\Phi(x)e^T PB) \quad (3.38)$$

Substituting (3.38) in (3.37) and putting $\Phi(x)e^T PB = Y$, we get

$$\begin{aligned} & \text{trace}(\Delta\theta^T \{\Gamma^{-1}\dot{\hat{\theta}} - \Phi(x)e^T PB\}\Lambda) \\ &= \sum_{i=0}^n (\hat{\theta} - \theta)^T_i (\Gamma^{-1}\text{Proj}(\hat{\theta}, \Gamma Y_j) - Y_j)\lambda_j \leq 0 \end{aligned} \quad (3.39)$$

$(\hat{\theta} - \theta)^T_i (\Gamma^{-1}\text{Proj}(\hat{\theta}, \Gamma Y_j) - Y_j) \leq 0$, $\lambda_j \geq 0$, and hence the trace term will be negative semidefinite.

$$\begin{aligned} \dot{V}(e, \Delta\theta) &= -e^T Q e + 2e^T P \xi(t) \\ &\leq -\lambda_{\min}(Q)\|e\|^2 + 2\|e\|\lambda_{\max}(P)\xi_{\max} \\ &= -\lambda_{\min}(Q)\|e\| \left(\|e\| - 2\frac{\lambda_{\max}(P)\xi_{\max}}{\lambda_{\min}(Q)} \right) \end{aligned} \quad (3.40)$$

$\dot{V}(e, \Delta\theta) < 0$ outside of the compact set

$$\begin{aligned} \Omega &= \left\{ (e, \Delta\theta) \in R^n \times R^{N \times m}: \|e\| \right. \\ &\quad \left. \leq 2\frac{\lambda_{\max}(P)}{\lambda_{\min}(Q)}\xi_{\max} \wedge \|\Delta\theta\|_F \leq \Delta\theta_{\max} \right\} \end{aligned} \quad (3.41)$$

$$\Delta\theta_{\max} = 2(\theta_1^{\max} \dots \theta_m^{\max}) = 2\theta_{\max}$$

where, θ_j^{\max} is the maximum allowable bound for the j^{th} column of θ . Hence all the signals of the closed loop system are uniformly ultimately bounded with this

adaptation law allowing the closed loop system to track the reference command with errors bounded as in (3.41).

A dead zone modification is applied on the tracking error e to make it more robust to bounded disturbance. Here the adaptation is stopped when the tracking error falls below the dead zone boundary. A continuous form of dead zone proposed in [69] is used. A Lipschitz-continuous modulation function in the form

$$\mu(\|e\|) = \max \left(0, \left(\min \left(1, \frac{\|e\| - \delta e_0}{(1 - \delta)e_0} \right) \right) \right) \quad (3.42)$$

where, $0 < \delta < 1$. Adaptive control law with continuous form of dead zone is

$$\dot{\hat{\theta}} = Proj(\hat{\theta}, \Gamma \Phi(x) \mu(\|e\|) e^T P B) \quad (3.43)$$

The projection operator ensures that the adaptive time-varying matrix $\hat{\theta}(t)$ do not exceed their pre-specified bounds (θ^{max}) and also ensures the negative semi-definiteness of the time derivative of the Lyapunov function. This is achieved by defining the convex function $f(\theta)$ in terms of the maximum upper bound of the adapted parameters (θ^{max}). This gives Uniform Ultimate Boundedness (UUB) of adapted parameters. For the launch vehicle attitude control problem, the convex function is defined as

$$f(\hat{\theta}) = \frac{(1 + \varepsilon_1) \|\theta\|^2 - (\theta_{max})^2}{\varepsilon_1 (\theta_{max})^2} \quad (3.44)$$

where, $\varepsilon_1 > 0$. The two convex sets can be defined as

$$\begin{aligned} \Omega_0 &= \{\theta: \in R^n | f(\theta) \leq 0\} = \left\{ \theta: \|\theta\| \leq \frac{\theta^{max}}{\sqrt{1 + \varepsilon_1}} \right\} \\ \Omega_1 &= \{\theta: \in R^n | f(\theta) \leq 1\} = \{\theta: \|\theta\| \leq \theta^{max}\} \end{aligned} \quad (3.45)$$

In the launch vehicle control problem, the gains are modified adaptively to get the required stability and performance. The bounds are selected in such a way that stability is maintained during the atmospheric phase of the flight.

Remark 1: Modification of the adaptation laws using projection operator ensures boundedness of the tracking error. Here the bounds on the adapted gains can be

specified in the convex function but the bounds on the tracking error cannot be specified.

Remark 2: In aerospace vehicles, both the gain margin and gain reduction margins are important. Hence the gains need to be limited within a maximum and minimum bound for certain applications. In such scenarios, the projection operator defined in (3.32) cannot be used as the convex function in (3.44) defined to constrain the gains lose its convexity when both minimum and maximum values of gains are specified.

3.3.2 Modified Control Parameter Update Law using BLF

Modification of the update mechanism using projection operator and quadratic Lyapunov functions ensures boundedness of the tracking error. Here the bounds on the adapted gains can be specified in the convex function but the bounds on the tracking error cannot be specified. For complex systems, it is very difficult to find out an explicit relation between the trajectory tracking error and the solution of the Lyapunov equation underlying the adaptive law. Hence BLF [30][31][32] is introduced to guarantee the boundedness of tracking error and adapted gains within the defined constraints. To establish the asymptotic convergence of the signals, the continuity properties of the derivative of the Lyapunov function can be analyzed using Barbalat's Lemma. This section explains the adaptive control strategy which constrains the tracking error and the deviations of the controller gains from the ideal control gains which satisfy the matching conditions.

Definition: A BLF is a scalar function $V(x)$, defined with respect to the system $\dot{x} = f(x)$ on an open region D containing the origin; that is continuous, positive definite, has continuous first-order partial derivatives at every point of D , has the property $V(x) \rightarrow \infty$ as x approaches the boundary of D , and satisfies condition: $\exists M, \forall t > 0 V(x(t)) < M$ along any system trajectory starting inside D .

Usually, it is assumed that D is a hyper-rectangle defined by $D = \{x: |x_i| \leq \Delta_{x_i}\}$.

Consider the plant dynamics

$$\dot{x} = Ax + B\Lambda(u + \Theta^T \Phi(x)) \quad (3.46)$$

$x \in R^n$, $u \in R^m$, $\theta \in R^{n \times m}$, $A \in R^{n \times n}$ is unstable, $B \in R^{n \times m}$, the pair (A, B) is controllable. $\Phi: D \rightarrow R^N$ is the regressor vector which is Lipschitz continuous. The term $\theta^T \Phi(x)$ captures both parametric and matched uncertainties. The MRAC system is designed to enable tracking of the reference model output. The model is as given in (3.19). Let the feedback control law be

$$u = K * [x^T \ u_c^T - \Phi(x)]^T = K\pi(t) \quad (3.47)$$

where $K = [K_x^T \ K_u^T - \theta^T]$ and $\pi(t) = [x^T(t), u_c^T(t), -\Phi^T(x)]^T$. The matching conditions are

$$\begin{aligned} A_m &= A + BK_x^T \\ B_m &= BK_u^T \end{aligned} \quad (3.48)$$

where, K is the ideal gain which satisfy the matching condition which cannot be found out as the plant parameters are uncertain. Hence, we have to find some estimates (K_e) of the ideal gain so that the control law (3.47) can be implemented. We want to get an accurate estimate of the ideal gains such that $\|K_e - K\|_F < \varepsilon$ where, ε is a small number. Let $e(t) = x(t) - x_m(t)$ is the trajectory tracking error and $\Delta K(t) = \widehat{K}(t) - K_e$ is the estimated adaptive gain's error and $\widetilde{\Delta K}(t) = \widehat{K}(t) - K$ is the adaptive gains error. Consider a compact, connected constraint set

$$C \triangleq \{(e, \Delta K) \in \mathbb{R}^n \times \mathbb{R}^{m \times (n+m+N)}: f(e^T M e, \Delta K \Gamma^{-1} \Delta K^T) \geq 0\} \quad (3.49)$$

where M and Γ are symmetric and positive-definite. This set captures the user defined constraints on the trajectory tracking error and the estimated adaptive gains' error. $f(e^T M e, \Delta K \Gamma^{-1} \Delta K^T)$ is continuously differentiable and such that $f(0,0) > 0$. The function f should be designed in such a way that it's derivative with respect to $e^T M e$ named as (f_e) and $\Delta K \Gamma^{-1} \Delta K^T$ named as (f_K) is negative definite for all $(e, \Delta K)$ inside the set C . A candidate function for this problem is

$$f(e^T M e, \Delta K \Gamma^{-1} \Delta K^T) = f_{max} - e^T M e - \Delta K \Gamma^{-1} \Delta K^T \quad (3.50)$$

Here f_{max} is selected as a positive number and $f_e = -1$ and $f_K = -I_m$. Using the control law (3.47), the tracking error dynamics can be written as

$$\begin{aligned}
\dot{e}(t) &= A_m e(t) + B \widetilde{\Delta K}(t) \pi(t) \\
e(t_0) &= x_0 - x_{m0}, \widetilde{\Delta K}(t) = \widehat{K}(t) - K, t > t_0, \\
\pi(t) &= [x^T(t), u_c^T(t), -\Phi^T(x)]^T
\end{aligned} \tag{3.51}$$

The Lyapunov function can be selected as

$$V(e, \Delta K) = \frac{e^T P e + \text{tr}(\Delta K \Gamma^{-1} \Delta K^T)}{f(e^T M e, \Delta K \Gamma^{-1} \Delta K^T)}, (e, \Delta K) \text{ inside } \mathcal{C} \tag{3.52}$$

This Lyapunov function goes to infinity, when f is zero, ie. $e^T M e + \Delta K \Gamma^{-1} \Delta K^T = f_{max}$. But inside \mathcal{C} , the function f is always positive. Maximum value of $V(e, \Delta K)$ inside \mathcal{C} is obtained when the tracking error and the deviation of the adaptive gain from ideal is zero. A set of adaptive gains $\widehat{K}(t)$ to be found out which ensure the negative definiteness of the derivative of Lyapunov function and $(e(t), \Delta K(t))$ is always inside the constraint set \mathcal{C} .

$$\begin{aligned}
\dot{V}(e, \Delta K) &= f^{-2} \{ f \cdot (e^T P \dot{e} + \dot{e}^T P e \\
&\quad + \text{tr}(\Delta K^T \Gamma^{-1} \dot{\Delta K} + \dot{\Delta K}^T \Gamma^{-1} \Delta K) \\
&\quad - (e^T P e + \text{tr}(\Delta K \Gamma^{-1} \Delta K^T)) \cdot f_e (e^T M \dot{e} + \dot{e}^T M e) \\
&\quad + f_k (\Delta K^T \Gamma^{-1} \dot{\Delta K} + \dot{\Delta K}^T \Gamma^{-1} \Delta K) \}
\end{aligned} \tag{3.53}$$

$$\begin{aligned}
\dot{V}(e, \Delta K) &= f^{-1} [e^T \cdot (A_m^T (P - V f_e M) + (P - V f_e M) A_m) e \\
&\quad + \pi^T \widetilde{\Delta K}^T B^T (P - V f_e M) e \\
&\quad + e^T (P - V f_e M) B \widetilde{\Delta K} \pi + \text{tr}(\dot{\Delta K}^T \Gamma^{-1} \Delta K \\
&\quad + \Delta K^T \Gamma^{-1} \dot{\Delta K}) (I_m - V f_k)
\end{aligned} \tag{3.54}$$

Define another set

$$\begin{aligned}
G_{\alpha, \pi} &= \{ -\alpha e^T e \\
&\quad + 2\varepsilon \text{trace}((\pi e^T [P \\
&\quad - V f_e M] B) (\pi e^T [P - V f_e M] B))^T)^{1/2} \}
\end{aligned} \tag{3.55}$$

Since u_c is bounded and A_m is Hurwitz x_m is bounded. If $e(t)$ is bounded then $\pi(t) \in \Pi$ where Π is a compact set. If both $e(t)$ and ΔK are bounded then there exists an extremum value (π^*) given by

$$\begin{aligned} \pi^* = \operatorname{argmax} & [-\alpha e^T e \\ & + 2\varepsilon \operatorname{tr}((\pi e^T [P \\ & - V f_e M] B)(\pi e^T [P - V f_e M] B))^T)^{\frac{1}{2}}] \end{aligned} \quad (3.56)$$

The set G_{α, π^*} captures the set where the total derivative of the Lyapunov function given in (3.52) is not guaranteed to be negative-definite. Also, the set G_{α, π^*} captures the effect of not being able to determine exactly the K for enforcing satisfactory trajectory tracking defined by the user. Assume that there exists a symmetric positive definite matrix P and $Q \geq \alpha I_n$ where $\alpha > 0$, such that

$$\begin{aligned} -Q(e^T M e, \Delta K \Gamma^{-1} \Delta K^T) = A_m^T [P - V f_e M] + [P - V f_e M] A_m, \\ (e, \Delta K) \in \text{inside } \mathcal{C} \end{aligned} \quad (3.57)$$

If $e(0), \Delta K(0) \in C^0 \setminus \{0\}$ then the control parameter update law

$$\dot{\hat{K}}^T = -\Gamma \pi(t) e^T(t) [P - V f_e M] B \times [I_m - V f_k]^{-1} \quad (3.58)$$

The control law (3.47) with the parameter update law given in (3.58) ensures that if the set $G_{\alpha, \pi^*} \subset C^0$ then $e(t), \Delta K(t) \in C^0$ for $t \geq t_0$. The derivation of the control law is given in Appendix – A.4.

3.3.3 Stable Adaptive Controller Design in the Presence of Actuator Constraints

Input saturation or actuator saturation is a characteristic of all physical systems. In addition, the control designer also introduces additional saturation as part of control allocation or to improve the system transient responses. A linear system becomes nonlinear with the introduction of saturation. This will introduce null controllable regimes where no control strategy can bring the system to a particular equilibrium. The best we can achieve is to maximise the domain of attraction within the boundaries imposed by these null control domains. This is a problem for both adaptive and non-adaptive control systems. Several strategies are

available for non-adaptive systems to tackle these problems. These strategies can be extended to the proposed controllers. The techniques available in the literature to handle the input saturation for adaptive controllers are limited.

Adaptive controllers proposed in sections 3.3.1 and 3.3.2 do not consider the actuator constraints such as position and slew rate constraints. Assuring stability of the adaptive controllers in the presence of actuator constraints is a very challenging problem. Theoretically justified and verifiable conditions for stable adaptation should be derived and control design should try to avoid actuator saturation criteria. Several design solutions are proposed in the literature which includes modification of the adaptation gains of the control input, tracking error and reference model. The positive μ - modification described in [70] is modified for the adaptive PID controller to avoid actuator position and rate saturation. The actuator model used in this section considers both position and slew rate constraints. The system state equation is defined as

$$\dot{x}(t) = Ax(t) + b\lambda u(t), x \in R^n, u \in R \quad (3.59)$$

where, A is the unknown plant matrix, b is the known control direction and $\lambda > 0$ is unknown positive constant which can be used to simulate actuator failures. A second order actuator model can be written as

$$\ddot{\delta} + 2\xi\omega\dot{\delta} + \omega^2\delta = \omega^2\delta_c \quad (3.60)$$

where, δ is the actuator output, δ_c is the input, ω is the actuator bandwidth and ξ is actuator damping. $u(t)$ in (3.59) is the actuator position δ . Actuator model in (3.60) is written in state space as

$$\begin{pmatrix} \dot{\delta} \\ \ddot{\delta} \end{pmatrix} = \begin{pmatrix} 0 & 1 \\ -\omega^2 & -2\xi\omega \end{pmatrix} \begin{pmatrix} \delta \\ \dot{\delta} \end{pmatrix} + \begin{pmatrix} 0 \\ \omega^2 \end{pmatrix} \delta_c \quad (3.61)$$

In order to impose the position constraint ($\pm\delta_{max}$) and slew rate constraint ($\pm\dot{\delta}_{max}$), we shall use projection operator described in (3.32) and modify the actuator dynamics as follows.

$$\dot{x}_{act} = Proj(x_{act}, A_{act}x_{act} + B_{act}\delta_c) \quad (3.62)$$

where, $\dot{x}_{act} = \begin{pmatrix} \dot{\delta} \\ \ddot{\delta} \end{pmatrix}$, $x_{act} = \begin{pmatrix} \delta \\ \dot{\delta} \end{pmatrix}$, $A_{act} = \begin{pmatrix} 0 & 1 \\ -\omega^2 & -2\xi\omega \end{pmatrix}$, $B_{act} = \begin{pmatrix} 0 \\ \omega^2 \end{pmatrix}$

For this model, a convex function $f(x_{act})=f_{act}(\delta,\dot{\delta})$ which defines the projection operator can be selected as

$$f_{act}(\delta,\dot{\delta}) = \frac{(1 + \varepsilon) \left(\frac{\delta^2}{\delta_{max}^2} + \frac{\dot{\delta}^2}{\dot{\delta}_{max}^2} \right) - 1}{\varepsilon} \quad (3.63)$$

This leads to the following two convex sets

$$\begin{aligned} \Omega_0 &= \{f_{act}(\delta,\dot{\delta}) \leq 0\} = \left\{ |\delta| \leq \frac{\delta_{max}}{\sqrt{1 + \varepsilon}} \wedge |\dot{\delta}| \leq \frac{\dot{\delta}_{max}}{\sqrt{1 + \varepsilon}} \right\} \\ \Omega_1 &= \{f_{act}(\delta,\dot{\delta}) \leq 1\} = \{|\delta| \leq \delta_{max} \wedge |\dot{\delta}| \leq \dot{\delta}_{max}\} \end{aligned} \quad (3.64)$$

From Lemma 3.2, it can be asserted that starting from any initial conditions in Ω_0 which satisfies the bounds on slew rate and position, the actuator states will not leave Ω_1 . The ideal reference model state equation of the plant in (3.59) can be written as

$$\dot{x}_m^*(t) = A_m x_m^*(t) + b_m r(t), x_m^* \in R^n, r \in R \quad (3.65)$$

Control command deficiency is defined as $\Delta u_c = \delta - u_c$. Here δ is the slew rate limited and position limited output of the actuator. Adaptive control law can be written as

$$u_c = k_x^T x + \mu \Delta u_c = u_{lin} + \mu \Delta u_c \quad (3.66)$$

where, $u_{lin} = k_x^T x$ and $\mu \Delta u_c$ is the control deficiency feedback.

Adaptive control with μ -modification is given as a convex combination of u_{lin} and δ_{lin} . Here δ_{lin} is the output of the actuator model in (3.62) when u_{lin} is the input to the actuator model. u_c is defined as

$$u_c = \frac{1}{1 + \mu} (u_{lin} + \mu \delta_{lin}) \quad (3.67)$$

Here u_c is a convex combination of u_{lin} and δ_{lin} , i.e., the coefficients $(\frac{1}{1+\mu})$ and $(\frac{\mu}{1+\mu})$ are positive and is equal to 1 when added. Substituting (3.66) in (3.59) we get the closed-loop state equation as

$$\begin{aligned}\dot{x} &= Ax + b\lambda u_c + b\lambda(u - u_c) \text{ where, } \Delta u = u - u_c \\ &= Ax + b\lambda u_{lin} + b\lambda(\mu\Delta u_c + \Delta u) \text{ where, } \Delta u_{lin} = \mu\Delta u_c + \Delta u \\ &= (A + b\lambda k_x^T)x + b\lambda u_{lin} + b\lambda(\Delta u_{lin})\end{aligned}\quad (3.68)$$

In order to satisfy the matching criteria, the reference state equation is modified as

$$\begin{aligned}\dot{x}_m &= A_m x_m + b_m(r(t) + k_u \Delta u_{lin}) \\ A + b\lambda k_x^T &= A_m ; b\lambda = b_m k_u\end{aligned}\quad (3.69)$$

Tracking error and Parameter errors are defined as

$$e = x - x_m ; \Delta k_x = k_x - k_x^* ; \Delta k_u = k_u - k_u^* \quad (3.70)$$

Tracking error dynamics

$$\dot{e} = A_m e + b\lambda(\Delta k_x^T x - b_m \Delta k_u \Delta u_{lin}) \quad (3.71)$$

Lyapunov function is

$$V(e, \Delta k_x, \Delta k_u) = e^T P e + \lambda(\Delta k_x^T \Gamma_x^{-1} \Delta k_x + \gamma_u^{-1} \Delta k_u^2) \quad (3.72)$$

Adaptation laws are derived for stability as given below

$$\begin{aligned}\dot{k}_x &= -\Gamma_x x e^T P b \\ \dot{k}_u &= -\gamma_u \Delta u_{lin} e^T P b_m\end{aligned}\quad (3.73)$$

This control law ensures the convergence of tracking error while maintaining the actuator deflections within the safe limit.

3.4 State Estimation and Noise Filtering Using EKF

The proposed control laws use full state feedback. In the case of launch vehicles, only attitude and attitude rate measurements are available. The remaining

states are to be estimated from the available measurements which can be noisy as seen from the simulation results presented in section 2.4. It is observed that the white noise added to the rate outputs enters the control loop; hence, control signals and responses are noisy. This has to be suppressed as the noise in the control signals can excite high frequency dynamics such as slosh and flexibility. An Extended Kalman Filter (EKF) is proposed for state estimation and noise filtering [71]. It has the advantage that the perturbations include only the state estimation errors, which are generally smaller than the deviations from any pre-defined nominal trajectory; hence, the linear approximations are good but have larger computational effort. Plant and measurement models are given below:

$$\text{Plant:} \quad \dot{x}(t) = f(x(t), t) + w(t), \quad w(t) \sim \mathcal{N}(0, Q(t)) \quad (3.74)$$

$$\text{Measurement:} \quad z(t) = h(x(t), t) + v(t), \quad v(t) \sim \mathcal{N}(0, R(t)) \quad (3.75)$$

Plant noise:

$$\begin{aligned} E\langle w(t) \rangle &= 0 \\ E\langle w(t)w^T(s) \rangle &= \delta(t - s)Q(t) \end{aligned} \quad (3.76)$$

Measurement noise:

$$\begin{aligned} E\langle v(t) \rangle &= 0 \\ E\langle v(t)v^T(s) \rangle &= \delta(t - s)R(t) \end{aligned} \quad (3.77)$$

Differential equation of the state estimate is

$$\dot{\hat{x}}_k(t) = f(\hat{x}(t), t) + \bar{K}(t)[z(t) - \hat{z}(t)] \quad (3.78)$$

Predicted Measurement

$$\hat{z}(t) = h(\hat{x}(t), t) \quad (3.79)$$

Linear approximation equations

$$\begin{aligned} F^{[1]}(t) &\approx \left. \frac{\partial f(x, t)}{\partial x} \right|_{x=\hat{x}(t)} \\ H^{[1]}(t) &\approx \left. \frac{\partial h(x, t)}{\partial x} \right|_{x=\hat{x}(t)} \end{aligned} \quad (3.80)$$

Kalman Gain

$$\begin{aligned} \dot{P}(t) &= F^{[1]}(t)P(t) + P(t)F^{[1]T}(t) - \bar{K}(t)R(t)\bar{K}^T(t) \\ \bar{K}(t) &= P(t)H^{[1]}(t)R^{-1}(t) \end{aligned} \quad (3.81)$$

3.5 Results and Discussions

In this chapter, the rigid body model presented in chapter 2 is augmented with slosh and flexibility dynamics. The adaptive control law is modified using projection operator and BLF. These controllers demand full state information for feedback and these are estimated from available noisy measurements using an EKF.

The proposed adaptive control laws are tested in two simulation conditions and the results are compared with the controller using quadratic Lyapunov functions. First, the tracking capability is demonstrated using a ramp input. The launch vehicle will be experiencing ramp commands in response to wind shears. An open-loop guidance profile that is biased to a wind measured on the day of launch is used. The typical guidance profile is used to demonstrate the tracking capability and stability of the various dynamics that are excited due to the variations in the command profile.

To show the superiority of the proposed control parameter update laws (i) studies are conducted to demonstrate the robustness by perturbing the plant parameters within specified limits as well as beyond and (ii) to show the wind disturbance rejection capability and the stability of various dynamics, a synthetic wind profile is injected to the nominal and perturbed plant.

Three adaptive controllers are designed for a plant with slosh and flexibility and the resulting closed-loop plants are simulated with ramp and typical guidance commands. The plant is simulated from lift-off till 100 s. During the atmospheric phase of the flight, the purpose of the controller is to stabilise the vehicle dynamics and follow the guidance commands to reduce the load on the vehicle. Gaussian white noise is applied to the rate sensor output and a nonlinear second order actuator model is used in simulations.

The reference models are varied with respect to time. These models are selected in such a way that the plant stability is ensured in the sense of classical control stability margins [aero margin (gain reduction margin), phase margin and

gain margin]. The bandwidth for the reference model is selected in such a way that actuator saturation is avoided.

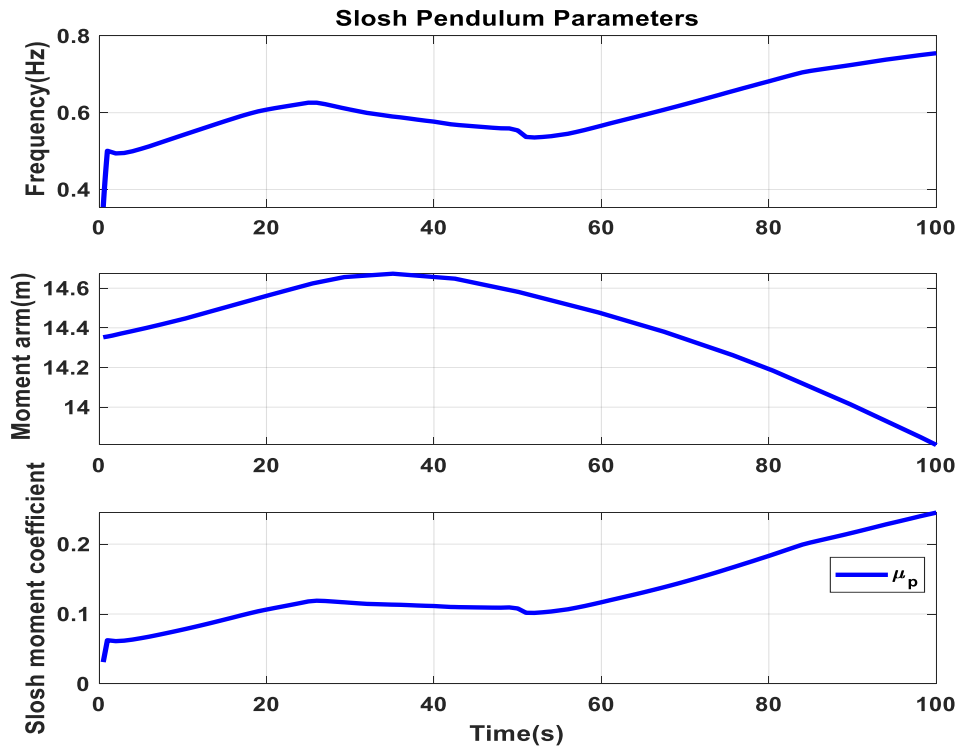


Figure 3.4 Slosh Parameter Variations

The plant parameters are varying with respect to time. Rigid body plant parameter and control parameter variations are already given in Chapter 2. Fig. 3.4 shows the slosh parameter (pendulum frequency, moment arm and moment coefficient) variations. The frequency of the slosh mode depends on the vehicle's acceleration and the slosh moment arm depends on the location of the hinge point of the pendulum with respect to the vehicle's center of gravity. Flexible mode frequency, generalised mass and mode shape are depending on the mass distribution and vary with respect to time.

3.5.1 Nominal Plant Simulated with a Ramp Command

In this case, nominal values of the plant parameters are considered and simulation is carried out for about 100 s. A ramp command is applied to the closed-loop plant. Fig. 3.5 and Fig. 3.6 show that attitude tracking is achieved in all three update algorithms with very low tracking error. In specific, the controller using BLF

responds to the ramp command with the least tracking error compared to the projection algorithm and quadratic Lyapunov functions.

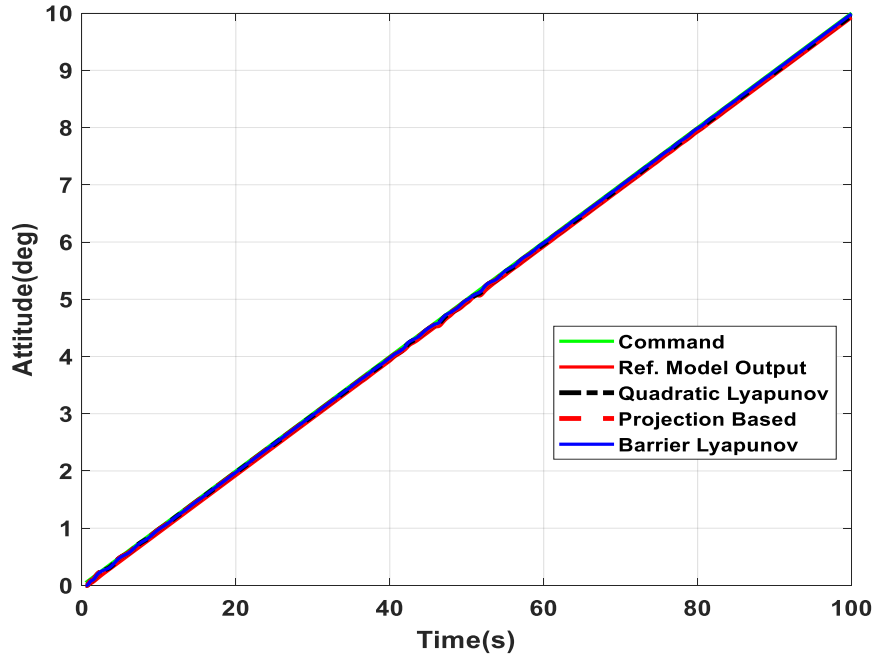


Figure 3.5 Attitude Tracking by Different Controllers with Ramp Command

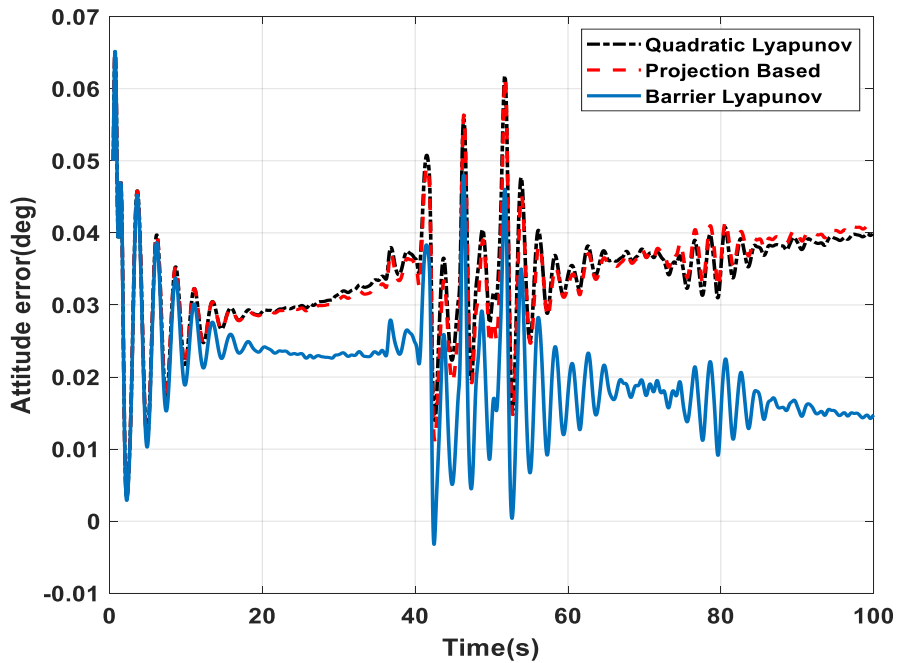


Figure 3.6 Attitude Tracking Error of Different Controllers with Ramp Command

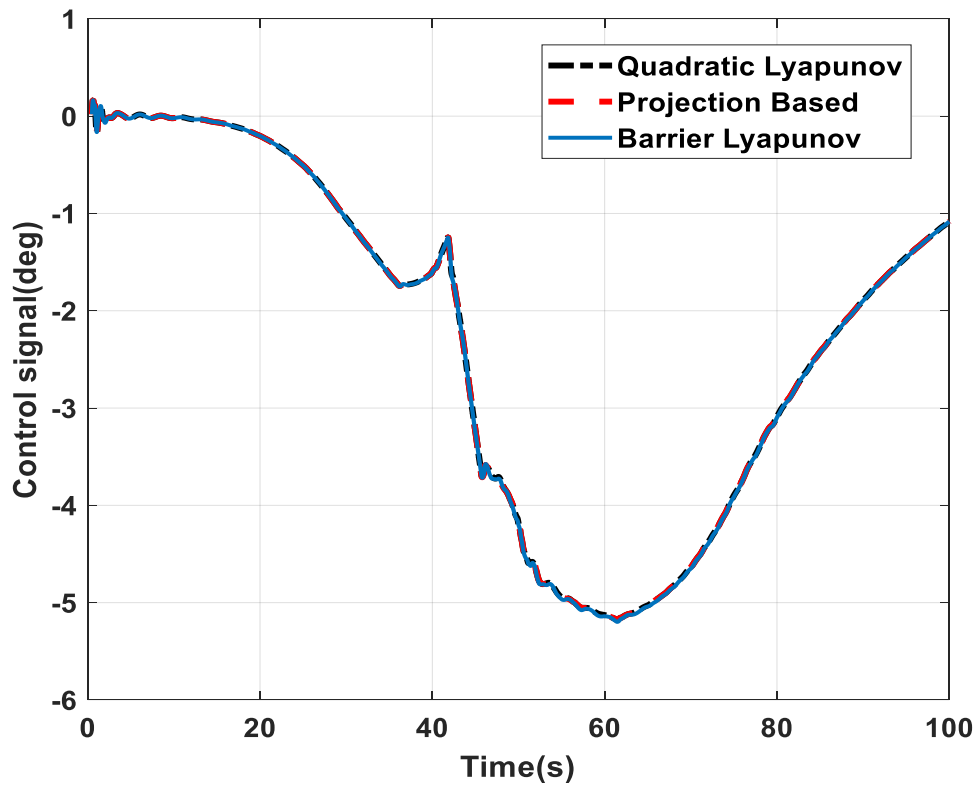


Figure 3. 7 Control Responses of Different Controllers for Ramp Command

Slosh and flexibility effects are not seen as significant in all the controller responses as shown in Fig. 3.7. This indicates that there is less interaction between control-structure and slosh dynamics. In general, slosh and flexible modes are excited whenever some excitations are in the command or some excursions are in the plant parameters. From Fig. 3.8, it is evident that the various modes excited are damped out; hence, the closed-loop stability is achieved for all modes. Fig. 3.9 shows the noisy rate output measured by the sensor, the actual rate from simulations and the rate estimated by EKF. It can be seen that the EKF gives a very accurate estimate of the original state from the noisy measurement.

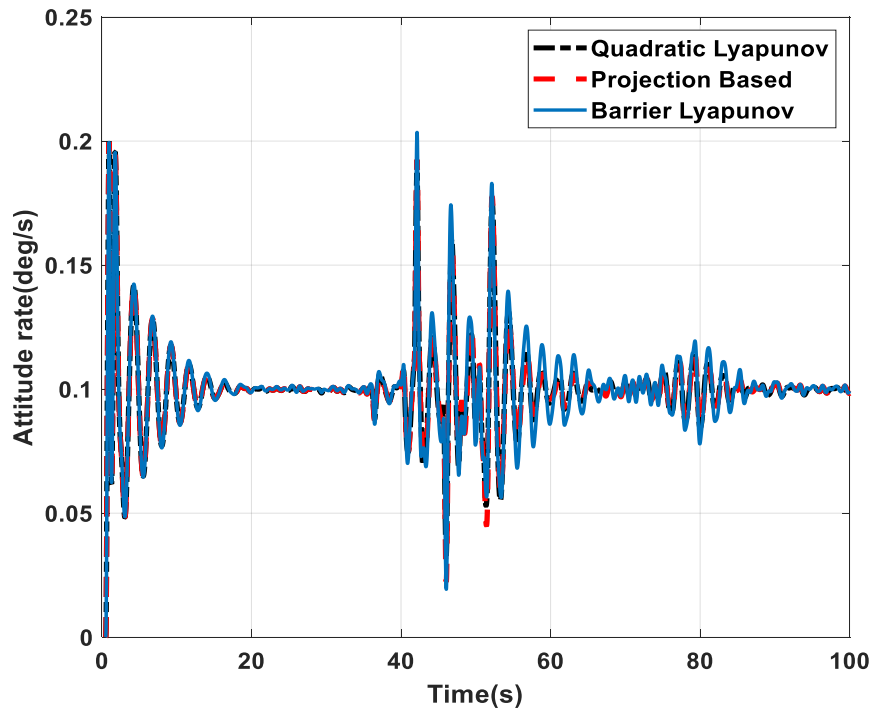


Figure 3. 8 Attitude Rate for Ramp Command Tracking

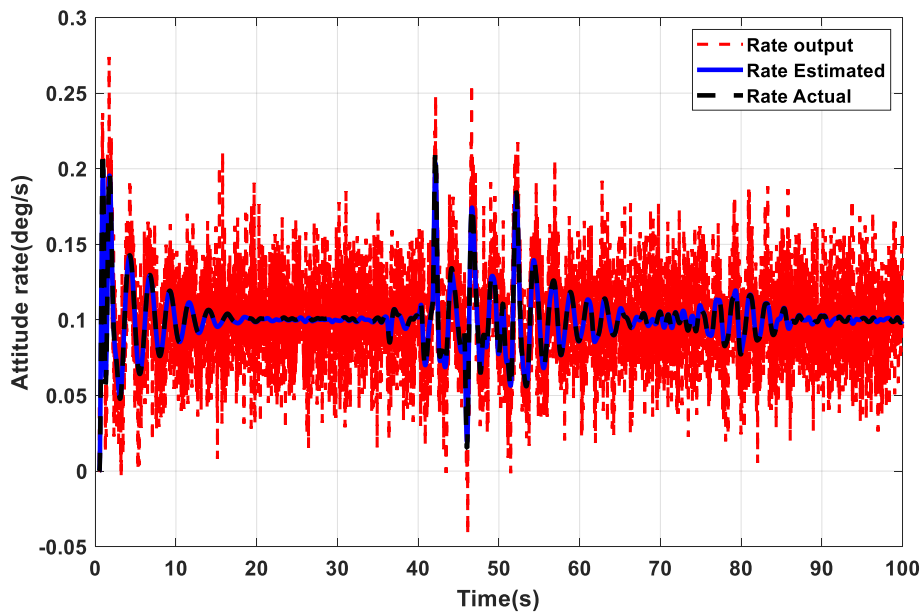


Figure 3. 9 Attitude Rate Estimated using EKF

3.5.2 Perturbed Plant Responses to a Ramp Command

In order to assess the robustness of the control schemes, plant (aero, flexibility and slosh) parameters are perturbed beyond $3\text{-}\sigma$ levels (ie. $\pm 10\%$ in

thrust, 30% in aerodynamic coefficients, $\pm 15\%$ in slosh and flexible mode frequency, 100% in mode shape perturbation with sign reversal, 15% in mass and inertia). Fig. 3.10 shows the rigid body plant parameters under perturbed conditions. Attitude tracking for the perturbed plant is shown in Fig. 3.11 and Fig. 3.12 show the attitude tracking error for various controllers. It is observed that integral absolute error is the least for projection based controller with the highest control demand. Plant parameter excursions due to aero perturbation are significant during the transonic regime (40-60 s). This causes a sudden jump in the control commands seen in Fig. 3.13. Fig. 3.14 gives the attitude rate due to slosh and flexible modes under excited conditions. The oscillations introduced in attitude rate due to slosh and flexible mode excitation are damped out quickly, showing the designed controllers' stability and robustness.

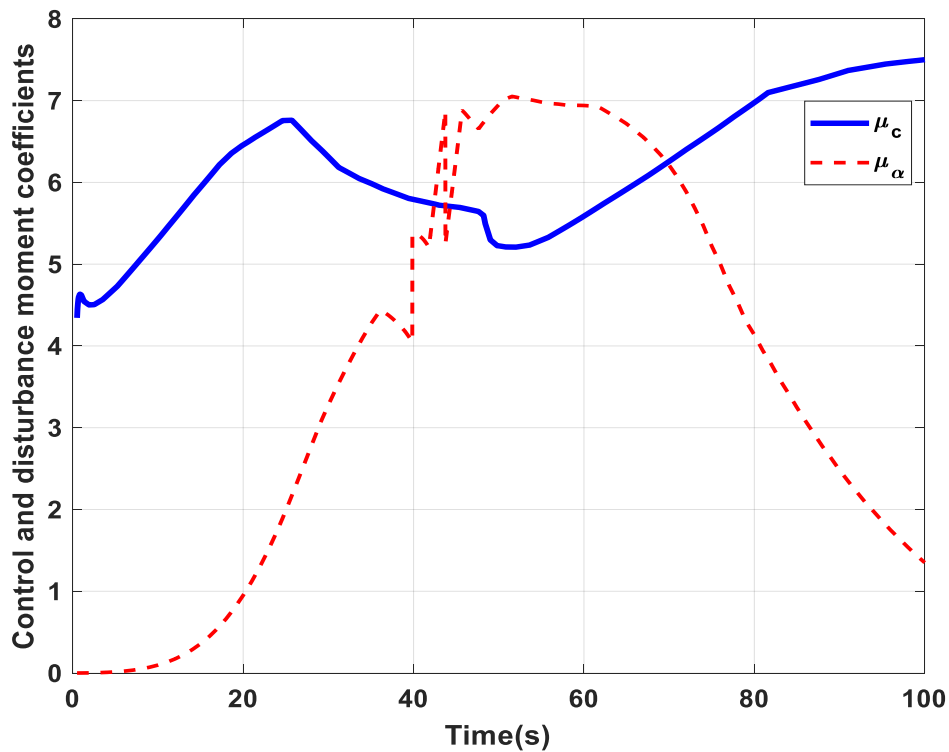


Figure 3.10 Perturbed Plant Parameters – Rigid Body

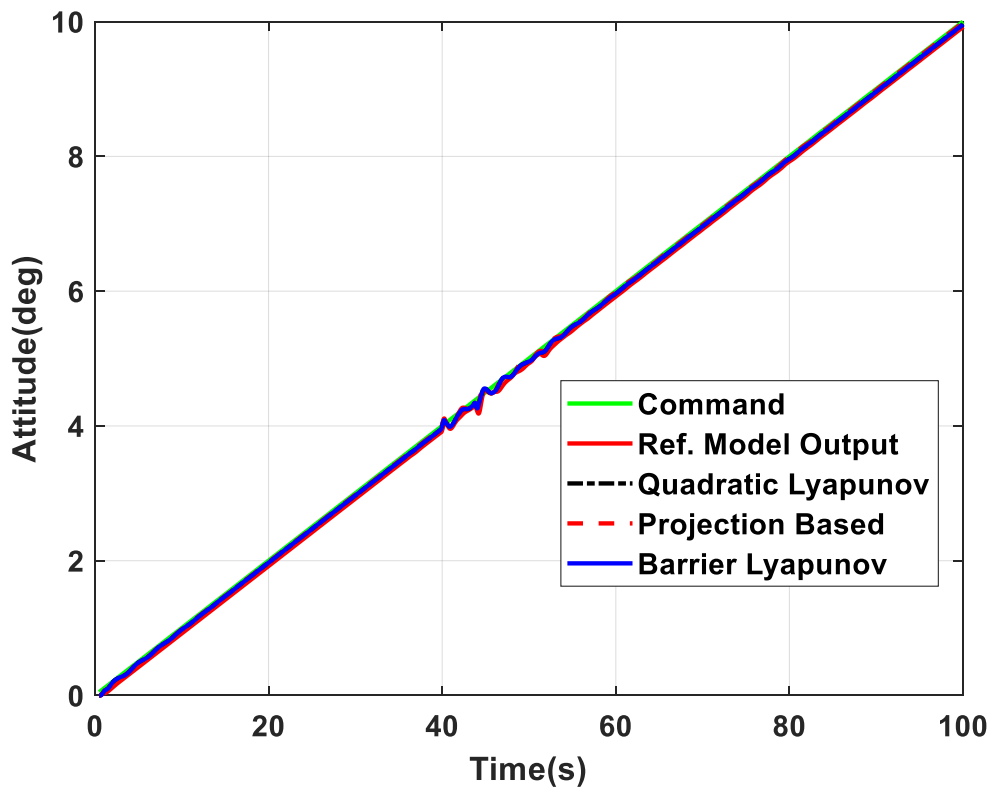


Figure 3.11 Attitude Tracking of Perturbed Plant for Ramp Command

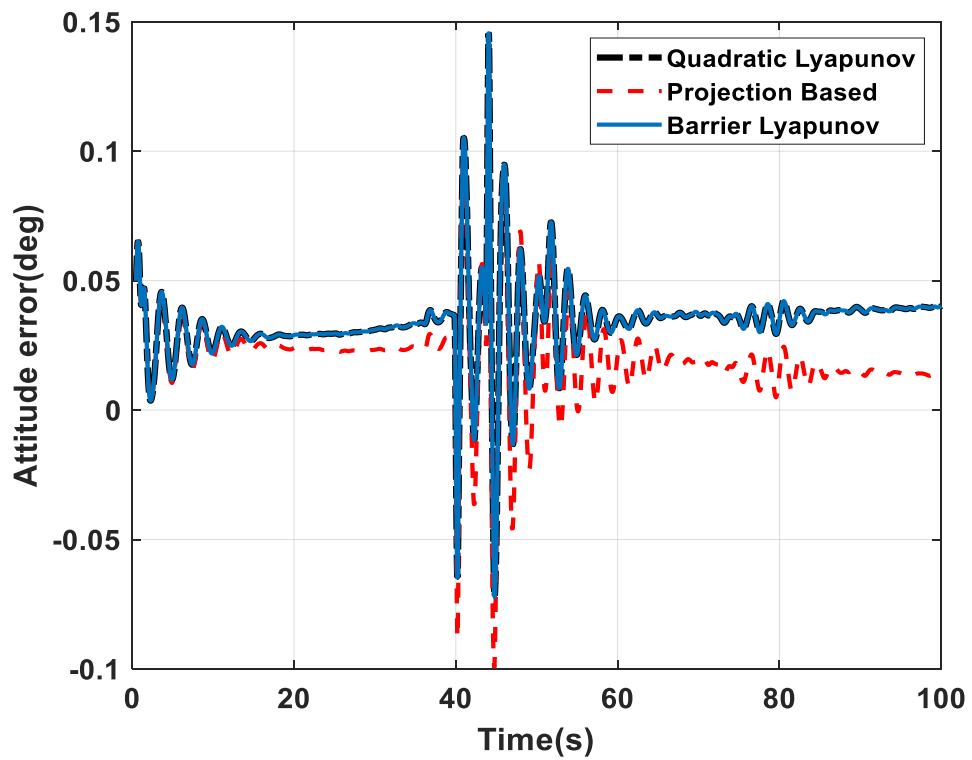


Figure 3.12 Attitude Tracking Error of Perturbed Plant for Ramp Command

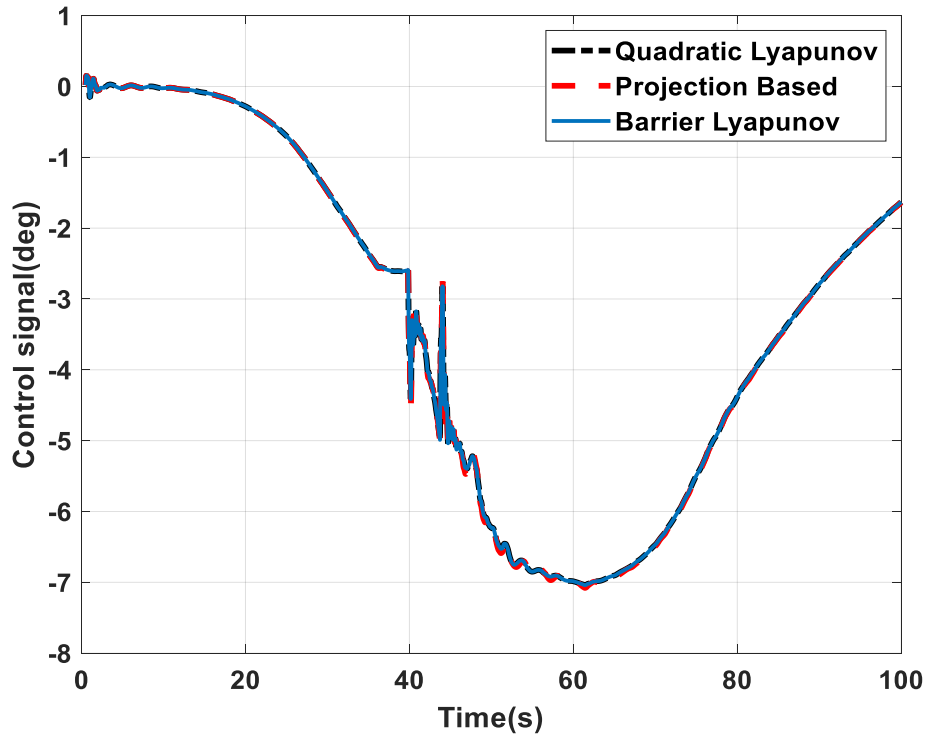


Figure 3.13 Control Responses of Perturbed Plant for Ramp Command

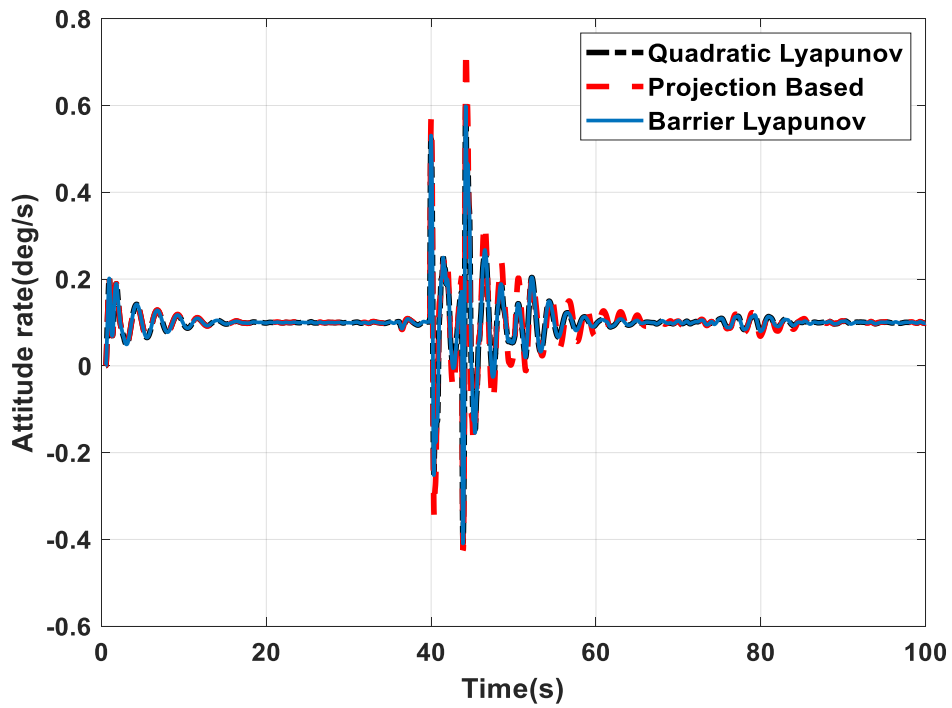


Figure 3.14 Attitude Rate of Perturbed Plant for Ramp Command

Results of the simulations with various controllers under nominal and off-nominal conditions are given in Table 3.1. It can be seen that the performances of all the controllers are comparable.

Table 3. 1 Performance Evaluation of Different Adaptive Controllers for a Ramp Command

Control Schemes	Under nominal condition			Under perturbed condition		
	Barrier Lyapunov	Projection Based	Quadratic Lyapunov	Barrier Lyapunov	Projection Based	Quadratic Lyapunov
Integral Absolute Error (deg)	0.0477	0.1176	0.1188	0.1270	0.0768	0.1379
Control effort (deg)	845.9551	841.55	841.32	1698.1	1707.2	1698.1

3.5.3 Robustness Verification

It is noted that the control signals are not saturated for the cases discussed in sections 3.5.1 and 3.5.2. In order to assess the limit of the robustness of the controllers, the perturbation levels of the aero parameters are increased such that control is saturated beyond which the system becomes uncontrollable. From Fig. 3.15, it can be inferred that the controller using BLF handles the highest level of aerodynamic parameter perturbation, followed by the controller using the projection operator. Fig. 3.16 shows the attitude tracking and Fig. 3.17 gives the controller output under this worst perturbation. Attitude rate signals shown in Fig. 3.18 have more oscillations with slower convergence for quadratic Lyapunov function, whereas the proposed methods show converging stable oscillations similar to nominal plant even with higher level of perturbation. Since BLF based controller handles higher perturbation levels, it shows more tracking error. This study indicates that BLF based controller is giving the best performance and stability (similar to nominal) for the highest level of perturbations, followed by projection based controller. Quadratic Lyapunov based controller lacks robustness

in presence of non-parametric uncertainties and un-modelled dynamics like non-linear actuator.

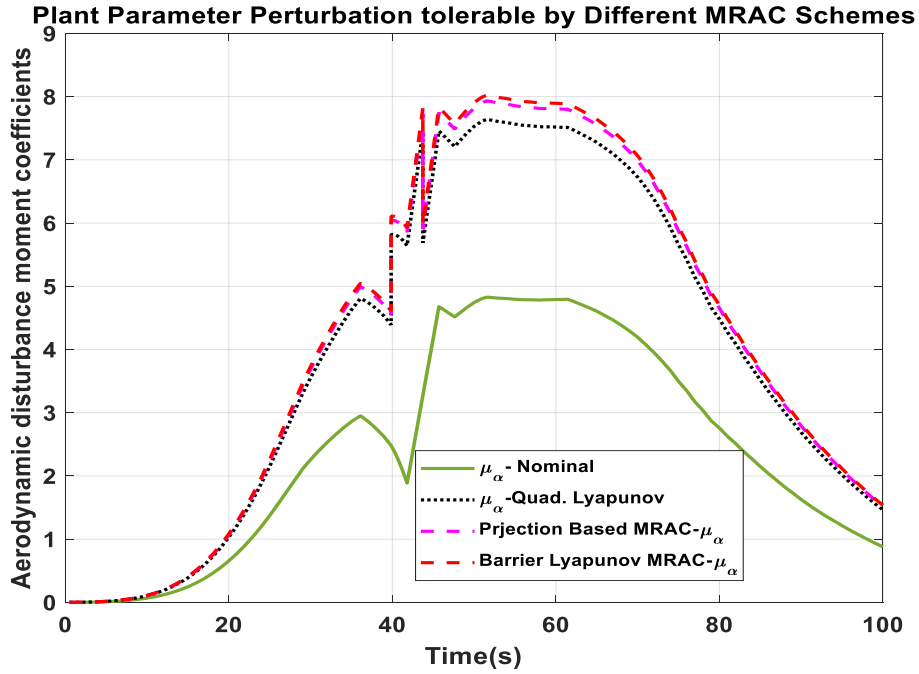


Figure 3. 15 Plant Parameter Perturbation Tolerable by Different Controllers

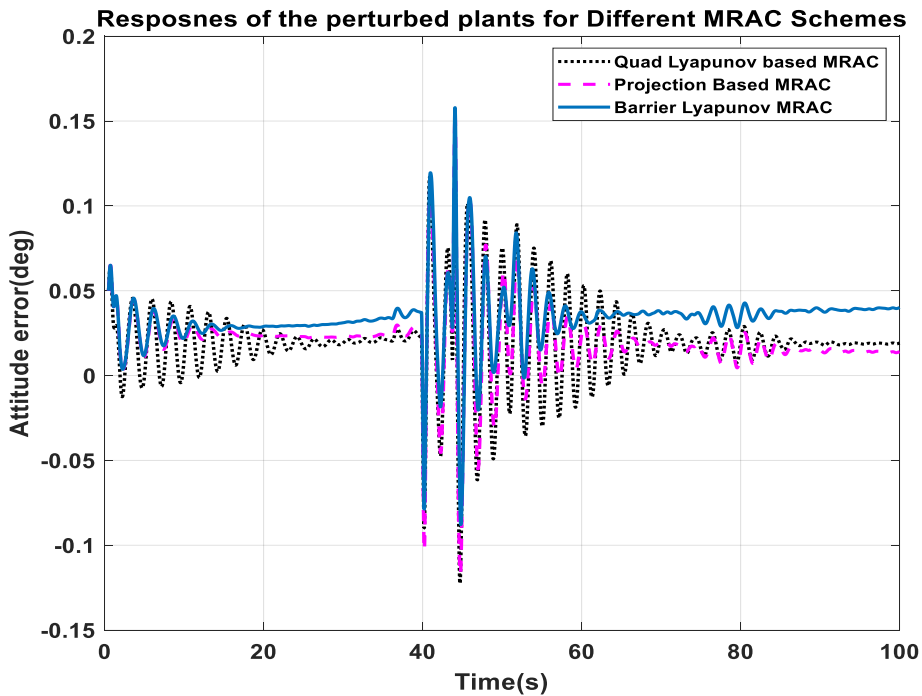


Figure 3. 16 Tracking of Ramp Commands by Different Controllers for the Plant Parameters Perturbed to the Limit

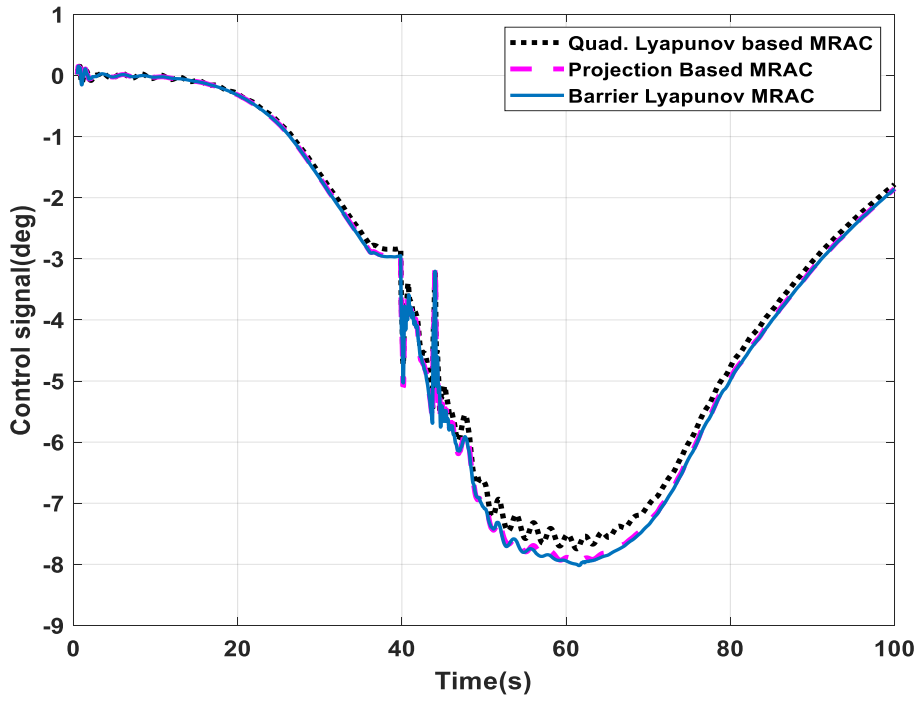


Figure 3. 17 Control Response of Different Controllers for the Plant Parameters Perturbed to the Limit

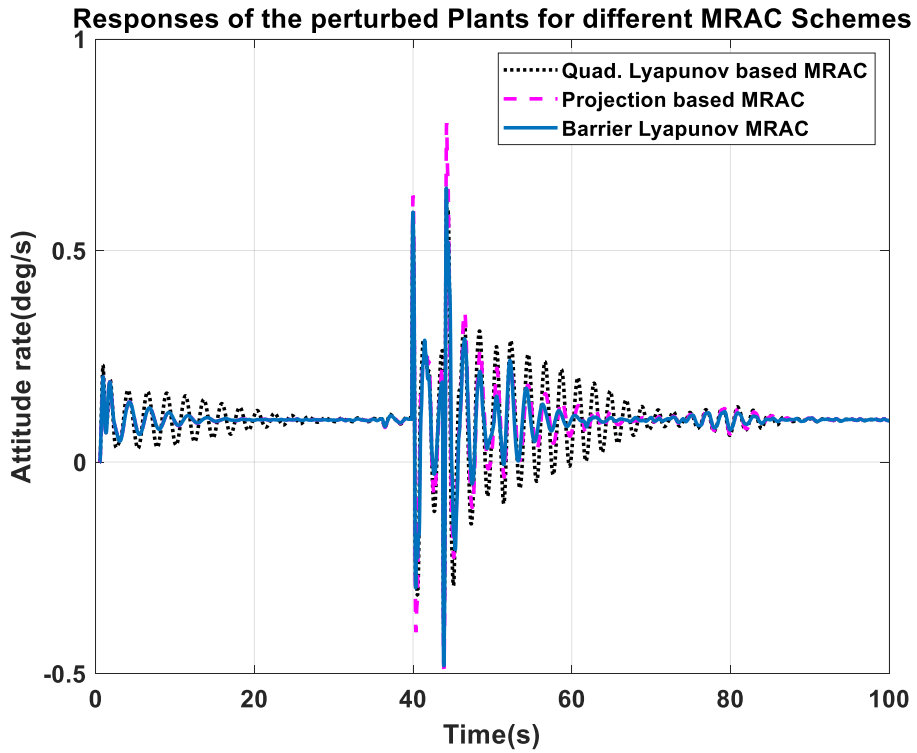


Figure 3. 18 Attitude Rate of Different Controllers for the Plant Parameters Perturbed to the Limit

3.5.4 Nominal Plant with a Typical Guidance Command

As explained in chapter 2, SLV's, during the atmospheric phase do not face continuous ramp commands. Closed Loop Guidance (CLG) typically will not be used during the atmospheric phase of flight. Attitude steering commands will be biased to a wind measured before the launch and will be stored onboard as a function of altitude to reduce the loads due to AoA build-up. CLG will start after the atmosphere is over to manoeuvre the SLV to the desired orbit. In the first stage, the autopilot should follow the open-loop guidance commands as close as possible to reduce the angle of attack build-up due to tracking error and reduce the trajectory deviations so that the CLG can start with benign initial conditions. This will increase the fuel margin, which is most desirable for guidance design.

Fig. 3.19 to Fig. 3.22 show the responses of various adaptive controllers compared with the responses of gain scheduled controller to a typical guidance command for a nominal plant. The plant simulated has high aerodynamic instability. Slosh and flexible mode frequency are very close to the rigid body frequency. Since the plant is having high $\sqrt{\mu_\alpha}$, the gain scheduled controller is designed with high bandwidth to ensure specified margins for rigid body. This causes interactions with slosh and flexibility dynamics. The open-loop steering command starts around 7 s and provides larger excitation to the slosh and flexible modes as seen in Fig. 3.22. The oscillations are converging, which shows the stability of the closed-loop system. The gain-scheduled controller is not able to provide sufficient stability and damping to the higher modes like adaptive controllers. This is the limitation of the gain scheduled controllers. It is observed that all adaptive controllers give almost the same performance for the nominal plant. Since similar observations are seen for the case of perturbed plant, figures are not included.

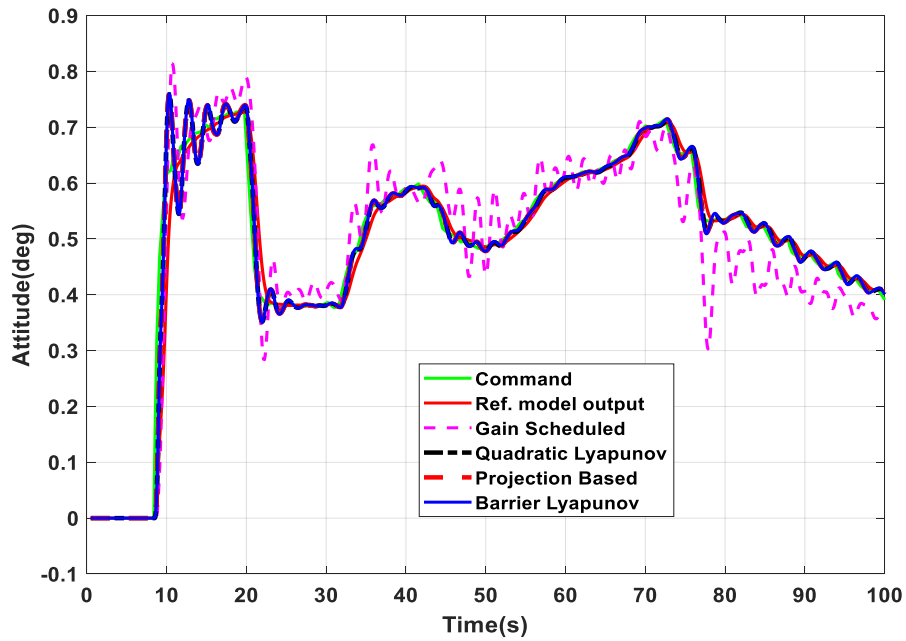


Figure 3.19 Attitude Tracking by Different Controllers for Nominal Plant with Typical Open Loop Guidance Command

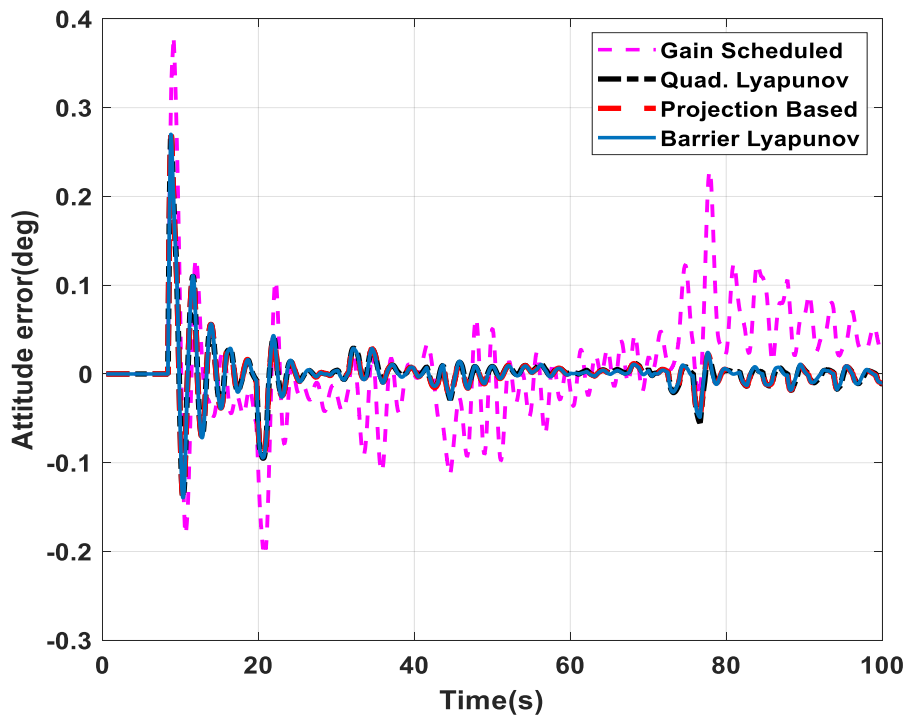


Figure 3.20 Attitude Tracking Error by Different Controllers for Nominal Plant with Typical Open Loop Guidance Command

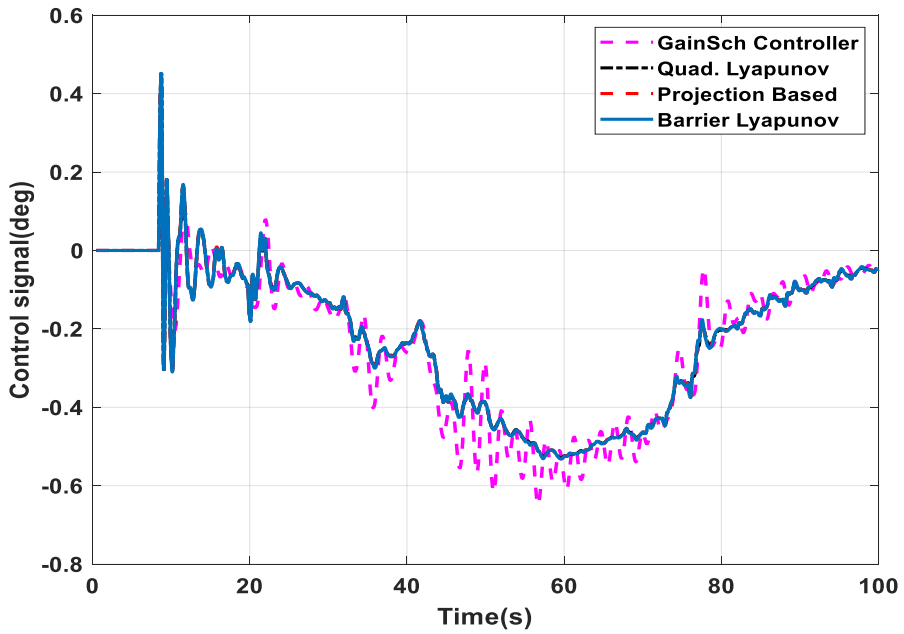


Figure 3. 21 Control Response for Typical Open Loop Guidance Command by Different Controllers for Nominal Plant

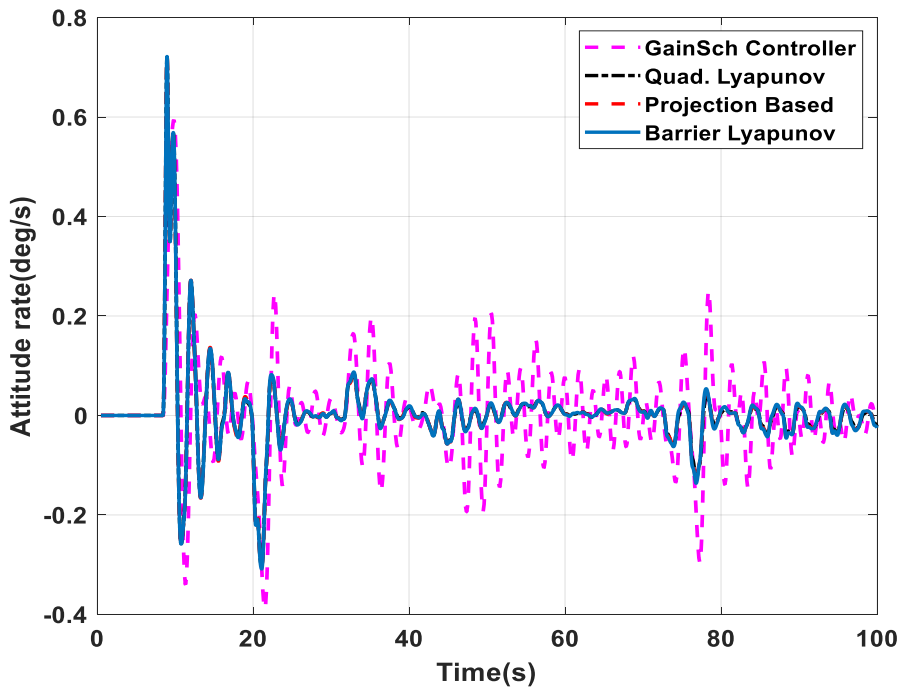


Figure 3. 22 Attitude Rate for Typical Open Loop Guidance Command by Different Controllers for Nominal Plant

The tracking error and control demand for the nominal and perturbed plant are given in Table 3.2. It is noted that the performances of all the controllers are very close under normal and perturbed plant conditions.

Table 3.2 Comparison of the Performance of Different Controllers for Typical Guidance Commands

Control Schemes	Under nominal condition			Under perturbed condition		
	Barrier Lyapunov	Projection Based	Quadratic Lyapunov	Barrier Lyapunov	Projection Based	Quadratic Lyapunov
Integral Absolute Error (deg)	0.0839	0.0833	0.0836	0.0836	0.0843	0.0836
Control effort (deg)	8.1524	8.1444	8.1302	16.5957	16.6606	16.5958

3.5.5 Disturbance Rejection Studies

A synthetic wind profile consists of shear and a tuned gust to excite the flexible and slosh modes. This profile is applied to the plant as a disturbance. Aerodynamic parameter variation is large between 40 to 50 s and the aerodynamic disturbance moment coefficient peaks around this time. The wind gust is applied around 45 s where the aerodynamic disturbance is at its peak. Wind disturbance rejection of various controllers are demonstrated in Fig. 3.23. All the controllers show almost the same performance until the wind gust is applied. After applying wind gust, the AoA oscillates at slosh and bending mode frequency which are very close. The tracking and disturbance rejection performance of the three controllers are given from Fig. 3.24 to Fig. 3.26. The wind gust, along with the jump in the plant parameters cause the control command to jump and hence the bending modes and slosh modes are excited.

Attitude tracking performance in the presence of wind is shown in Fig. 3.24 and Fig. 3.25. It can be seen that tracking is good till 40 s where a large wind shear comes. At 45 s, a gust is also applied. Fig. 3.26 and Fig. 3.27 show the control signals and Fig. 3.28 gives the attitude rates. Slosh pendulum angles are shown in Fig. 3.29 and Fig. 3.30. Corresponding bending mode generalised co-ordinates are

given in Fig. 3.31. It can be seen that the slosh pendulum and the bending mode are excited due to the wind shear, gust and control signal. Slosh pendulum angles and bending mode signals converge, showing the controllers' stability property. But the convergence is poor for quadratic Lyapunov based controller compared to the other two controllers. Projection based controller shows the highest stability compared to the other schemes. This is because the convex function used in the projection based controller is defined in such a way that the controller gains are allowed to vary only between the stability boundaries.

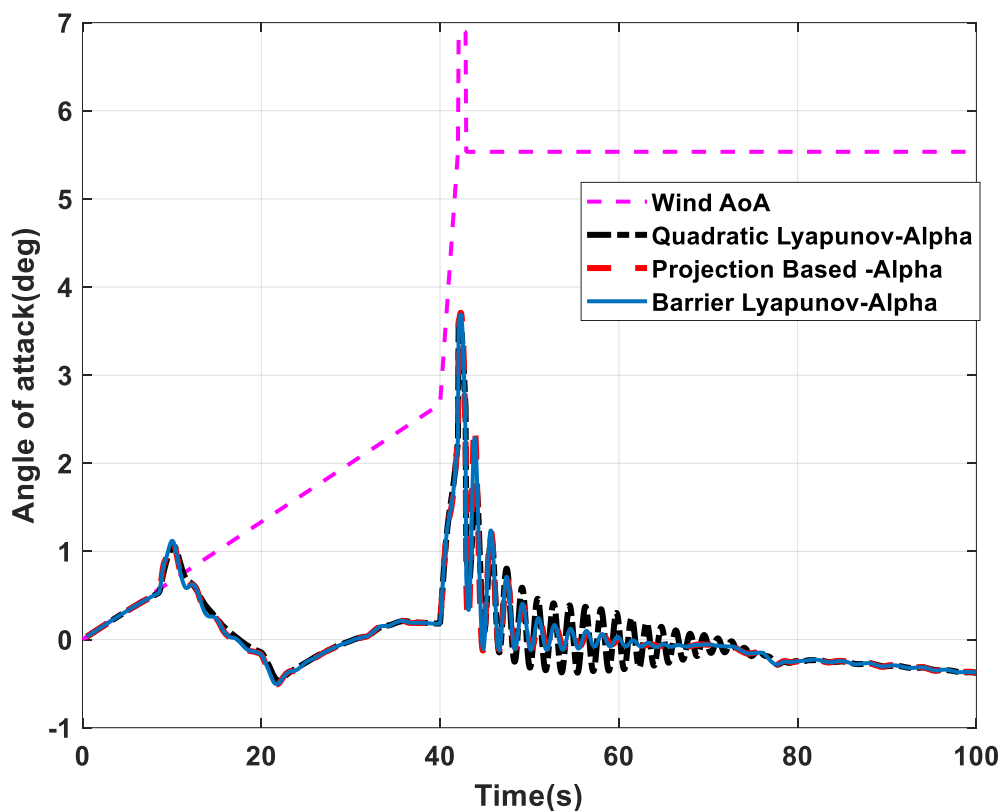


Figure 3.23 Comparison of Wind Disturbance Rejection Capability of Different Controllers for Perturbed Plant

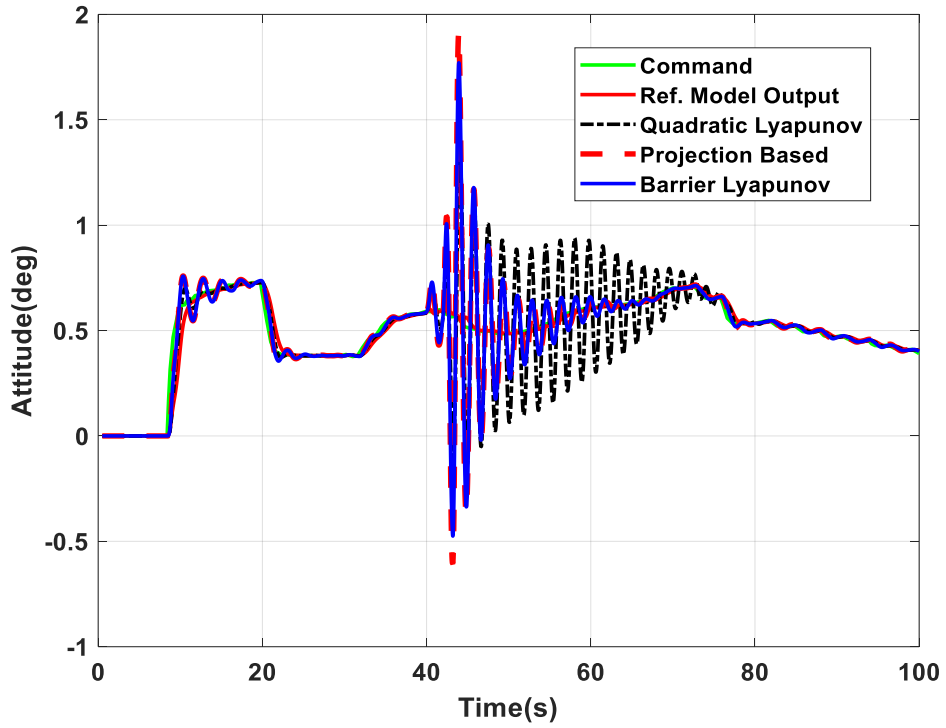


Figure 3.24 Attitude Tracking and Wind Disturbance Rejection for Typical Guidance Command by Different Controllers for Perturbed Plant

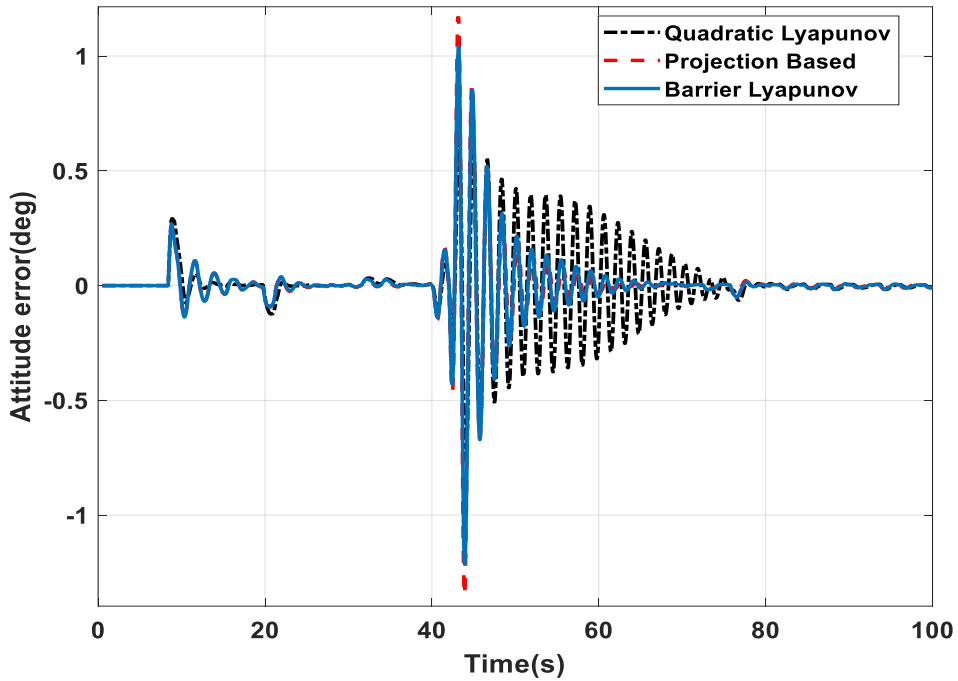


Figure 3.25 Attitude Tracking Error for Typical Guidance Command by Different Controllers for Perturbed Plant with a Wind Disturbance

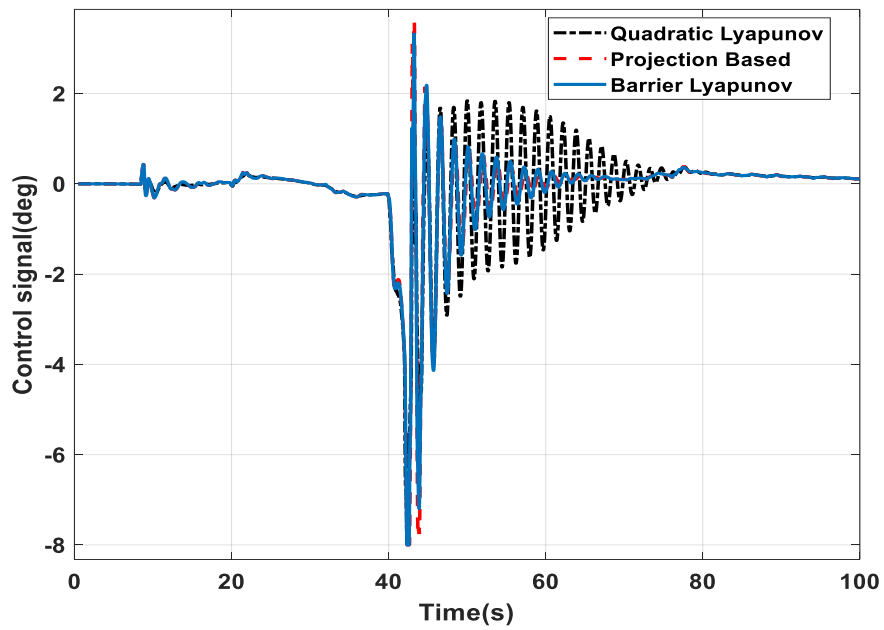


Figure 3. 26 Control Response for Typical Guidance Command by Different Controllers for Perturbed Plant with a Wind Disturbance

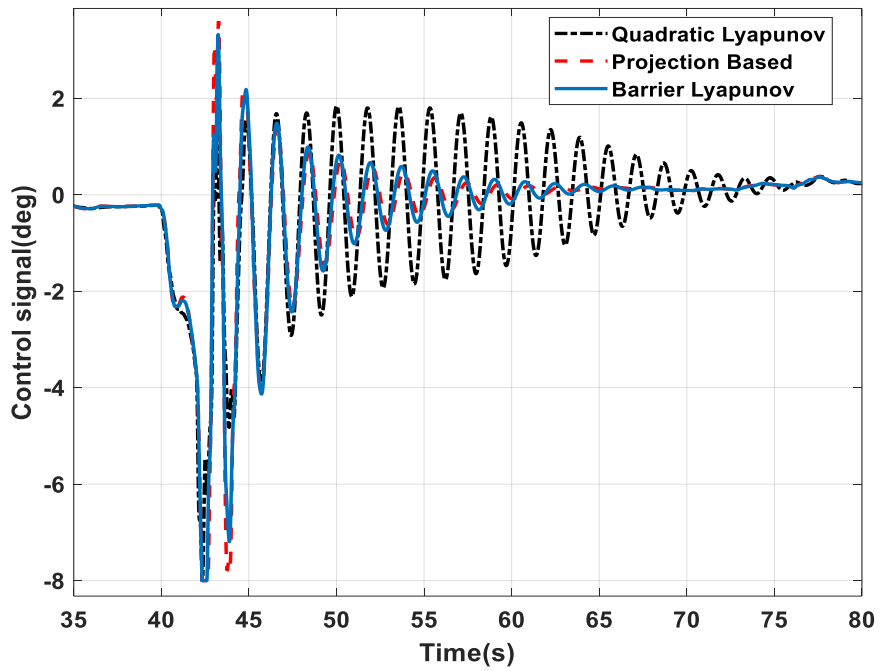


Figure 3. 27 Control Response by Different Controllers: Fig.3.26 Zoomed from 35 s to 80 s

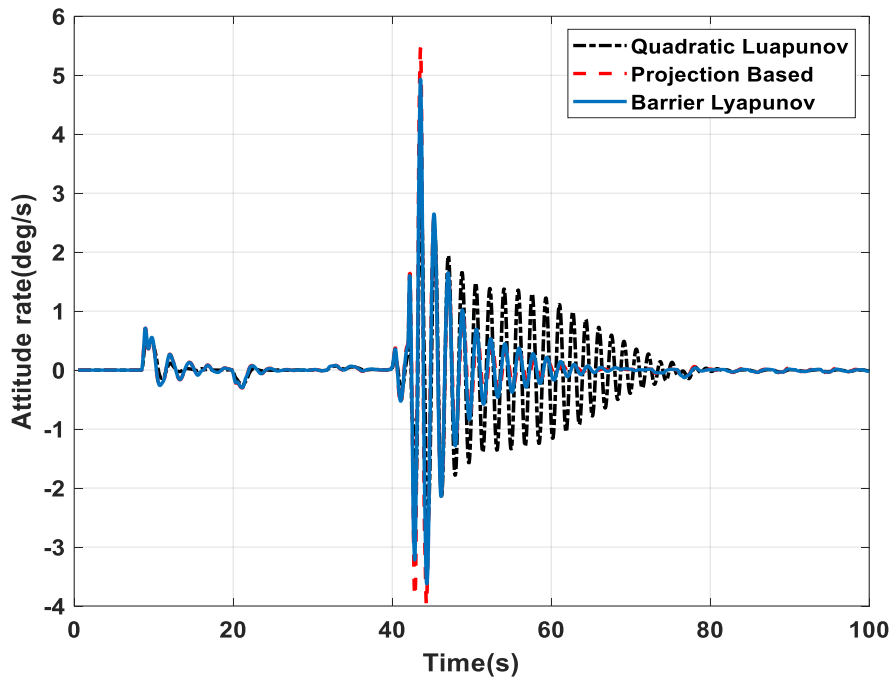


Figure 3.28 Attitude Rate Response for Typical Guidance Command by Different Controllers for Perturbed Plant with a Wind Disturbance

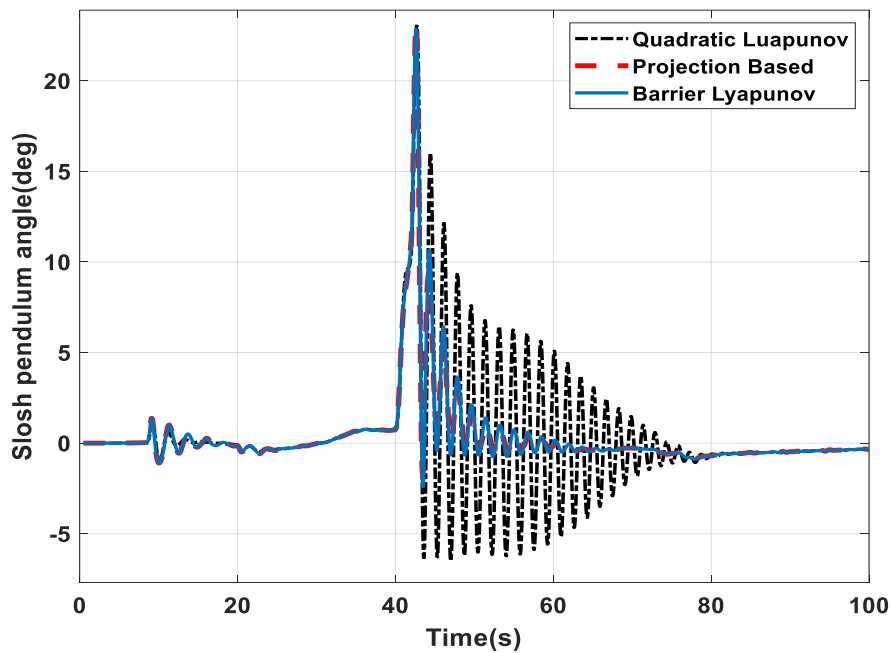


Figure 3.29 Slosh Pendulum Angles in Response to Typical Guidance Commands for Perturbed Plant with Wind Disturbance

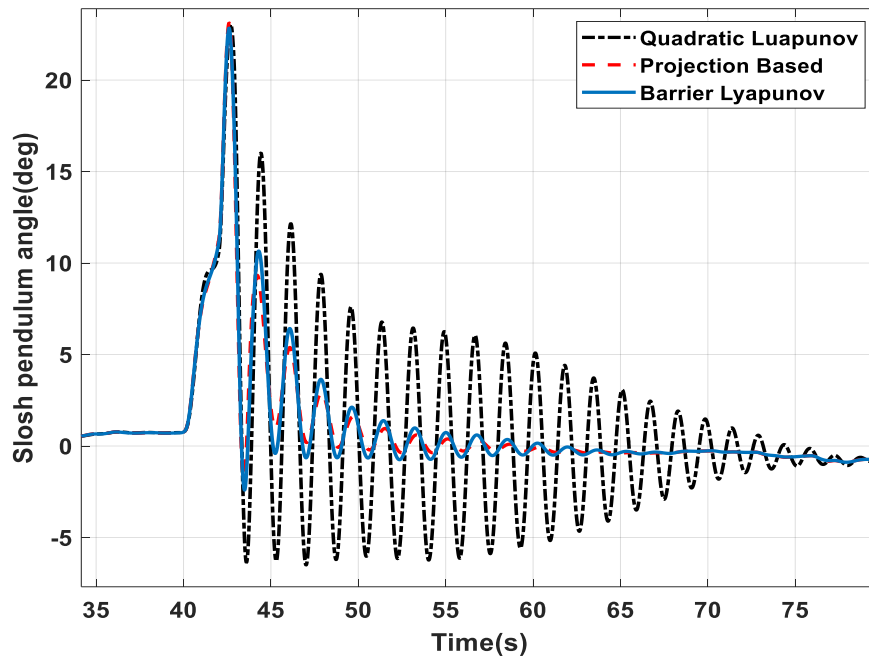


Figure 3. 30 Slosh Pendulum Angles for Perturbed Plant: Fig 3.29 Zoomed from 35 s to 80 s

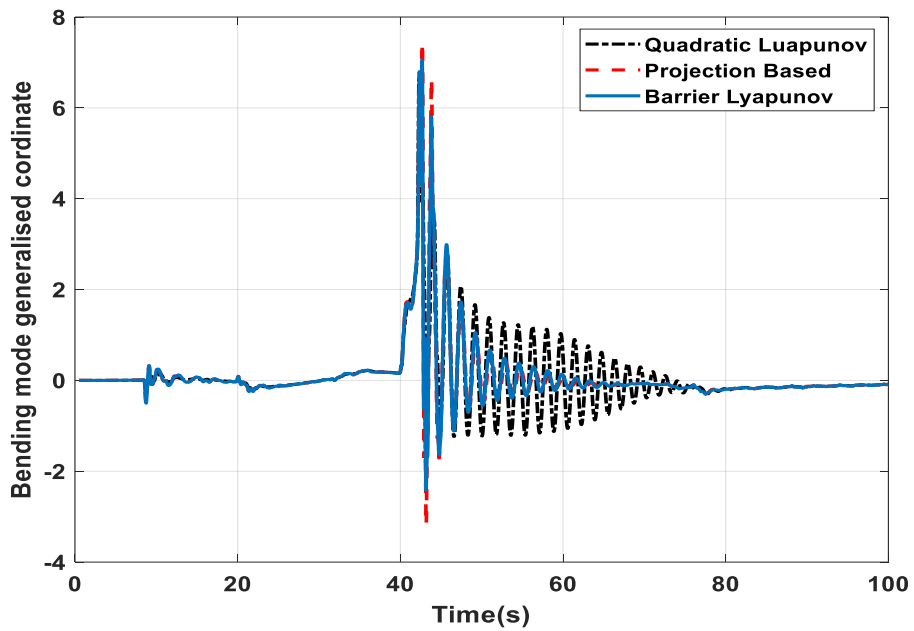


Figure 3. 31 Bending Mode Generalised coordinate in Response to Typical Guidance Commands for Perturbed Plant with Wind Disturbance

3.5.6 Studies with Actuator Saturation Avoidance Algorithm

Studies are done on the perturbed plant with the adaptive controller, which avoids actuator saturation. The non-linear actuator is modelled using a projection operator, which imposes a limit on actuator position and slew rate with a safe limit. Actuators are nearly saturated during the high dynamic pressure regime for the perturbed plant when a ramp command is applied. The algorithm tries to limit the actuator commands within the safe limit. This causes oscillations in the control signal, which excites the slosh and bending mode dynamics.

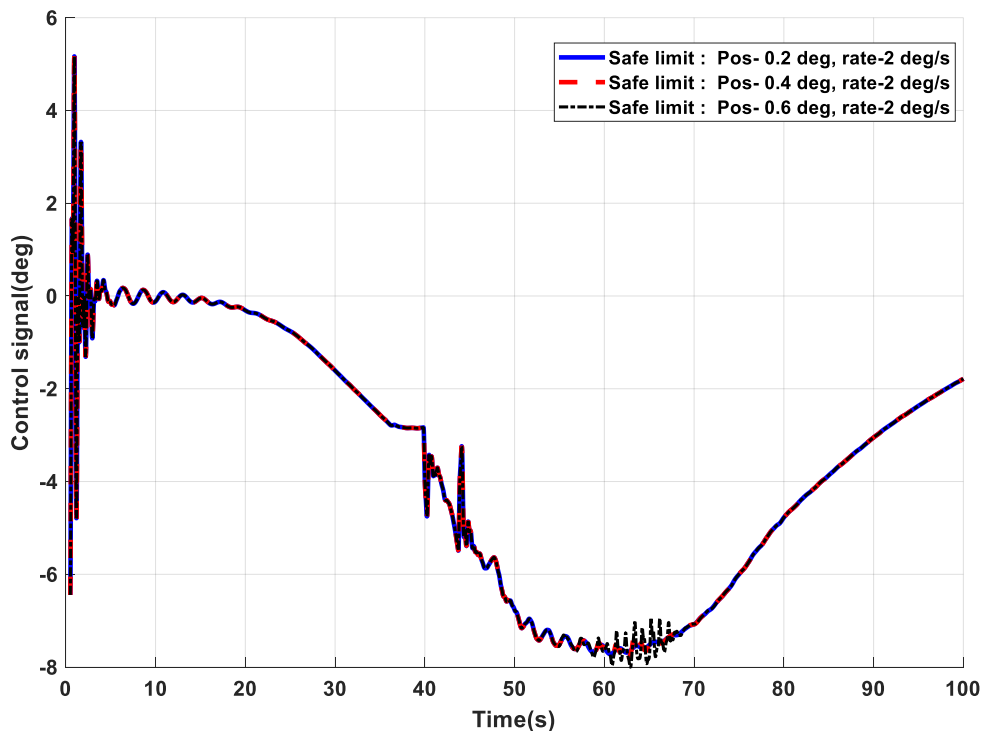


Figure 3. 32 Control Output of the Stable Adaptive Controller that Avoids Actuator Saturation

Fig. 3.32 and Fig. 3.33 show the control signals for different safe limits on actuator position and slew rate. When the safe limit is increased, the amplitude of the control oscillations increases and results in higher mode excitations, as observed in Fig. 3.34 - Fig. 3.36. Control signals were oscillating at slosh frequency in the high Q regime due to aero parameter variations till the safe limit of the control deflection was exceeded. Because of the oscillations in the control signal, flexibility also gets

excited, as evident from Fig. 3.34. Since this control algorithm is causing excitations of the higher modes, it is not proposed for the SLV plant with slosh and flexibility during the atmospheric phase of flight. However, this algorithm can be proposed for the upper stages under actuator failure conditions. This can be a future research direction. Actuator saturation can be avoided in the projection based and BLF based controllers through proper selection of the bounds and the reference model.

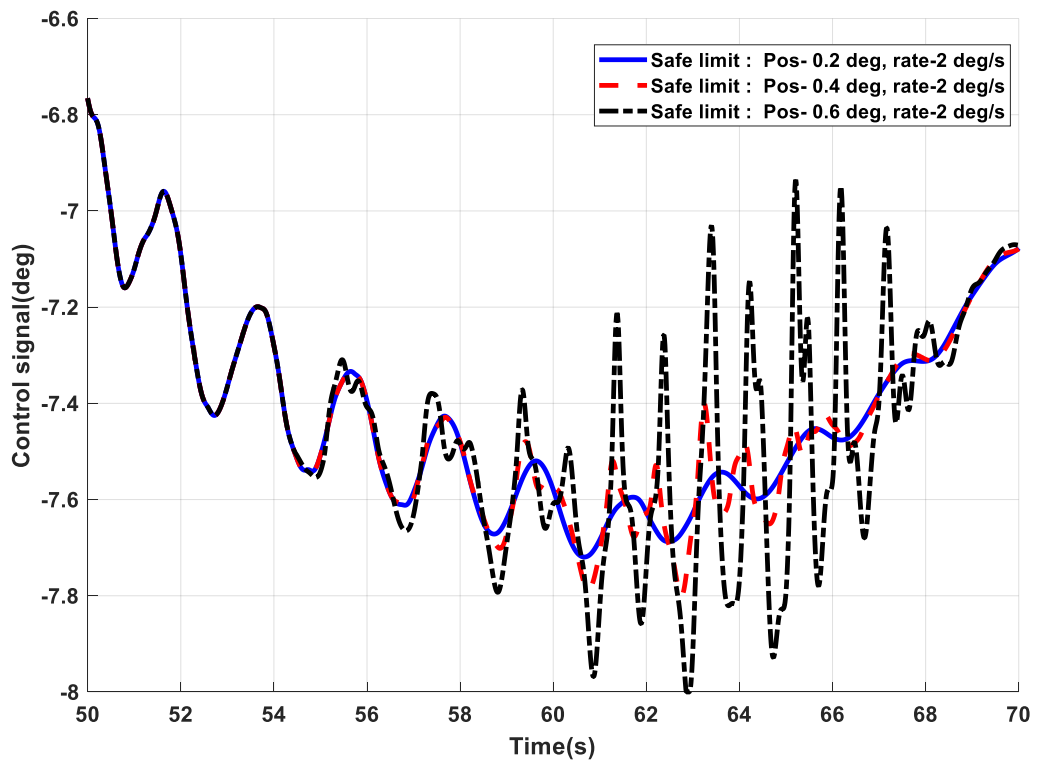


Figure 3. 33 Control Output of the Stable Adaptive Controller that Avoids Actuator Saturation – Fig 3.32 Zoomed from 50 s to 70 s

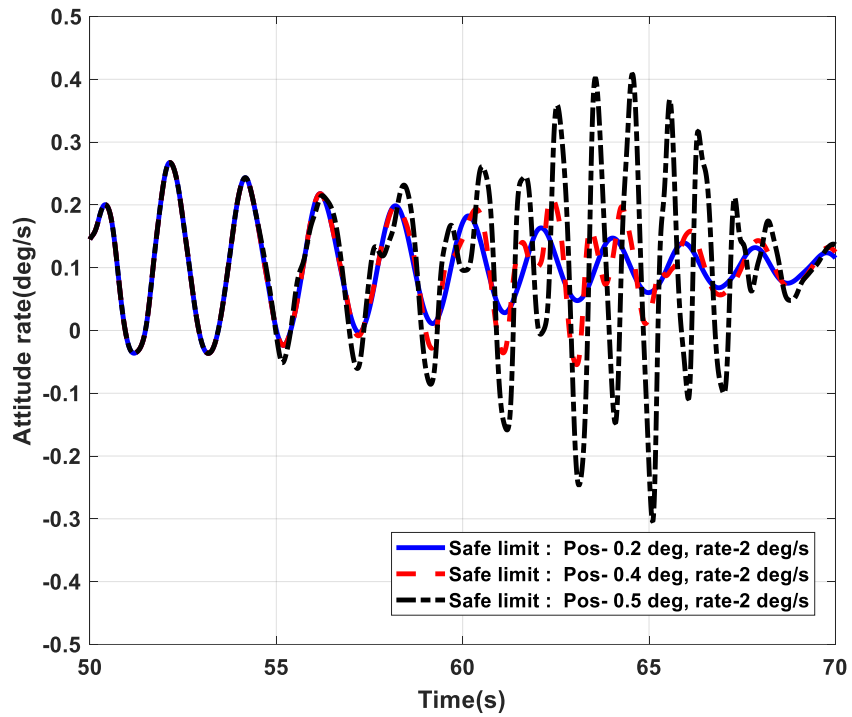


Figure 3.34 Attitude Rate Response of the Stable Adaptive controller that Avoids Actuator Saturation–Zoomed from 50 s to 70 s

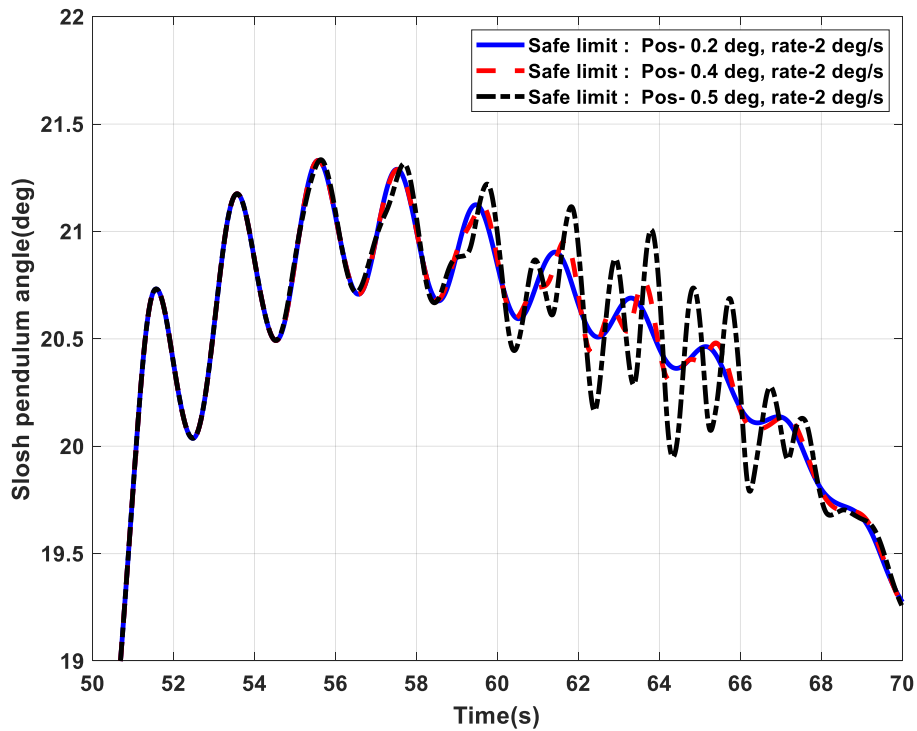


Figure 3.35 Slosh Pendulum Angles –Zoomed from 50 s to 70 s

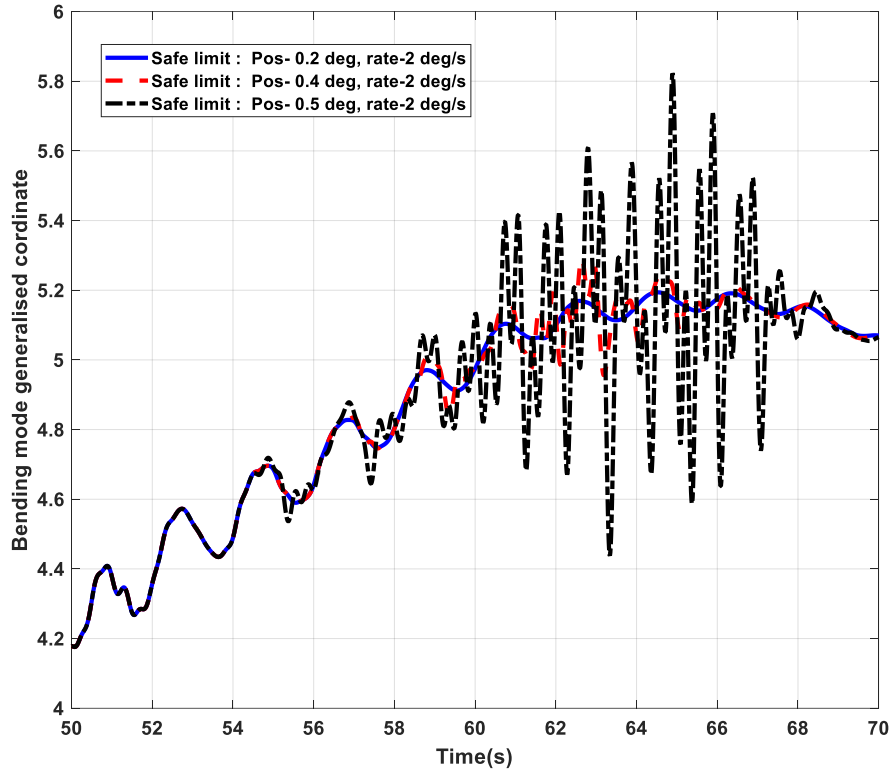


Figure 3.36 Bending Mode Generalized coordinates –Zoomed

3.6 Summary

Major contributions in this chapter are as follows:

Slosh and flexibility dynamics are introduced in the existing rigid body SLV model and states of those dynamics are estimated using EKF from available noisy measurements. The projection operator and BLF are used to update the parameters of the MRAC. Robustness of the proposed algorithms to parametric uncertainties and unmodelled dynamics are demonstrated. The results are compared with existing Quadratic Lyapunov based MRAC and the gain scheduled classical controller. A control scheme is developed using Lyapunov theory to ensure the stability and performance of the proposed adaptive controllers in the presence of actuator

nonlinearities like position saturation and slew rate saturation. A set of theoretically justifiable and verifiable condition for stability of the adaptive controllers is found out. This algorithm excites the high frequency modes when the actuator operates near the safe limit and hence not proposed.

The simulation studies indicated that adaptive controllers based on Projection/Barrier Lyapunov functions provide excellent tracking error performance and robustness to parameter perturbations. All three controllers have shown almost the same performance for typical guidance commands. Adaptive control using BLF provided the least integral of absolute error for nominal plant whereas projection based controller has shown minimum integral of absolute error for perturbed plant compared to quadratic Lyapunov based controller.

It is found that the Barrier Lyapunov and projection based adaptive control provides the highest robustness to parameter perturbations during tracking, whereas quadratic Lyapunov method offers limited robustness. During the perturbed condition, projection based adaptive controller exhibits maximum disturbance rejection followed by other methods. However, the quadratic Lyapunov based controller shows the least stability under perturbed condition.

Use of BLF and projection operators allows higher adaptation gains and tracking error was minimal in both cases. Both schemes restrict the adapted parameters within the specified boundary and remain stable throughout the simulation. The proposed control schemes are similar in performance under parameter perturbation and disturbance conditions.

Chapter 4

Adaptive Control Designs for a Winged Re-Entry Vehicle

4.1. Introduction

Reusable launch vehicles are getting developed to use multiple times to have low-cost access to space. The major challenge is the re-entry of the vehicle from outer space into the earth's atmosphere. During the re-entry phase, several stringent constraints and unknown uncertainties come into action. Though RLV's look like aircraft, they have to work for a large flight envelope, starting with hypersonic Mach numbers at the time of re-entry to landing at subsonic Mach numbers. There are several challenges unique to the RLV that makes the goal of such a "full envelope" flight control system more difficult to achieve than for a conventional airplane. The RLV experiences a wider range of dynamic pressure, Mach number, and mass properties during nominal and off-nominal flight. The dynamics of RLV change dramatically as the velocity and altitude go through a wide range of flight envelope during its re-entry process. As a result, the dynamic model of RLV is highly nonlinear, strongly coupled and fast time-varying, with large parameter uncertainties, environmental disturbances and un-modelled dynamics. Hence the flight control system for RLV should be robust, adaptive and reconfigurable. Thus, to assure a safe and reliable re-entry flight, it is significant for an RLV to track the guidance commands more accurately and rapidly while improving the robust performance.

Flight control system design for open loop stable aircraft is done using conventional classical analytical tools. These methods are iterative in which the nonlinear, coupled, time-varying plant dynamics is decoupled and linearised about several operating points in the flight envelope [6]. For such systems, classical controllers are designed for large stability margins about the operating points,

ensuring robustness towards the parameter perturbations. On the other hand, modern aircraft and winged re-entry vehicles have highly coupled nonlinear dynamics and has to work for a large flight envelope. Hence the system nonlinearities can be handled by designing nonlinear controllers which are free from approximations. For these systems, large parameter variations can be handled by building adaptive mechanisms in the controller [3]. However, ensuring stability and robustness to large parameter variations with different environmental conditions is challenging.

The modified adaptive controllers developed in chapter 3 are applied to a winged re-entry vehicle to track the angle of attack and bank angle commands during the approach and landing phase of an RLV mission. The six DoF rigid body equations are developed and a control design-oriented model is developed from these equations using various assumptions. Here the projection operator is re-defined to constrain the gains within the upper and lower bounds. Both the trajectory tracking error and gains are constrained using BLF. Tracking capability, robustness and disturbance rejection properties are demonstrated using extensive simulations.

4.2. Modelling of an RLV in the Descent Phase

The model of RLV during the descent phase is same as that of an aircraft. Six-degrees-of-freedom (6-DoF) rigid body equations for an aircraft can be obtained based on Newton's second law of motion [72][73][74][75]. These equations are derived in the aircraft-fixed body axes coordinate system as shown in Fig. 4.1. The origin is fixed at the CG of the vehicle.

The dynamics consists of 3 translational and 3 rotational DoF. The translational motion is described by the forward velocity u along the fuselage (x axis), lateral velocity v along the right wing (y axis) and the vertical velocity w positive down and along the body z axis. The three rotational DoF are given by body roll rate p about the x axis, pitch rate q about y axis and yaw rate r about z axis. The 6-DoF rigid body equations for an RLV can be written as follows.

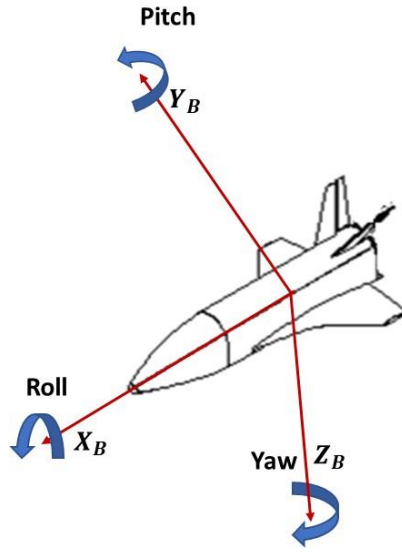


Figure 4. 1 RLV Co-ordinate System

The translational dynamics is

$$\begin{aligned}
 m \begin{pmatrix} \dot{u} \\ \dot{v} \\ \dot{w} \end{pmatrix} = - \left[\begin{pmatrix} p \\ q \\ r \end{pmatrix} \times m \begin{pmatrix} u \\ v \\ w \end{pmatrix} \right] + \begin{pmatrix} F_x \\ F_y \\ F_z \end{pmatrix} \\
 + m \|\vec{g}\| \begin{pmatrix} -\sin(\theta) \\ \cos(\theta) \sin(\varphi) \\ \cos(\theta) \cos(\varphi) \end{pmatrix}
 \end{aligned} \tag{4.1}$$

The rotational dynamics is

$$I \begin{pmatrix} \dot{p} \\ \dot{q} \\ \dot{r} \end{pmatrix} = - \left[\begin{pmatrix} p \\ q \\ r \end{pmatrix} \times I \begin{pmatrix} p \\ q \\ r \end{pmatrix} \right] + \begin{pmatrix} L \\ M \\ N \end{pmatrix} \tag{4.2}$$

where, m is the mass of the RLV, \vec{g} is the gravity vector which is expressed in the body axes coordinates and I is the inertia matrix and L, M, N are the moments about the X_B, Y_B, Z_B axes. Here φ is the vehicle bank angle (positive when aircraft right wing is down), θ is the pitch angle (positive when the nose is up) and ψ is the true heading angle (clockwise rotation of the aircraft nose from the true north direction is positive). The three Euler angles (θ, ψ, φ) are the inertial angular orientation of the rigid body or the instantaneous orientation of the body coordinate system with

respect to earth fixed (inertial) frame of reference. The kinematic relation between the Euler angle dynamics with the body rates is

$$\begin{pmatrix} \dot{\phi} \\ \dot{\theta} \\ \dot{\psi} \end{pmatrix} = \begin{pmatrix} 1 & \sin(\varphi) \tan(\theta) & \cos(\varphi) \tan(\theta) \\ 0 & \cos(\varphi) & -\sin(\varphi) \\ 0 & \frac{\sin(\varphi)}{\cos(\theta)} & \frac{\cos(\varphi)}{\cos(\theta)} \end{pmatrix} \begin{pmatrix} p \\ q \\ r \end{pmatrix} \quad (4.3)$$

F_x , F_y and F_z are the components of forces due to aerodynamics and propulsion acting on the vehicle. In this study, the RLV is performing an unpowered flight during descent phase. Hence the forces are due to aerodynamics and are often resolved into two perpendicular components. The lift force is perpendicular to the vehicle true air speed vector (V_T) and the drag force is opposing the vehicle motion along the airspeed direction. These forces depend on the angle-of-attack (α), which is the angle between the longitudinal (x) axis, the projection of the true airspeed vector on the plane of symmetry (xz plane) and dynamic pressure $Q = \frac{1}{2}\rho V_T^2$ where, ρ is the air density which is dependent on the altitude (h). The aero data measurements (V_T, α, β) can be written as

$$\begin{aligned} V_T &= \sqrt{u^2 + v^2 + w^2} \\ \alpha &= \tan^{-1}\left(\frac{w}{u}\right), \beta = \sin^{-1}\left(\frac{v}{V_T}\right) \end{aligned} \quad (4.4)$$

The lift and drag forces can be resolved into the body coordinate system as follows:

$$\begin{aligned} X_a &= L \sin(\alpha) - D \cos(\beta) \cos(\alpha) \\ Y_a &= D \sin(\beta) \\ Z_a &= -L \cos(\alpha) - D \cos(\beta) \sin(\alpha) \end{aligned} \quad (4.5)$$

Substituting (4.5) in (4.1), we get

$$\begin{aligned} \dot{u} &= rv - qw + \frac{L}{m} \sin(\alpha) - \frac{D}{m} \cos(\beta) \cos(\alpha) - \|\vec{g}\| \sin(\theta) \\ \dot{v} &= pw - ru + \frac{D}{m} \sin(\beta) + \|\vec{g}\| \cos(\theta) \sin(\varphi) \end{aligned} \quad (4.6)$$

$$\dot{w} = qu - pv - \frac{L}{m} \cos(\alpha) - \frac{D}{m} \cos(\beta) \sin(\alpha) + \|\vec{g}\| \cos(\theta) \cos(\varphi)$$

In order to write the position dynamics equations, we need to consider the relationship between the body fixed velocities (u, v, w) and inertial velocities in north-east-down frame $(\dot{x}, \dot{y}, \dot{h})$.

$$\begin{pmatrix} \dot{x} \\ \dot{y} \\ -\dot{h} \end{pmatrix} = \begin{pmatrix} 1 & 0 & 0 \\ 0 & \cos(\varphi) & \sin(\varphi) \\ 0 & -\sin(\varphi) & \cos(\varphi) \end{pmatrix} \begin{pmatrix} \cos(\theta) & 0 & -\sin(\theta) \\ 0 & 1 & 0 \\ \sin(\theta) & 0 & \cos(\theta) \end{pmatrix} \begin{pmatrix} \cos(\psi) & \sin(\psi) & 0 \\ -\sin(\psi) & \cos(\psi) & 0 \\ 0 & 0 & 1 \end{pmatrix} \begin{pmatrix} u \\ v \\ w \end{pmatrix} \quad (4.7)$$

The inertial positions (x, y, h) are derived by integrating these velocities. Inertial position and velocity information is required by the guidance algorithm design. This information is very significant during landing and take-off. This is a fully coupled 6 DoF model and there are 12 states, namely, $u, v, w, p, q, r, \varphi, \theta, \psi, x, y, h$.

The RLV considered here is an unpowered vehicle. The control in pitch, yaw and roll planes is achieved by deflecting the control surfaces. Usual aircraft, roll control is through differential deflection of two ailerons (on the left and right wings) and pitch control is through elevators near the tail. The rudders, which are control surfaces on the vertical tail, control the yawing motion. For the RLV, for which the control design is attempted, pitch control and roll control are through a set of elevons (elevator + aileron) on the two wings. However, for modelling purposes, the control deflection required for roll (δ_{ail}), pitch (δ_e) and yaw (δ_{rud}) are taken separately. Hence the input vector is

$$\vec{u} = (\delta_{ail}, \delta_e, \delta_{rud})^T \quad (4.8)$$

The vehicle dynamics can be modified and manoeuvred through appropriate selection of the control input. The RLV is fitted with several sensors on its body to measure different physical variables. The body angular rates (p, q, r) are measured by the gyroscopes usually located near the CG of the vehicle. These measurements

can be used to get the Euler angles (φ, θ, ψ) . In addition to these, accelerometers are used to measure the body acceleration A_x, A_y, A_z (load in longitudinal, lateral and vertical). The air-data system measures the true airspeed, AoA and angle of side-slip. Hence, the output vector is

$$\vec{y} = [A_x, A_y, A_z, V_T, \alpha, \beta, p, q, r, \varphi, \theta, \psi]^T \quad (4.9)$$

This fully coupled 6 DoF model will result in impractical control solutions if used for control design. Hence there is a strong requirement to make a simplified control design-oriented model so that the resulting control solution will be simple, robust and works well with the real plant. The nonlinearities present in the model can be handled by using nonlinear controllers like dynamic inversion and backstepping control. These techniques avoid the linearisation of the plant dynamics about various operating points and gain scheduled controller design. Dynamic inversion requires the perfect model of the system to be controlled (which is practically impossible), so that all the nonlinearities are cancelled and desired dynamics are added [76][77][78][79]. Backstepping is a Lyapunov based method which ensures the stability of the system, but representing the performance specifications in the Lyapunov function is a challenge. In this chapter, the plant is linearized about the operating point and design adaptive controllers, ensuring stability and performance in the entire flight envelope.

The 6 DoF equations can be linearised about an operating point (trim point). Trimming an aircraft means finding a balance between aerodynamic, propulsive and gravitational forces and moments that are acting on the vehicle constantly. It is done by deflecting primary controls to values that would result in the specified steady state conditions. In the case of RLV, only the moments can be balanced and the forces are continuously changed by the guidance system (trajectory controller) to satisfy various constraints and to safely land on the desired location. The adaptive controllers described in the following sections, control the rotational dynamics of the vehicle. The translational dynamics is being controlled by a guidance system.

When the vehicle is trimmed about an operating point, the dynamics gets decoupled into longitudinal dynamics and lateral-directional dynamics. The

longitudinal dynamics describe the motion of the vehicle in forward, vertical planes and the rotation about the pitch (Y_B) axis. These dynamics can be further decomposed into fast (short period) and slow (phugoid) modes. The short period dynamics describes the fast coupling between the AoA (α) and the pitch rate (q). The phugoid mode is much slower compared to the short period mode. This represents the dynamical interchange between the vehicle's kinetic and potential energy or the vehicle attitude and the airspeed. The aircraft longitudinal equations of motion after trimming with respect to an operating point can be written as

$$\begin{pmatrix} \dot{v}_T \\ \dot{\alpha} \\ \dot{q} \\ \dot{\theta} \end{pmatrix} = \begin{pmatrix} X_V & X_\alpha & 0 & -g \cos(\gamma_0) \\ \frac{Z_V}{V_0} & \frac{Z_\alpha}{V_0} & 1 + \frac{Z_q}{V_0} & \frac{-g \sin(\gamma_0)}{V_0} \\ M_V & M_\alpha & M_q & 0 \\ 0 & 0 & 1 & 0 \end{pmatrix} \begin{pmatrix} v_T \\ \alpha \\ q \\ \theta \end{pmatrix} + \begin{pmatrix} X_{\delta_e} \\ \frac{Z_{\delta_e}}{V_0} \\ M_{\delta_e} \\ 0 \end{pmatrix} \delta_e \quad (4.10)$$

where, X_V and X_α are the aerodynamic stability derivatives of the forces in the X axis and X_{δ_e} is the force coefficient with respect to elevon deflection. Z_V, Z_α are the force coefficient in Z axis and Z_q derivative of force in Z direction with respect to q . M_V, M_α and M_q are the moment coefficients about the pitch axis and M_{δ_e} is the pitching moment derivative with respect to elevon deflection. V_0 is the trimmed velocity and α_0 is the trimmed angle of attack.

$\gamma_0 = \theta_0 - \alpha_0$ is the trimmed flight path angle and θ_0 is the trimmed pitch angle.

The short period mode is defined by:

$$\begin{pmatrix} \dot{\alpha} \\ \dot{q} \end{pmatrix} = \begin{pmatrix} \frac{Z_\alpha}{V_0} & 1 + \frac{Z_q}{V_0} \\ M_\alpha & M_q \end{pmatrix} \begin{pmatrix} \alpha \\ q \end{pmatrix} + \begin{pmatrix} \frac{Z_{\delta_e}}{V_0} \\ M_{\delta_e} \end{pmatrix} \delta_e \quad (4.11)$$

Short period mode is controlled by the attitude controller and the phugoid mode is controlled by the guidance system.

Lateral-directional dynamics

Using the kinematic relationship between the Euler angle dynamics with the body rates as defined in (4.3), the Euler roll equation is written as follows

$$\dot{\varphi} = p + \tan(\theta)(q \sin(\varphi) + r \cos(\varphi)) \quad (4.12)$$

Let θ_0 be the trimmed pitch angle, then the linear approximation of (4.12) around the trim point ($\varphi_0 = p_0 = q_0 = r_0 = 0$) is

$$\dot{\varphi} = p + r \tan(\theta_0) \quad (4.13)$$

Stability axis roll and yaw rates (p_s, r_s) are related to the body axis roll and yaw rates (p, r) in the following way:

$$\begin{aligned} p_s &= p \cos(\alpha) + r \sin(\alpha) \\ r_s &= -p \sin(\alpha) + r \cos(\alpha) \end{aligned} \quad (4.14)$$

At the trim point this relation becomes

$$\begin{aligned} p_s &= p \cos(\alpha_0) + r \sin(\alpha_0) \\ r_s &= -p \sin(\alpha_0) + r \cos(\alpha_0) \end{aligned} \quad (4.15)$$

In order to get the body rates, inverse is taken

$$\begin{aligned} p &= p_s \cos(\alpha_0) - r_s \sin(\alpha_0) \\ r &= p_s \sin(\alpha_0) + r_s \cos(\alpha_0) \end{aligned} \quad (4.16)$$

Substituting (4.16) in (4.13), we get

$$\begin{aligned} \dot{\varphi} &= p_s \cos(\alpha_0) - r_s \sin(\alpha_0) \\ &\quad + (p_s \sin(\alpha_0) + r_s \cos(\alpha_0)) \tan(\theta_0) \\ &= p_s (\cos(\alpha_0) + \sin(\alpha_0) \tan(\theta_0)) + r_s (-\sin(\alpha_0) \\ &\quad + \cos(\alpha_0) \tan(\theta_0)) \end{aligned} \quad (4.17)$$

We have, at zero bank angle and sideslip angle

$$\alpha_0 = \theta_0 - \gamma_0 \quad (4.18)$$

$$\begin{aligned}
& \therefore \cos(\alpha_0) + \sin(\alpha_0) \tan(\theta_0) \\
& \quad = \cos(\theta_0 - \gamma_0) + \sin(\theta_0 - \gamma_0) \tan(\theta_0) \\
& \quad = \frac{\cos(\gamma_0)}{\cos(\theta_0)} \\
& -\sin(\alpha_0) + \cos(\alpha_0) \tan(\theta_0) = \frac{\sin(\gamma_0)}{\cos(\theta_0)}
\end{aligned} \tag{4.19}$$

Hence the bank angle dynamics can be written as

$$\dot{\varphi} = \frac{\cos(\gamma_0)}{\cos(\theta_0)} p_s + \frac{\sin(\gamma_0)}{\cos(\theta_0)} r_s \tag{4.20}$$

Assuming small angles, the angle of sideslip dynamics can be written as

$$\begin{aligned}
\dot{\beta} = \frac{1}{V_0} (Y_\beta \beta + Y_p p_s + Y_r r_s + Y_{\delta_{ail}} \delta_{ail} + Y_{\delta_{rud}} \delta_{rud}) \\
+ \left(\frac{g \cos(\theta_0)}{V_0} \right) \varphi - r_s
\end{aligned} \tag{4.21}$$

where, Y_β, Y_p, Y_r are the derivatives of the side force Y with respect to β, p_s and r_s and $Y_{\delta_{ail}}, Y_{\delta_{rud}}$ correspond to those with respect to control deflections δ_{ail} and δ_{rud} . The dynamics of p_s and r_s can be written as

$$\begin{aligned}
\dot{p}_s &= L_\beta \beta + L_p p_s + L_r r_s + L_{\delta_{ail}} \delta_{ail} + L_{\delta_{rud}} \delta_{rud} \\
\dot{r}_s &= N_\beta \beta + N_p p_s + N_r r_s + N_{\delta_{ail}} \delta_{ail} + N_{\delta_{rud}} \delta_{rud}
\end{aligned} \tag{4.22}$$

where, L_β, L_p and L_r are the rolling moment coefficients with respect to lateral-directional states β, p_s, r_s . $L_{\delta_{ail}}, L_{\delta_{rud}}$ are rolling moment coefficients due to control surface deflections. Similarly, $N_\beta, N_p, N_r, N_{\delta_{ail}}$ and $N_{\delta_{rud}}$ are the yawing moment coefficients with respect to $\beta, p_s, r_s, Y_{\delta_{ail}}$ and $Y_{\delta_{rud}}$.

Using (4.20) to (4.22), the state-space representation of linearised lateral-directional dynamics can be written as

$$\begin{aligned}
\begin{pmatrix} \dot{\varphi} \\ \dot{\beta} \\ \dot{p}_s \\ \dot{r}_s \end{pmatrix} &= \begin{pmatrix} 0 & 0 & \frac{\cos(\gamma_0)}{\cos(\theta_0)} & \frac{\sin(\gamma_0)}{\cos(\theta_0)} \\ g \frac{\cos(\theta_0)}{V_0} & \frac{Y_\beta}{V_0} & \frac{Y_p}{V_0} & \frac{Y_r}{V_0} - 1 \\ 0 & L_\beta & L_p & L_r \\ 0 & N_\beta & N_p & N_r \end{pmatrix} \begin{pmatrix} \varphi \\ \beta \\ p_s \\ r_s \end{pmatrix} \\
&+ \begin{pmatrix} 0 & 0 \\ \frac{Y_{\delta_{ail}}}{V_0} & \frac{Y_{\delta_{rud}}}{V_0} \\ L_{\delta_{ail}} & L_{\delta_{rud}} \\ N_{\delta_{ail}} & N_{\delta_{rud}} \end{pmatrix} \begin{pmatrix} \delta_{ail} \\ \delta_{rud} \end{pmatrix}
\end{aligned} \tag{4.23}$$

This model has 2 inputs (δ_{ail} , δ_{rud}) and four outputs φ , β , p , r . From these measurements, p_s and r_s can be obtained by using AoA measurement. Here, both these inputs affect all the states. Also, an increase in side-slip angle can cause both yaw rate and roll rate. Hence this plant model is highly coupled and Multi Input Multi Output (MIMO) design techniques have to be used for the controller design.

4.3. Adaptive Control Design

Longitudinal and lateral-directional models developed in the above section are used for the adaptive control development. Adaptive controllers developed in the previous chapter, for a flexible SLV can be used for this MIMO plant. However, a different projection operator is used for this plant, which will constrain the controller parameters within a minimum and maximum bound.

4.3.1 Using Rectangular Projection Operator

In section 3.3, it is proven that the MRAC law derived using a standard quadratic Lyapunov function is not robust to non-parametric uncertainties. Hence, this control law is modified to achieve more robustness using the projection operator and BLF. In this section, an adaptive control law is derived using a rectangular projection operator to constrain the controller parameters within an upper and lower limit. The design philosophy is similar to that given in section

3.3.1. To derive a rectangular projection based control law, the plant and reference models are re-written here.

$$\begin{aligned}\dot{x} &= Ax + B\Lambda(u + \theta^T \Phi(x)) + B_m u_c + \xi(t) \\ y &= Cx\end{aligned}\tag{4.24}$$

$\xi(t)$ is the uniformly bounded disturbance in R^n and $\|\xi(t)\| \leq \xi_{max}$ where, $\xi_{max} \geq 0$. The diagonal positive-definite matrix $\Lambda \in R^{m \times m}$ and constant matrix $\theta \in R^{N \times m}$ represent the matched uncertainties. The pair $(A, B\Lambda)$ is controllable. The reference model for MRAC is given by

$$\begin{aligned}\dot{x}_m &= A_m x_m + B_m u_c \\ y_m &= C_m x_m\end{aligned}\tag{4.25}$$

The control has to be designed in such a way that the system output (y) tracks the command u_c in the presence of uncertainties keeping all the signals uniformly bounded in time. The feedback control law can be chosen in the form

$$u = -\widehat{\Theta}^T \Phi(x)\tag{4.26}$$

where, $\widehat{\Theta} \in R^{N \times m}$ is the matrix of parameters to be adapted. Using (4.26), the error dynamics can be written as

$$\dot{e} = A_m e - B\Lambda\Delta\theta^T \Phi(x) + \xi(t)\tag{4.27}$$

Lyapunov function is chosen as

$$V(e, \Delta\theta) = e^T P e + \text{trace}(\Delta\theta^T \Gamma_\theta^{-1} \Delta\theta \Lambda)\tag{4.28}$$

where, $e = x - x_m$, $\Delta\theta = \widehat{\Theta} - \theta$ is the parameter estimation error. P is a positive definite matrix which is the solution of the algebraic Lyapunov equation $PA_m + A_m^T P = -Q$, $Q = Q^T > 0$.

$$\begin{aligned}\dot{V}(e, \Delta\theta) &= -e^T Q e + 2\text{trace}(\Delta\theta^T (\Gamma_\theta^{-1} \dot{\widehat{\Theta}} - \Phi e^T P B) \Lambda) \\ &\quad + 2e^T P \xi(t)\end{aligned}\tag{4.29}$$

The adaptation law should ensure the negative semi-definiteness of the derivative of the Lyapunov function ie. $2\text{trace} \left(\Delta\theta^T \left(\Gamma_\theta^{-1} \dot{\hat{\Theta}} - \Phi e^T P B \right) \Lambda \right) \leq 0$ and all the adapted parameters should be uniformly bounded in time. To impose minimum and maximum limit for the adapted gains, a rectangular formulation of the projection operator is used. Consider a convex hypercube in R^n ,

$$\Omega = \{ \theta \in R^n : (\theta_i^{min} \leq \theta_i \leq \theta_i^{max})_{i=1,2,\dots,n} \} \quad (4.30)$$

where, $(\theta_i^{min}, \theta_i^{max})$ are the minimum and maximum bounds for the i^{th} component of the n -dimensional parameter vector θ . Define another hypercube

$$\Omega_\delta = \{ \theta \in R^n : (\theta_i^{min} + \delta \leq \theta_i \leq \theta_i^{max} - \delta)_{i=1,2,\dots,n} \} \quad (4.31)$$

such that $\Omega_\delta \subset \Omega$. A rectangular version of the projection operator can be defined for two 'n' dimensional vectors (θ, y) as

$$\begin{aligned} & Proj_i(\theta, y) \\ &= \begin{cases} \left(\frac{\theta_i - \theta_i^{min}}{\delta} \right) y_i, & [(\theta_i < \theta_i^{min} + \delta) \wedge (y_i < 0)] \\ \left(\frac{\theta_i^{max} - \theta_i}{\delta} \right) y_i, & [(\theta_i > \theta_i^{max} - \delta) \wedge (y_i > 0)] \\ y_i, & \text{otherwise} \end{cases} \end{aligned} \quad (4.32)$$

Suppose that $\theta^* \in \Omega_\delta$ is a constant vector. Then it can be proven that for any $\theta \in \Omega$ and for any $y \in R^n$, the following inequality holds good

$$(\theta - \theta^*)^T (Proj(\theta, y) - y) \leq 0 \quad (4.33)$$

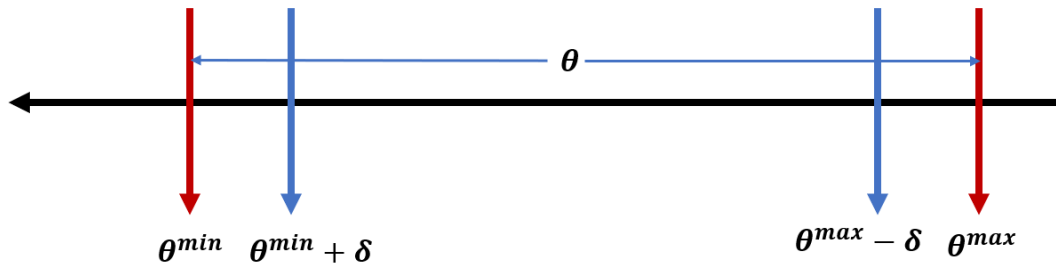


Figure 4.2 Pictorial Representation of Rectangular Projection Operator

Proof: Referring to Figure 4.2, we can see that

When $(\theta_i < \theta_i^{min} + \delta) \wedge (y_i < 0)$, two cases arise:

When $\theta_i < \theta_i^{min} \wedge (y_i < 0)$,

$$\underbrace{(\theta_i - \theta^*)^T}_{<0} \underbrace{\left(\frac{\theta_i - \theta_i^{min}}{\delta}\right) y_i - y_i}_{>0} < 0 \quad (4.34)$$

When $\theta_i > \theta_i^{min} \wedge (\theta_i < \theta_i^{min} + \delta) \wedge (y_i < 0)$,

$$\underbrace{(\theta_i - \theta^*)^T}_{<0} \underbrace{\left(\frac{\theta_i - \theta_i^{min}}{\delta}\right) y_i - y_i}_{>0} < 0 \quad (4.35)$$

When $\theta_i < \theta_i^{min} + \delta \wedge (y_i \geq 0)$, then $Proj(\theta, y_i) = y_i$,

$$\therefore \underbrace{(\theta_i - \theta^*)^T}_{<0} \underbrace{(y_i - y_i)}_{=0} = 0 \quad (4.36)$$

Similarly, when $(\theta_i > \theta_i^{max} - \delta) \wedge (y_i > 0)$, again two cases arise.

When $(\theta_i > \theta_i^{max} - \delta) \wedge (\theta_i < \theta_i^{max}) \wedge (y_i > 0)$, then $\left(\frac{\theta_i^{max} - \theta_i}{\delta}\right) < 1$

$$\underbrace{(\theta_i - \theta^*)^T}_{>0} \underbrace{\left(\frac{\theta_i^{max} - \theta_i}{\delta}\right) y_i - y_i}_{<0} < 0 \quad (4.37)$$

When $(\theta_i > \theta_i^{max}) \wedge (y_i > 0)$, then $\left(\frac{\theta_i^{max} - \theta_i}{\delta}\right) < 0$

$$\underbrace{(\theta_i - \theta^*)^T}_{>0} \underbrace{\left(\frac{\theta_i^{max} - \theta_i}{\delta}\right) y_i - y_i}_{<0} < 0 \quad (4.38)$$

when $(\theta_i > \theta_i^{max} - \delta) \wedge (y_i \leq 0)$, then $Proj(\theta, y_i) = y_i$,

$$\underbrace{(\theta_i - \theta^*)^T}_{>0} \underbrace{(y_i - y_i)}_{=0} = 0 \quad (4.39)$$

Hence, $(\theta - \theta^*)^T (Proj(\theta, y_i) - y_i) \leq 0$ is proved. With the adaptive control law

$$\hat{\theta} = Proj(\hat{\theta}, \Gamma \Phi(x) e^T P B) \quad (4.40)$$

Substituting (4.40) in $2\text{trace}(\Delta\theta^T(\Gamma^{-1}\dot{\hat{\theta}} - \Phi e^T P B)\Lambda)$ and putting $\Phi(x)e^T P B = Y$, we get

$$\begin{aligned} & \text{trace}(\Delta\theta^T\{\Gamma^{-1}\dot{\hat{\theta}} - \Phi(x)e^T P B\}\Lambda) \\ &= \sum_{i=0}^n (\hat{\theta} - \theta)^T_i (\Gamma^{-1}\text{Proj}(\hat{\theta}, \Gamma Y_j) - Y_j)\lambda_j \leq 0 \end{aligned} \quad (4.41)$$

$(\hat{\theta} - \theta)^T_i (\Gamma^{-1}\text{Proj}(\hat{\theta}, \Gamma Y_j) - Y_j) \leq 0$, $\lambda_j \geq 0$, and hence the trace term will be negative semidefinite.

$$\begin{aligned} \dot{V}(e, \Delta\theta) &= -e^T Q e + 2e^T P \xi(t) \\ &\leq -\lambda_{\min}(Q)\|e\|^2 + 2\|e\|\lambda_{\max}(P)\xi_{\max} \\ &= -\lambda_{\min}(Q)\|e\| \left(\|e\| - 2\frac{\lambda_{\max}(P)\xi_{\max}}{\lambda_{\min}(Q)} \right) \end{aligned} \quad (4.42)$$

$\dot{V}(e, \Delta\theta) < 0$ outside of the compact set

$$\begin{aligned} \Omega = \left\{ (e, \Delta\theta) \in R^n \times R^{N \times m}: \|e\| \leq 2\frac{\lambda_{\max}(P)}{\lambda_{\min}(Q)}\xi_{\max} \wedge \|\Delta\theta\|_F \right. \\ \left. \leq \Delta\theta_{\max} \wedge \|\Delta\theta\|_F \leq \Delta\theta_{\min} \right\} \end{aligned} \quad (4.43)$$

where, θ_i^{\max} is the maximum allowable bound for the i^{th} column of θ and θ_i^{\min} is the minimum bound. Hence all the signals of the closed-loop system are UUB with this adaptation law allowing the closed-loop system to track the reference command with errors bounded as in (4.43).

The projection operator ensures that the adaptive time-varying matrix $\hat{\theta}(t)$ do not exceed their pre-specified bounds $(\theta^{\min}, \theta^{\max})$ and also ensures the negative semi-definiteness of the time derivative of the Lyapunov function. This gives UUB of adapted parameters. The advantage of this update law is that the method can provide a higher adaptation rate and more robustness towards parametric and non-parametric uncertainties.

4.3.2 Using Barrier Lyapunov Functions

Adaptive control parameter update law based on BLF is the same as that explained in section 3.3.2. Here the bounds on the adapted gains can be specified in the convex function but the bounds on the tracking error cannot be specified. For complex systems, it is very difficult to find an explicit relation between the trajectory tracking error and the solution of the Lyapunov equation underlying the adaptive law. Hence BLF is introduced to guarantee the boundedness of tracking error and adapted gains within the defined constraints. To establish the asymptotic convergence of the signals, the continuity properties of the derivative of the Lyapunov function can be analyzed using Barbalat's Lemma.

4.4. Results and Discussions

RLV systems are designed to perform multiple missions. There are two major flight phases for a mission, (i) Ascent phase in which the RLV ascends through the dense atmosphere to the orbit and (ii) Descent phase. The descent phase is further divided into deboost phase in which the RLV is de-orbited from an orbit of 400 km and brought to the re-entry point and the re-entry phase. The re-entry phase starts from around 120 km. During this phase of RLV flight, almost all vehicle energy is dissipated through atmospheric drag and this phase extends from hypersonic Mach to supersonic Mach numbers. Next is the Terminal Area Energy Management (TAEM) phase in which energy level of vehicle is further decreased. The last phase is the approach and landing phase where the vehicle is prepared for automatic landing.

In this work, adaptive controllers are designed to control the rotational dynamics of RLV. The closed loop guidance system controls the translational dynamics. Entry guidance system steers the vehicle to the TAEM transit point meeting the range requirements and satisfying the constraints. Usually, optimal control techniques are used for launch vehicle guidance system design. But this results in non-linear two-point boundary value problem which is difficult to solve.

Entry guidance algorithms available in the literature mostly use a trajectory planner to generate a feasible trajectory and a tracker to follow the planned trajectory [80]. The re-entry guidance system commands the AoA and bank angles to control the trajectory and to bring the vehicle to the desired landing site.

This chapter describes the attitude control responses of the RLV during the approach and landing phase. The function of the attitude control system is to follow AoA (α_c), bank angle (σ_c) commands from the guidance system and angle of sideslip (β) is regulated. For the RLV considered in this simulation, both pitch and roll control are by elevons and the yaw control is by rudders. Integrator states are also augmented to the longitudinal and lateral directional plant dynamics in alpha, beta and sigma channels.

RLV plant is simulated with open-loop guidance commands and the modified adaptive controllers. The performance of these controllers is compared with the regular Lyapunov based adaptive control law. These controllers require full state feedback and the measurements of all the states are available. To assess the stability and robustness of the controllers, extensive perturbation studies are conducted. The actuator dynamics is not considered during the design of the controllers. But in simulations, a nonlinear second order actuator model for both rudder and elevons with a limit on the maximum deflection, slew rate limit and angular acceleration is included.

4.4.1 Studies with Nominal RLV Plant

In this study, only the approach and landing phase of RLV is simulated. Open-loop guidance commands (α_c and σ_c) are applied to the nominal plant. Here it is assumed that the RLV is dropped from a helicopter and when the dynamic pressure picks up, a pull up manoeuvre is performed followed by a flare manoeuvre and landing. Aggressive bank angle commands are given to the plant to demonstrate the tracking performance in the lateral plane. The attitude controller should follow the guidance commands without much tracking error to achieve the precise landing point.

Tracking responses for a nominal plant is shown from Fig. 4.3 to Fig. 4.7. It can be seen from Fig. 4.4 that all the three controllers follow the AoA (α_c) command closely. Projection based controller gives the least tracking error. AoA error is more during the initial phase, since the control force is minimum as the dynamic pressure is less. Projection based controller demands maximum rate to track the alpha command which in turn produces the least tracking error. Control deflection requirement is slightly higher for the BLF based controller in the alpha channel during initial capture where the dynamic pressure and control effectiveness is less. This causes slight oscillations in the longitudinal responses for BLF based controller. As per formulation, BLF based controller tries to limit the tracking error within the user defined limit by demanding maximum control deflection. This can be reduced by proper tuning of the reference model or reduction in the tracking error weightage matrix used to define the constraint set and BLF. Bandwidth of the reference model can be reduced initially during the low control effectiveness regime.

Banking manoeuvre starts from 15 s onwards and a 10 deg/s command is given for 5 s. A bank reversal is performed at 23 s with the same rate as seen from Fig. 4.4. It can be observed that all three controllers show very good tracking of bank angle commands (σ) and the angle of sideslip (Beta- β) is regulated. Least β build up is exhibited by the controller using BLF for parameter update followed by projection-based controller. Fig. 4.5 shows the tracking error when various controllers are simulated during banking manoeuvre. Barrier Lyapunov based controller gives the least tracking error followed by the projection based controller and quadratic Lyapunov based controller. Fig. 4.6 shows the control demand in pitch/yaw/roll planes. Control demand in yaw and roll planes comes when the bank angle command tracking starts. This causes a build-up in beta and the rudders generate commands to regulate this beta. Tracking of σ command is achieved by deflecting elevons in a differential manner. Control demand in yaw/roll planes is slightly higher for projection based controller. In the lateral-directional plane barrier Lyapunov is giving a slightly better performance (in terms of σ tracking error and beta build up) compared to other two control schemes. Fig. 4.7 give the

control command to the various effectors. All the three controllers demand the same control for the nominal case.

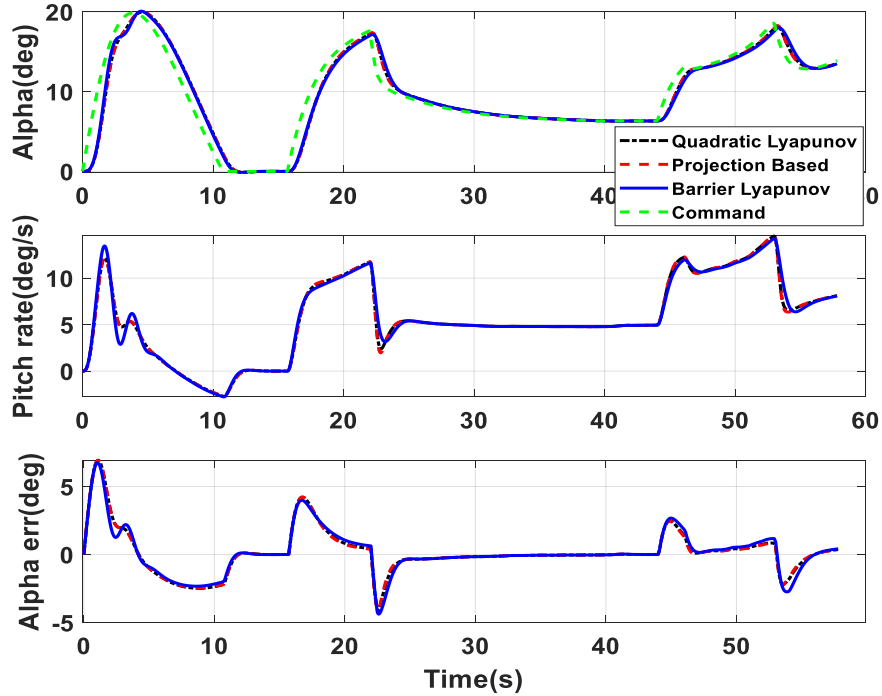


Figure 4.3 Longitudinal Plane Responses for Nominal Case

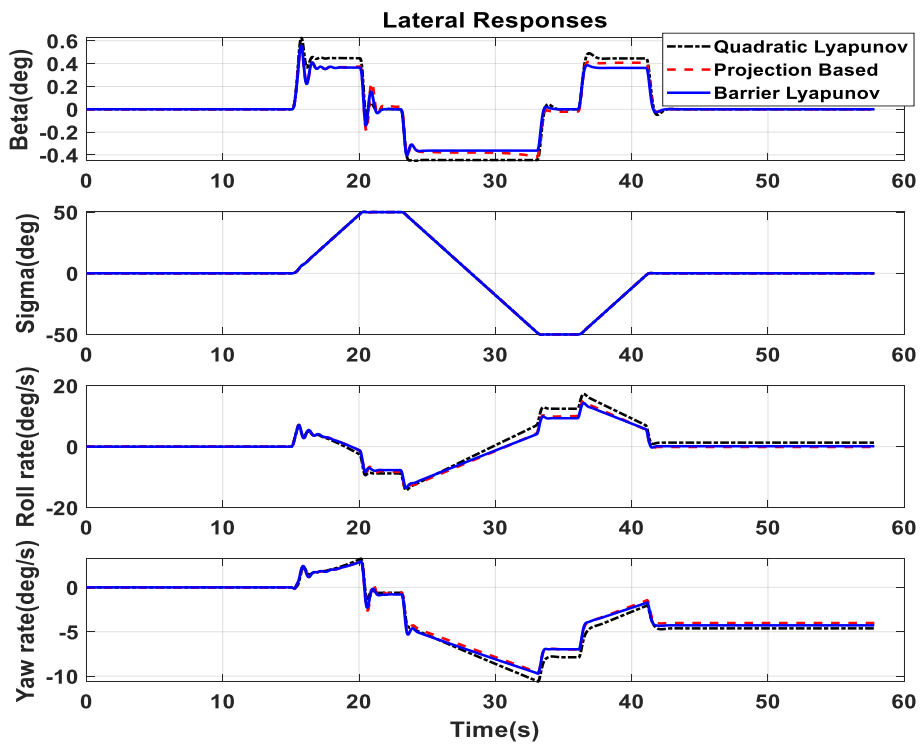


Figure 4.4 Lateral Plane Responses for Nominal Case

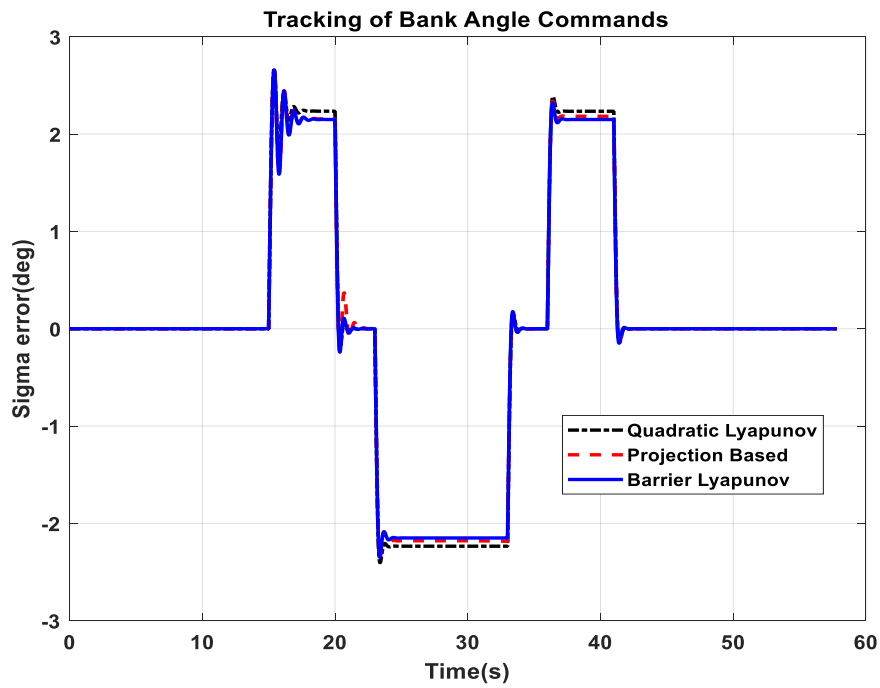


Figure 4.5 Bank Angle Tracking Error for the Nominal Case

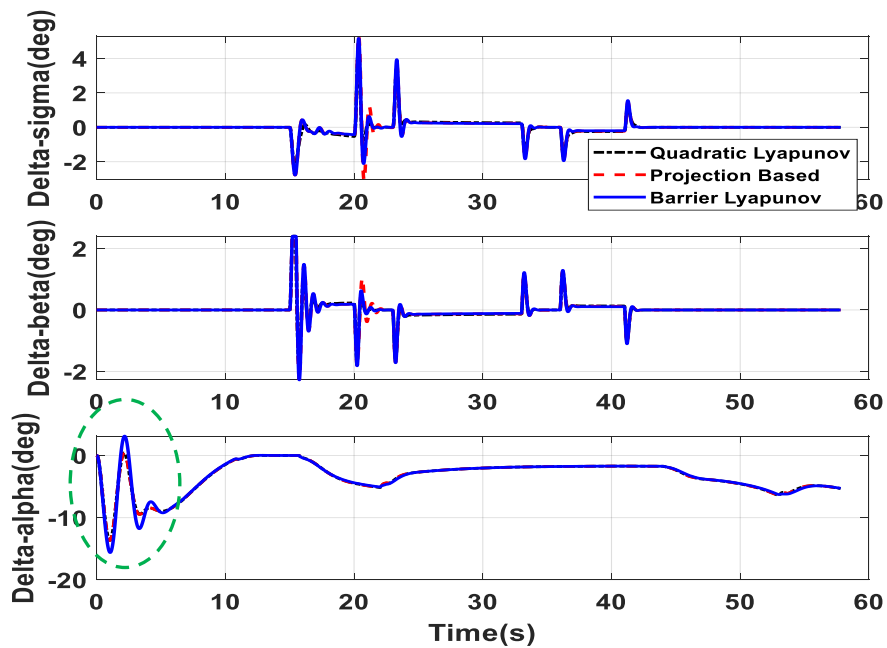


Figure 4.6 Control Demand in Roll/Yaw/Pitch Planes for the Nominal Case

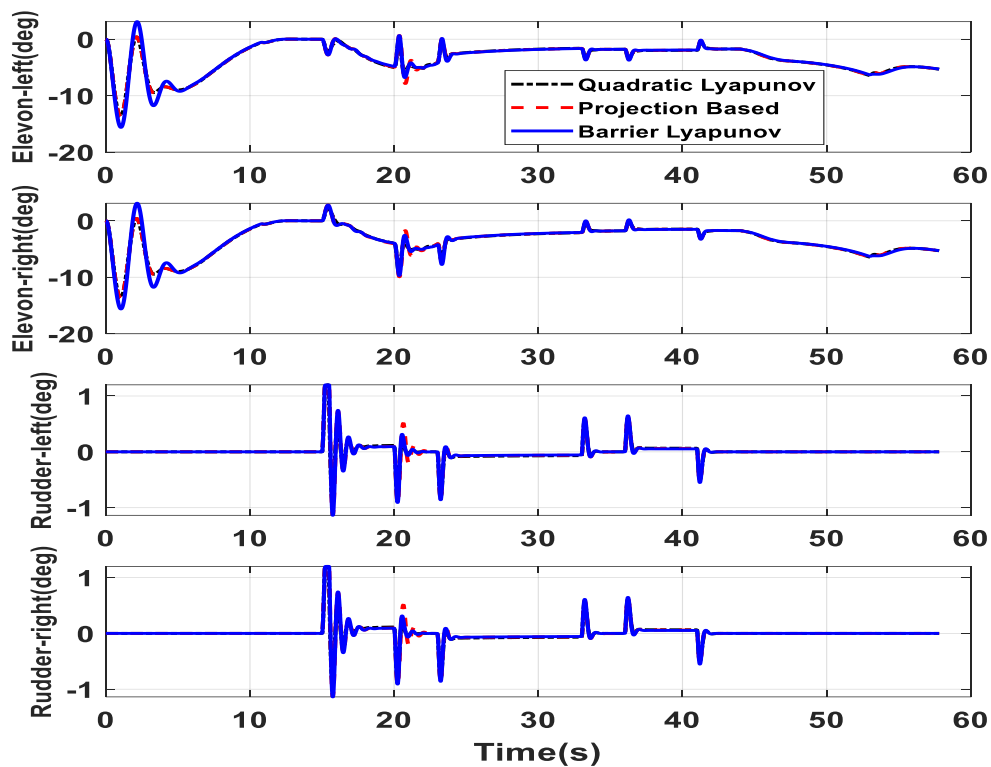


Figure 4.7 Control Deflection of Various Effectors for the Nominal Case

4.4.2 Studies with Perturbed RLV Plant

Plant parameter perturbation studies are done to assess the robustness of the various adaptive controllers. Parameters are perturbed in such a way as to increase the disturbance moments, coupling and to decrease the control efficiency. To study the gain margin loss, control effectiveness is increased beyond the specifications and disturbance moments are minimised. These perturbations are consolidated in Table 4.1.

Results of the perturbation studies are shown in the following figures and it is consolidated in Table 4.2. In Case 2, perturbations are given in such a way that the aero disturbances are maximised and the control moments are minimised. Responses are given in Fig. 4.8 to Fig. 4.11.

Table 4. 1 Plant Parameter Perturbations for Different Cases

Case	Condition	Remarks
1	Nominal	
2	$C_m=45\%; C_z=40\%; C_{m_{\delta e}}=-20\%;$ $C_{m_{\delta r}}=-50\%$	Perturbations in longitudinal plane: - Aero disturbance moment increased and control moment reduced
3	$C_m=-40\%; C_z=-30\%; C_{m_{\delta e}}=40\%;$ $C_{m_{\delta r}}=20\%;$	Perturbations in longitudinal plane: - Aero disturbance moment reduced and control moment increased
4	$C_m=20\%; C_n=120\%; C_l=140\%;$ $C_z=20\%; C_y=20\%; C_{m_{\delta e}}=-30\%;$ $C_{m_{\delta r}}=40\%; C_{l_{\delta e}}=-90\%; C_{n_{\delta e}}=-$ $90\%; C_{l_{\delta r}}=440\%; C_{n_{\delta r}}=-20\%$	Combined worst case perturbation in longitudinal and lateral
5	$C_m=50\%; C_n=220\%; C_l=240\%;$ $C_z=20\%; C_y=20\%; C_{m_{\delta e}}=-20\%;$ $C_{m_{\delta r}}=-50\%; C_{l_{\delta e}}=-50\%; C_{n_{\delta e}}=0\%;$ $C_{l_{\delta r}}=-60\%; C_{n_{\delta r}}=-50\%$	Combined worst case perturbation in longitudinal and lateral

Tracking of α_c command is shown in Fig. 4.8. All the controllers are trying to follow the command, the proposed controllers are giving better performance compared to the quadratic Lyapunov based controller. When the dynamic pressure is low at the beginning (during drop), barrier Lyapunov is trying to reduce the tracking error (as formulated in the Lyapunov equation) by increasing the control deflection and hence slightly oscillatory response is observed during the initial capture. But as time progresses, barrier Lyapunov based controller is giving a better performance in terms of tracking error and stability. Projection based controller maintains a consistent performance always as it is maintaining the controller parameters within the allowable limits. Quadratic Lyapunov based control deflections abruptly saturate as the parameters are perturbed and the longitudinal plane responses are oscillatory near the touch down point. Such abrupt change in behaviour is not acceptable for a flight control system. The control responses should gracefully degrade in presence of nonlinear actuator and parameter perturbations.

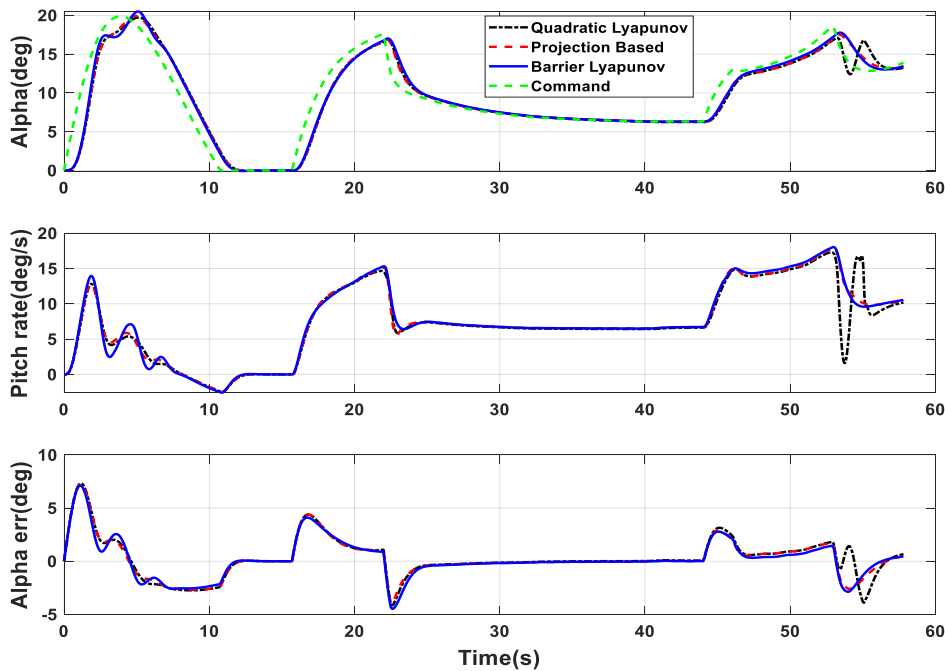


Figure 4. 8 Longitudinal Plane Responses for Perturbed Case 2

Fig. 4.9 gives the lateral plane responses which is similar to nominal case. Beta build up is maximum for quadratic Lyapunov based controller and barrier Lyapunov gives the least sideslip angle. The bank angle tracking error is the least for barrier Lyapunov followed by Projection based controller and quadratic Lyapunov based controller. Fig. 4.10 gives the control demand in all channels and Fig. 4.11 gives the individual control deflections of various effectors. Control demand in alpha channel during the initial drop phase is high (nearly saturated) for barrier Lyapunov based controller. This controller is trying to minimise the trajectory tracking error during the low dynamic pressure regime by increasing the control deflection. This resulted in small oscillations at the beginning but later it is giving the best performance.

When a sigma command with a rate of 10 deg/s is given at 15 s, all three adaptive controllers give oscillatory response, but gradually improve with barrier Lyapunov giving the least tracking error. Control deflections for quadratic Lyapunov controller is more during the later stages and gets saturated near the landing phase. This causes oscillations in the longitudinal responses, whereas the other two controllers perform as in nominal simulations.

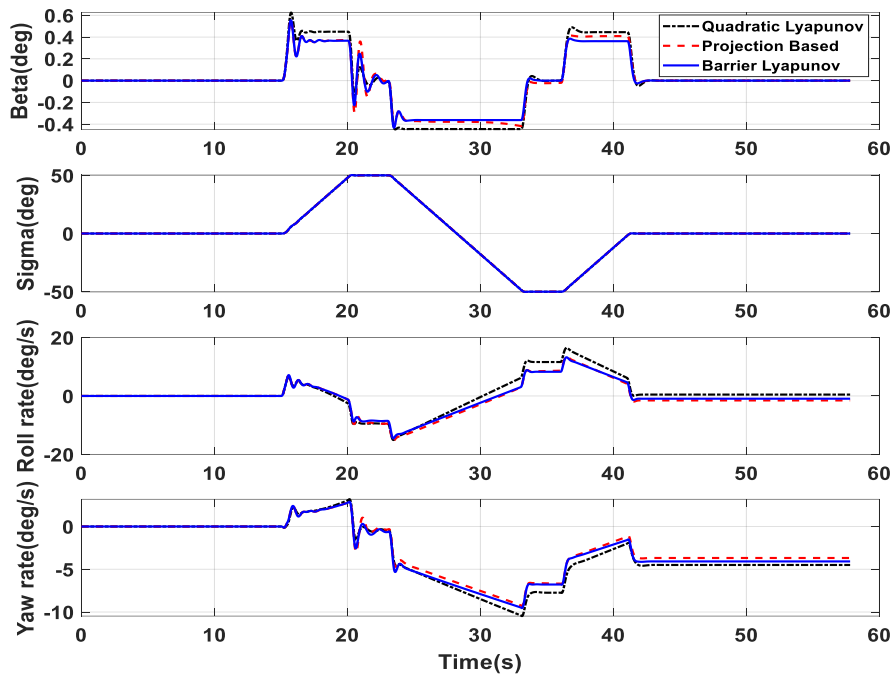


Figure 4. 9 Lateral Plane Responses for Perturbed Case 2

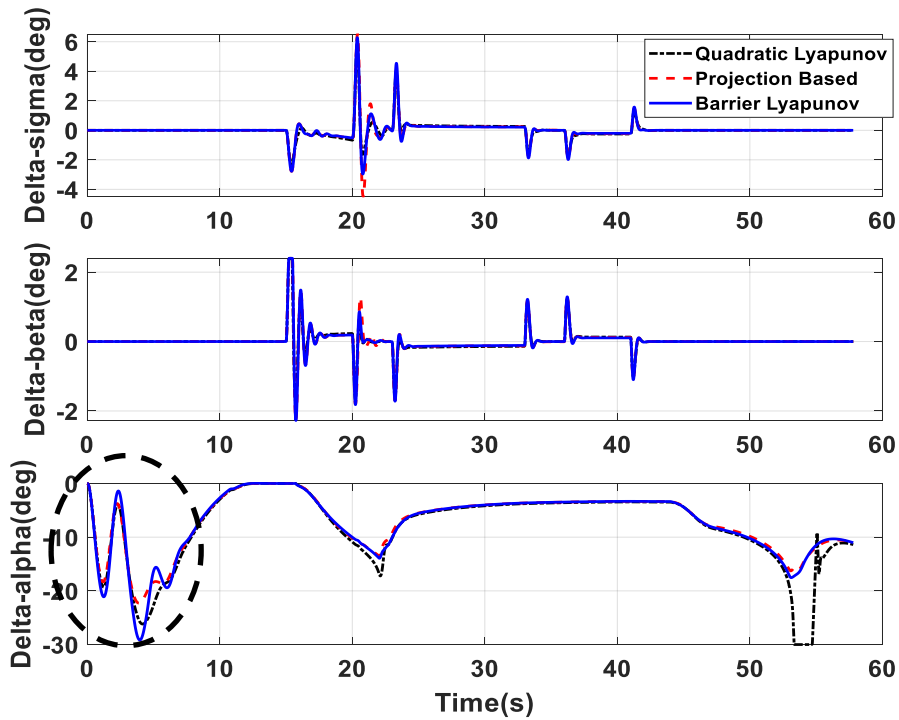


Figure 4. 10 Control Demands in Roll/Yaw/Pitch Channels for Perturbed Case 2

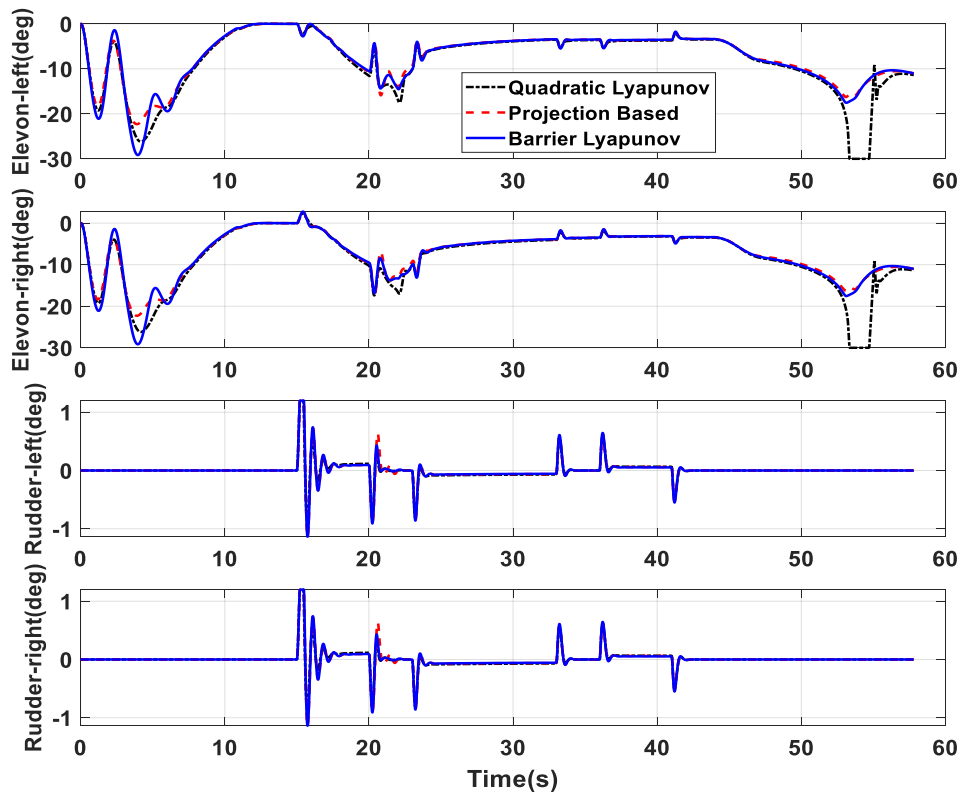


Figure 4. 11 Control Deflections of Effectors for Perturbed Case 2

In case 3, a gain margin loss case is simulated in which the control deflections are increased and the aerodynamic disturbances are minimised. Fig. 4.12 gives longitudinal plane responses. Attitude rates and angles are diverging for simulations with quadratic Lyapunov based controller. Here the actuators are not saturated. Fig. 4.13 gives the control demands in various planes. Projection based and BLF based controllers are giving near nominal performance with slightly higher control deflections.

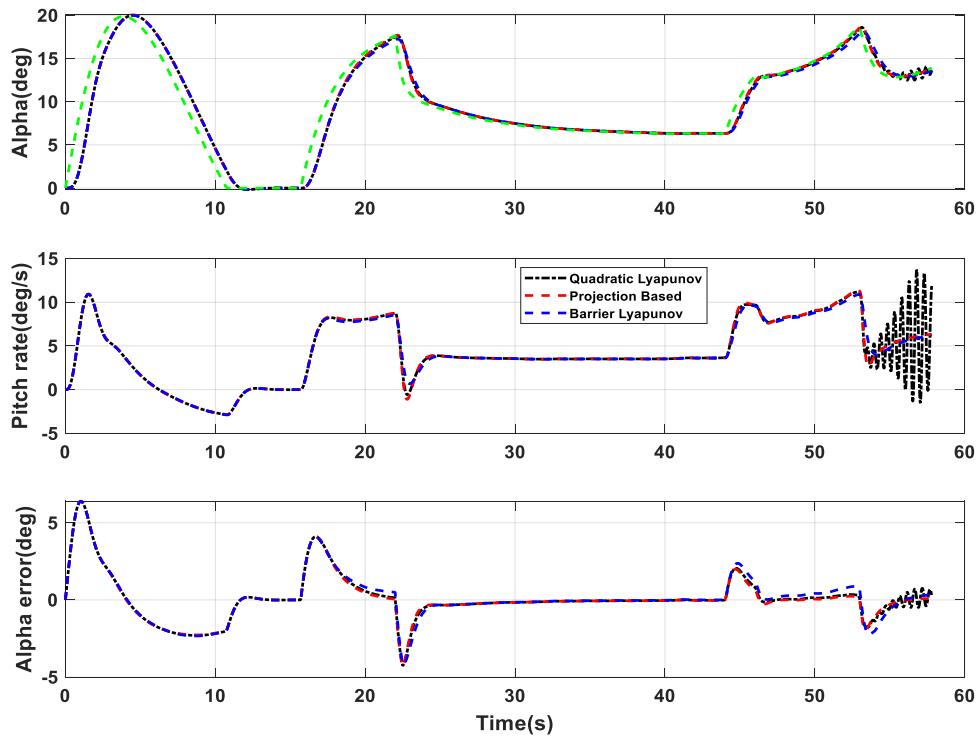


Figure 4. 12 Longitudinal Plane Responses for Case 3

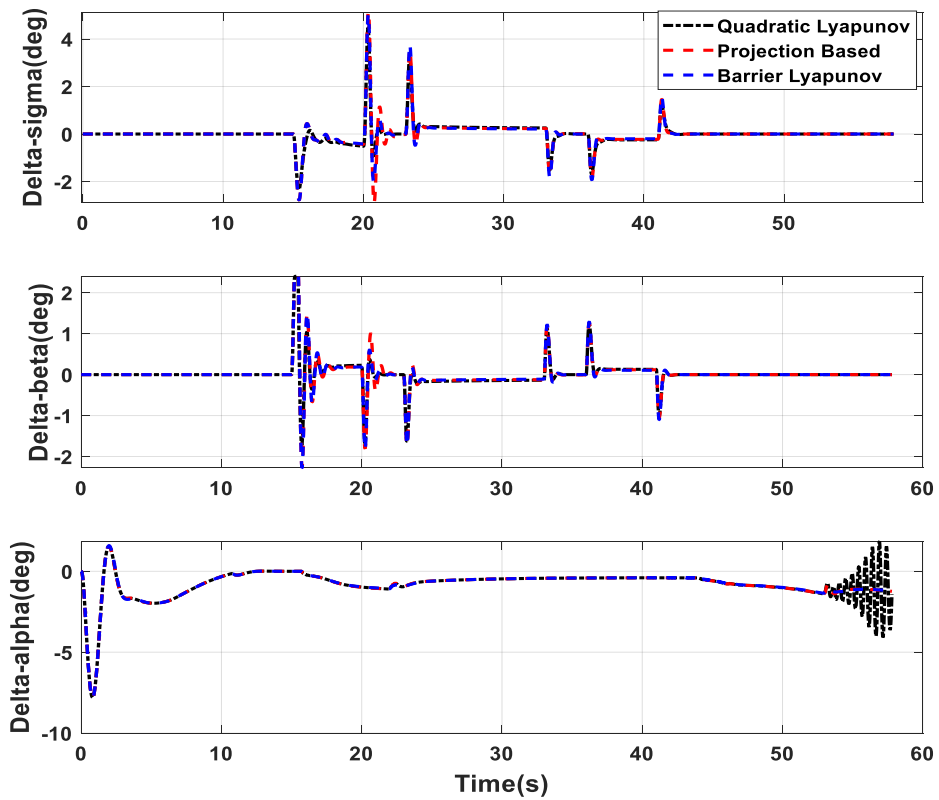


Figure 4. 13 Control Demands in Roll/Yaw/Pitch Channels for Case 3

Cases 4 and 5 are combined worst case perturbations in both longitudinal and lateral channels. The performances are comparable for all three controllers for case 4. The control is saturated for barrier Lyapunov based adaptive scheme during the initial drop phase but recovers fast. The corresponding responses are shown from Fig. 4.14 to Fig. 4.16.

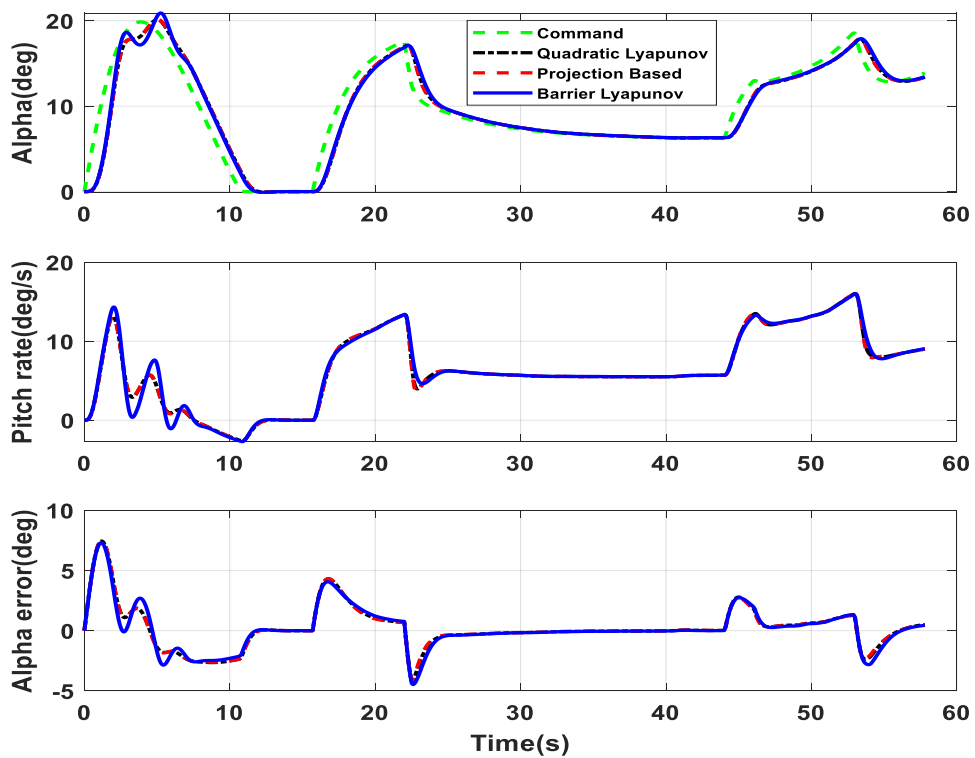


Figure 4. 14 Longitudinal Plane Responses for Case 4

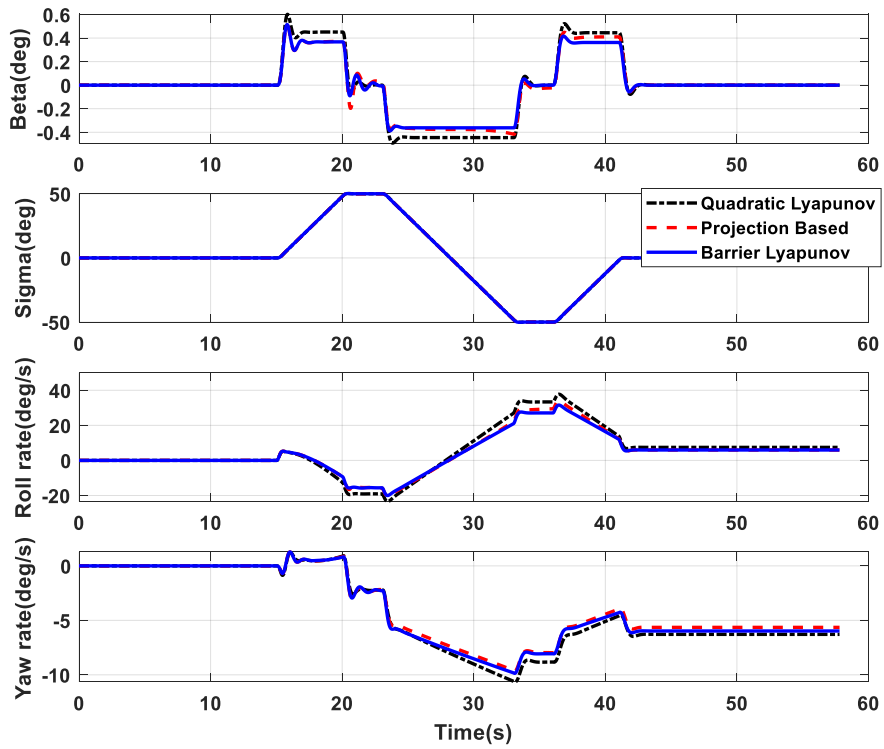


Figure 4.15 Lateral Plane Responses for Case 4

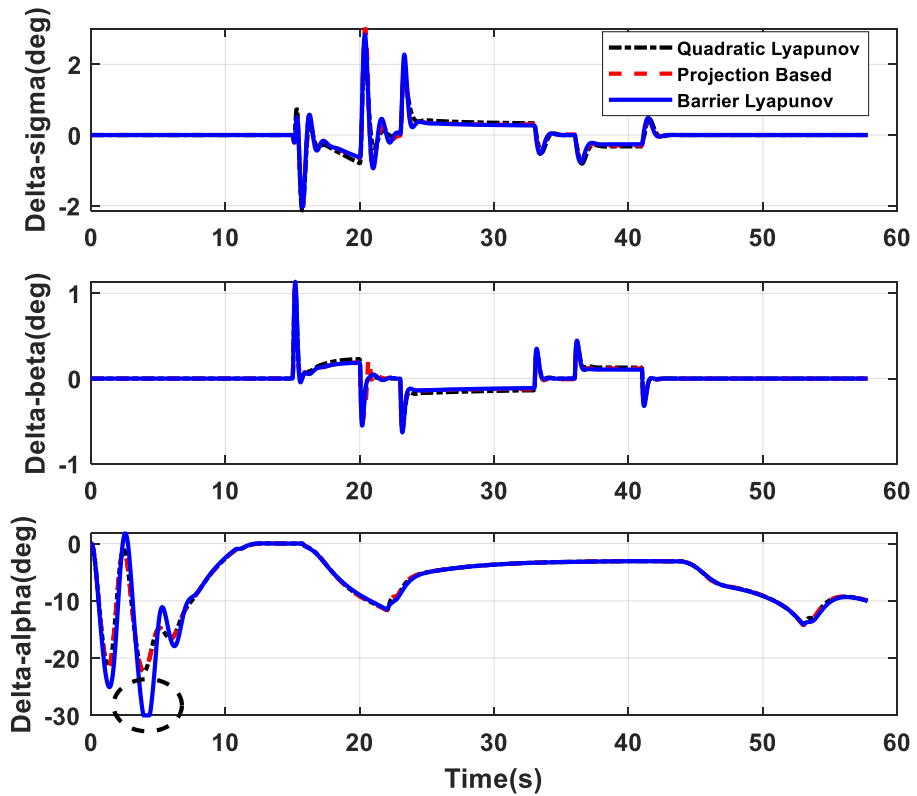


Figure 4.16 Control Demands in Roll/Yaw/Pitch Channels for Case 4

For case 5, simulation fails for adaptive control with quadratic Lyapunov functions. Other controllers give a near nominal performance. Here severe perturbations are given in both longitudinal plane and lateral-directional plane. For the quadratic Lyapunov based controller, slew rate limits of the actuators are touched for the elevon actuators and system become unstable. Hence oscillations started when a large sigma command is provided. Finally, it fails in the longitudinal plane also. The performance of the proposed controllers also is slightly degraded due to large perturbations. The corresponding responses are shown from Fig. 4.17 to Fig. 4.19. This simulation shows that the proposed adaptive controllers based on rectangular projection operator and BLF are more robust towards non-linear actuator dynamics and is able to handle more parameter perturbations.

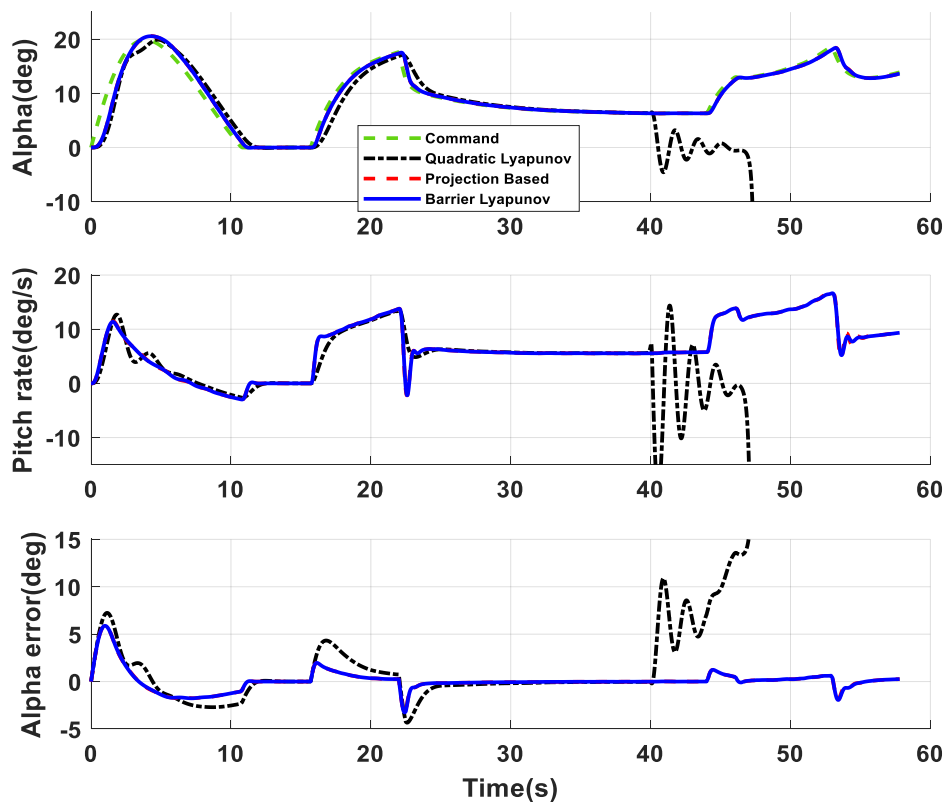


Figure 4. 17 Longitudinal Plane Responses for Case 5

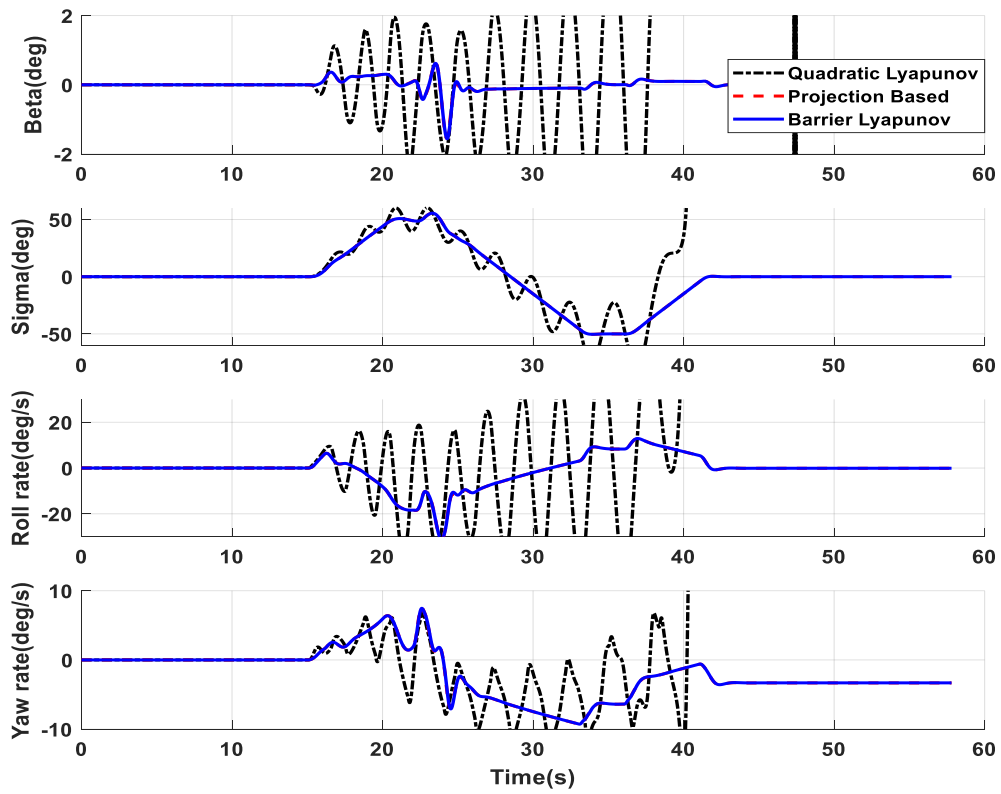


Figure 4.18 Lateral Plane Responses for Case 5

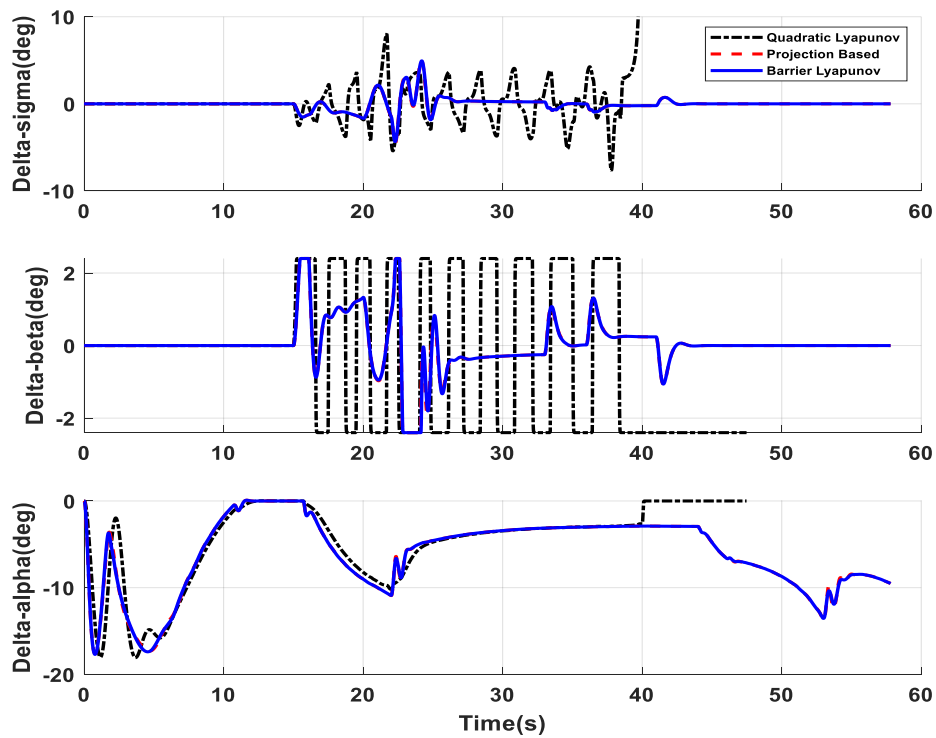


Figure 4.19 Control Demands in Roll/Yaw/Pitch Channels for Case 5

The results of the simulations are consolidated in Table 4.2.

Table 4. 2 Performance Evaluation of Various Controllers During Approach and Landing Phase of RLV

Case Definition	Control Schemes	Simulation passed/ Not	Max. Alpha Error (deg)	Steady State Sigma error (deg)	Max. Beta (deg)	Max. Elevon Deflection (deg)	Max. Rudder Deflection (deg)	Remarks
Case 1 Nominal	Barrier Lyapunov	Y	6.7	2.15	0.36	-15.57	1.2	Normal
	Projection Based	Y	6.87	2.18	0.40	-13.5	1.2	Normal
	Quadratic Lyapunov	Y	6.94	2.23	0.468	-13.6	1.2	Normal
Case 2	Barrier Lyapunov	Y	7.11	2.15	0.36	-29.15	1.2	Control near saturation
	Projection Based	Y	7.27	2.18	0.4	-22.12	1.2	Normal
	Quadratic Lyapunov	Y	7.32	2.4	0.49	-30	1.2	Control saturated
Case 3	Barrier Lyapunov	Y	6.3	2.15	0.36	-7.77	1.2	Normal
	Projection Based	Y	6.4	2.18	0.4	-7.6	1.2	Normal
	Quadratic Lyapunov	Y	6.41	2.4	0.49	-7.7	1.2	Divergence in longitudinal response
Case 4	Barrier Lyapunov	Y	7.3	2.15	0.36	-30	0.21	Control saturated
	Projection Based	Y	7.5	2.2	0.41	-22	0.23	Normal
	Quadratic Lyapunov	Y	7.6	2.5	0.5	-23	0.25	Normal
Case 5	Barrier Lyapunov	Y	7.44	2.312	0.414	-18.1	2	Normal
	Projection Based	Y	7.54	2.427	0.433	-17.8	2	Normal
	Quadratic Lyapunov	N	-	-	-	-	2	Failure in lateral/longitudinal plane

From Table 4.2 it can be inferred that projection based controller gives maximum stability for combined worst case perturbations. The gains are allowed to vary strictly between the stability boundaries specified by the gains' upper bound and lower bound values. Barrier Lyapunov based controller also show very good performance. In certain extreme perturbation cases, this controller tries to minimise the tracking error by increasing the control effort, which results in control saturation.

4.4.3 Disturbance Rejection Studies

Wind disturbance rejection studies are conducted by injecting wind gusts of different magnitudes in alpha and beta channels. All three controllers are exhibiting similar performance in these studies. Fig. 4.20 gives the longitudinal responses of the controllers. Here wind gusts are applied at 14 s, 35 s, 40 s and at 55 s near the landing time. At 35 s and 40 s, alpha was already ramping down with a body rate of 5 deg/s. When wind gust is applied, control commands and body rates show oscillatory behaviour at these points as observed from Fig. 4.21 to Fig. 4.22. In the lateral channel, barrier Lyapunov shows the least tracking error and better disturbance rejection as observed from Fig. 4.23 to Fig. 4.24.

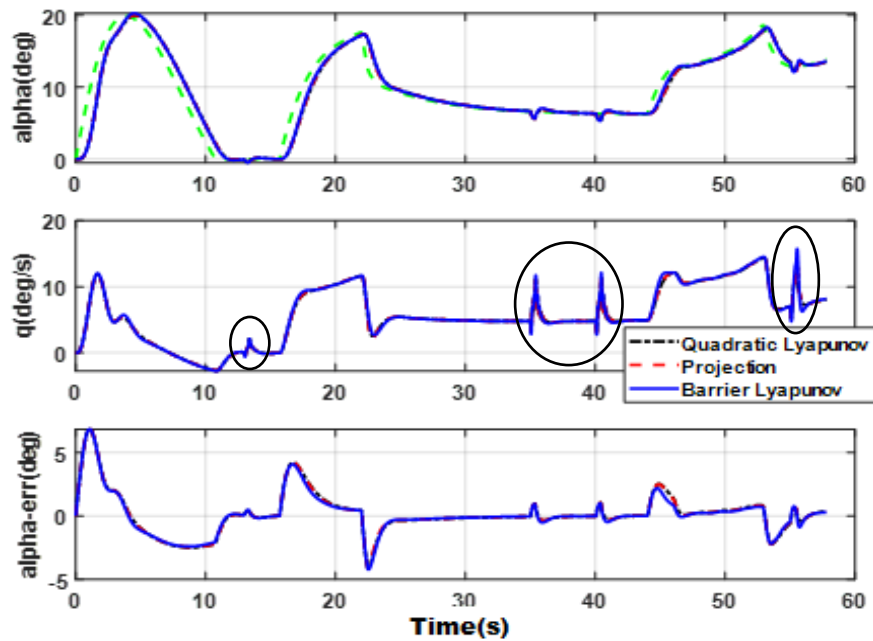


Figure 4. 20 Longitudinal Plane Responses with Wind Gust

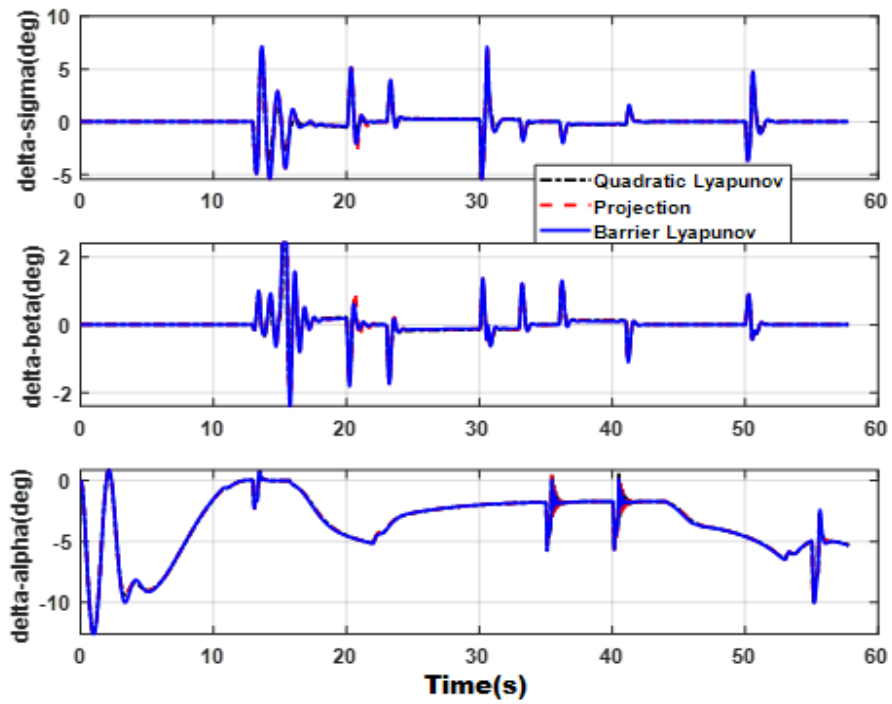


Figure 4. 21 Control Demands in Roll/Yaw/Pitch Channels with Wind Gust

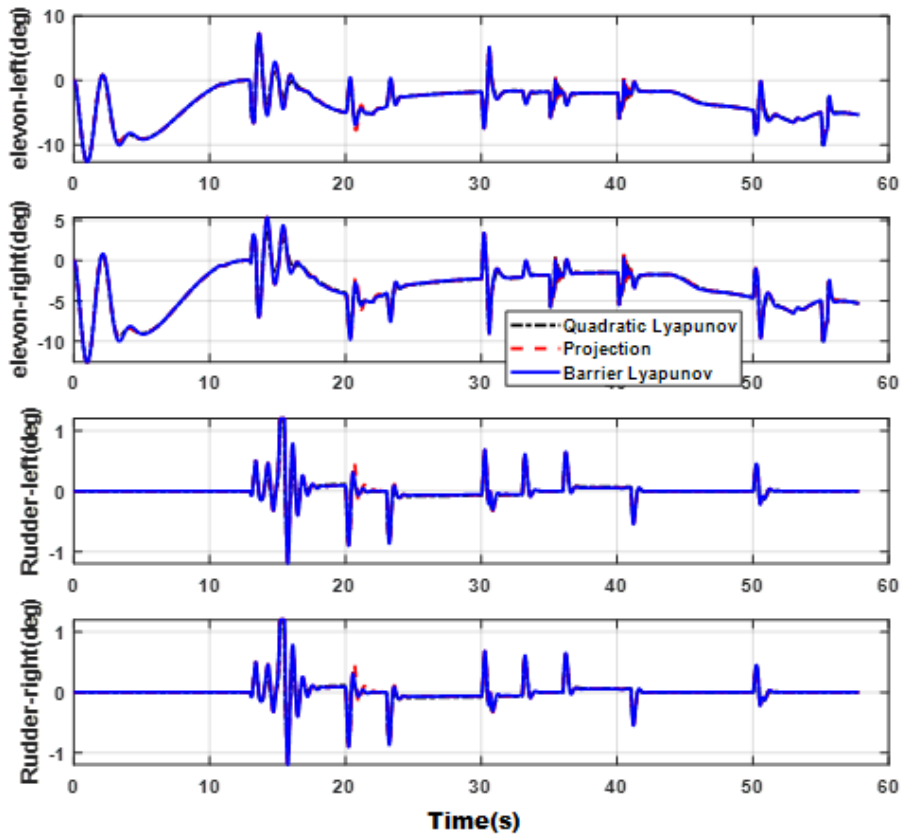


Figure 4. 22 Control Deflections of Effectors with Wind Gust

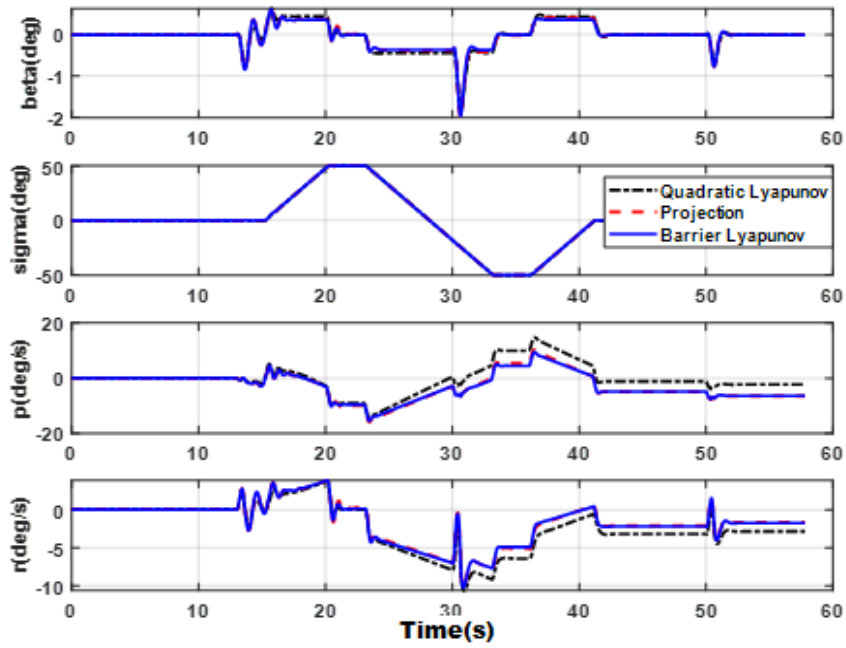


Figure 4.23 Lateral Plane Responses with Wind Gust

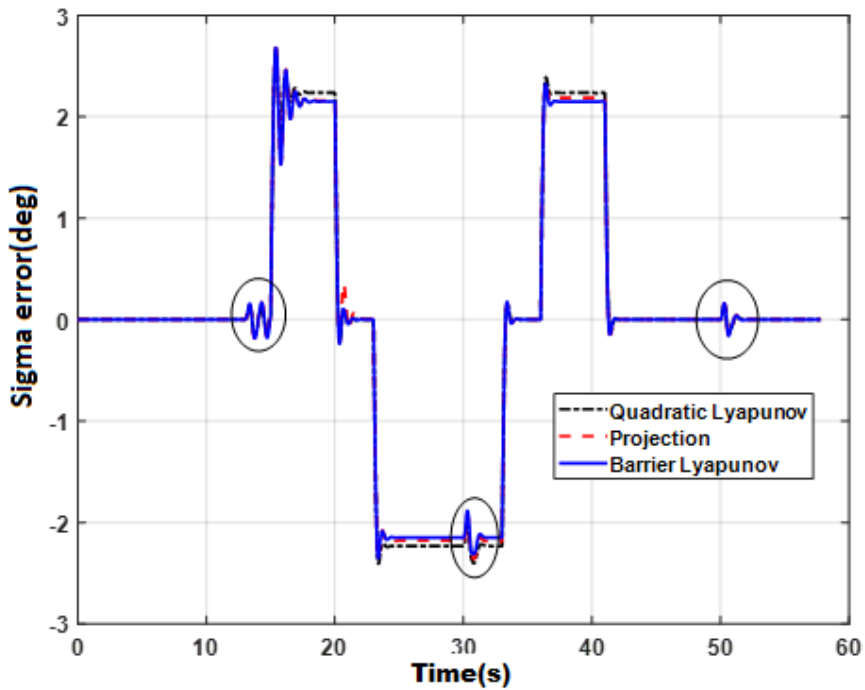


Figure 4.24 Bank Angle Tracking with Wind Gusts Applied

4.5. Summary

Adaptive control laws designed for the approach and landing phase of a winged re-entry vehicle using BLF and a rectangular projection operator are presented in this chapter. Extensive simulation is carried out for the proposed update laws under normal and perturbed conditions and results are compared with existing quadratic Lyapunov based controller update law. Under normal conditions (without perturbations), all the three controllers provided excellent performance. For conditions in which aero disturbance moment is maximised and control effectiveness is reduced, the quadratic Lyapunov based control showed control saturation and oscillatory response. Barrier Lyapunov and projection based controller gave near nominal responses. Control effort required is more for barrier Lyapunov based controller. For the combined worst-case perturbation, simulation failed for the quadratic Lyapunov based controller and control goes near saturation for the proposed updated laws but responses are good.

Chapter 5

Conclusions and Future Scope

A set of dynamic models for a flexible launch vehicle and a winged re-entry vehicle were developed. These models are complex and as such cannot be used for control design purpose. Hence control design models were developed stating various assumptions used for the derivation. The need for advanced control system design for the futuristic STS was emphasized with an appropriate literature survey.

The rigid body equations were derived and reduced to a simplified transfer function model. This was converted to a second order state-space model. Adaptive PD/PID controllers were developed in MRAC framework using standard quadratic Lyapunov function for the time varying launch vehicle plant in the atmospheric phase. It was proved using Lyapunov stability and Barbalat's Lemma that the time-varying system is robust to parametric uncertainties and all the signals are bounded. The performance of the designed controllers was compared with existing gain scheduled PD/PID controllers.

The rigid body model of the SLV was augmented with slosh and flexibility. The adaptive controller based on the quadratic Lyapunov law was not robust to bounded disturbance. Hence modifications were proposed on the controller parameter update law based on projection operator and barrier Lyapunov functions. It was proved that these adaptive controllers provide excellent tracking of the guidance commands and all the other signals are bounded even in the presence of non-parametric uncertainties. This was demonstrated using extensive simulations. An EKF was used to estimate all the states of the plant from noisy measurements which are used for feedback. An adaptive control algorithm to avoid actuator saturation was studied for this plant. Here both control input and reference model dynamics are varied to avoid both position and slew rate saturation of the actuator.

The proposed adaptive controllers based on projection and BLF were applied to a winged re-entry vehicle to track the angle of attack and bank angle commands during the approach and landing phase. 6 DoF rigid body equations were developed and a control design oriented model was developed from these equations using various assumptions. Here the projection operator was re-defined to constrain the gains within the upper and lower bounds simultaneously. Both the trajectory tracking error and gains were constrained using barrier Lyapunov functions. Tracking capability, robustness and disturbance rejection properties are demonstrated using extensive simulations.

5.1 Future Scope

This section provides potential future directions of research in continuation of this work. As mentioned in the introduction section, adaptive controllers are not widely used in the flight control systems because of the difficulty in translating the flight control certification guidelines defined for classical controllers to the adaptive control domain. Major questions raised against the use of adaptive controllers in flight control systems are the following:

- (i) Is there any possibility that the adaptive controllers can cause the loss of the vehicle?
- (ii) Is it possible for the adaptive controllers to recover back from a failure in adaptation?
- (iii) Is it possible to test the adaptive controllers in flight safely?

The first two questions are related to the incorrect learning of the adaptive controller. It is very difficult to show that an adaptive controller will not learn incorrectly. After learning incorrectly, whether it will be able to come back is the next issue to be addressed. Future adaptive control systems for flight should address these questions correctly to get it certified for flight. Third question is regarding the testability. Limited tests only will be possible during the flight. Extensive simulations are to be performed in ground to demonstrate the robustness and

stability of the controllers. This is the case with classically designed gain scheduled controllers also. Hence flight control certification requirements of the adaptive control should be clearly spelt out. This is another future research direction.

It is very difficult to ensure transient responses of the adaptive controller. In order to improve the transient response characteristics of adaptive controllers, the use of closed loop reference models is proposed in literature. The proposed control laws can be modified using these closed loop reference models in which an observer like gain is added in the reference model with feedback from the plant states.

The proposed adaptive controllers are designed for a slender flexible launch vehicle and for an RLV in the descent phase of flight. Hypersonic air breathing propulsion is the key technology needed for a sustained hypersonic cruise and improving the payload capability of the launch vehicle. Here the airframe will be integrated with scramjet/ramjet propulsion. For an air breathing launch vehicle, there is large interaction between aerodynamics, structure and propulsion system.

In hypersonic propulsion, the entire aerodynamic configuration must be considered as part of the propulsion system. The stability and control of the hypersonic vehicle becomes sensitive to changes in the angle of attack as it induces variations in the thrust vector magnitude and direction. Significant elastic and rigid body interactions are likely at hypersonic speeds. This in turn influences the flow conditions at the engine inlet. The need for low structural weight calls for low frequency bending modes. These couplings have to be considered in flight control system design. The extension of the proposed adaptive controllers to such highly coupled systems is another future direction. In this scenario, the function approximation technique based approaches can very well be used in which the flexible modes and their interactions with rigid body and aerodynamics can be modelled as unstructured uncertainties. This is an interesting future direction. Intelligence-based control strategies such as neural networks, fuzzy systems etc. can also be explored for such systems.

Bibliography

- [1] Karl J. Astrom and Bjorn Wittenmark, *Adaptive Control*, Second Edition, Pearson Education, 1994.
- [2] Petros A. Ioannou, Jing Sun, *Robust Adaptive Control*, Dover Publications, Inc, New York, 2012.
- [3] Eugene Lavretsky, Kevin A. Wise, *Robust and Adaptive Control with Aerospace Applications*, Springer, London, 2013.
- [4] Greensite, A. L., *Control Theory: Volume II – Analysis and Design of Space Vehicle Flight Control Systems*, Spartan Books, Mcamillan & Co. Ltd., London, UK, 1970.
- [5] Wie, B., *Space Vehicle Dynamics and Control*, AIAA Education Series, 1998.
- [6] Blakelock, J., *Automatic Control of Aircraft and Missiles*, John Wiley & Sons, New York, 1991.
- [7] Sankar Sastry and Mark Bodson, *Adaptive Control – Stability, Convergence and Robustness*, Prentice Hall, NJ, 1989.
- [8] Jeb S. Orr, Tannen S. VanZwieten, “Robust, Practical Adaptive Control for Launch Vehicles”, *AIAA Guidance, Navigation and Control Conference*, Minneapolis, Minnesota, August 2012.
- [9] Evgeny Kharisov, Irene M. Gregory, Chengyu Cao, Naira Hovakimyan, “L1 Adaptive Control Law for Flexible Space Launch Vehicle and Proposed Plan for Flight Test Validation”, *AIAA Guidance, Navigation and Control Conference and Exhibit*, August, 2008.
- [10] Uzair Ansari, Saqib Alam and Syed Minhaj un Nabi Jafri, “Trajectory optimization and Adaptive Fuzzy based Launch Vehicle Attitude Control”, *20th Mediterranean Conference on Control & Automation (MED)*, 2012.

- [11] Clinton E. Plaisted, Alexander Leonessa, “Expendable Launch Vehicle Adaptive Autopilot Design”, *AIAA Guidance, Navigation and Control Conference and Exhibit*, August, 2008.
- [12] Jonathan A. Muse, Anthony J. Calise, “Adaptive Attitude and Vibration Control of the NASA Ares Crew Launch Vehicle”, *AIAA Guidance, Navigation and Control Conference and Exhibit*, August, 2008.
- [13] Johnson, E. N., Calise, A. J., & Corban, J. E., “Adaptive guidance and control for autonomous launch vehicles”, (pp. 2669–2682). *Institute of Electrical and Electronics Engineers*, 2002.
- [14] Man Wang, Jianying Yang, Guozheng Qin and Yingxin Yan, “Adaptive Fault-tolerant Control with Control Allocation for Flight Systems with Severe Actuator Failures and Input Saturation”, *American Control Conference (ACC)*, June 17-19, 2013.
- [15] Wang Yao, Yang Lingyu, Zhang Jing and Shen Gongzhang, “An Observer Based Multivariable Adaptive Reconfigurable Control Method for the Wing Damaged Aircraft”, *11th IEEE International Conference on Control & Automation (ICCA)*, June, 2014.
- [16] Daniele Tancredi, Yu Gu, Haiyang Chao, “Fault Tolerant Formation Flight Control Using Different Adaptation Techniques”, *International Conference on Unmanned Aircraft Systems (ICUAS)*, May, 2013.
- [17] M. Poderico, G. Morani, and M. Ariola, “Reconfigurable Flight Control Laws for Re-Entry Vehicles”, *Mediterranean Conference on Control & Automation (MED)*, June 25-28, 2013
- [18] Choong-Seok Oh, C. S., Bang, H., & Park, C. S. “Attitude control of a flexible launch vehicle using an adaptive notch filter: Ground experiment”, *Control Engineering Practice*, 16(1), 30–42, 2008.
- [19] Khoshnood, A. M., Roshanian, J., Jafari, A. A., & Khaki-Sedigh, A. “An Adjustable Model Reference Adaptive Control for a Flexible Launch

- Vehicle”. *Journal of Dynamic Systems, Measurement, and Control*, 132(4), 041010, 2010.
- [20] Mathew Englehart, James Krause, “An adaptive control concept for flexible launch vehicles”, *Astro dynamics Conference*, 1992.
- [21] Benoit Clement, Gilles Duc, Sophie Mauffrey, “Aerospace launch vehicle control: a gain scheduling approach”, *Control Engineering Practice*, 13(3), 333-347, 2005.
- [22] Lalithambika, V. R., S. Dasgupta, “Launch Vehicle Autopilot Robustness to Multilinear Uncertainties: Analysis in Kharitonov Framework”, *Journal of Guidance, Control and Dynamics*, Vol. 30(4), July- August, 2007, pp. 1179–1182.
- [23] Minnan Piao, Youan Zhang, Mingwei Sun, Zhihong Yang, Zenghui Wang and Zengqiang Chen, “Adaptive aeroservoelastic mode stabilization of flexible airbreathing hypersonic vehicle”, *Journal of Vibration and Control* 2019.
- [24] Sangbum Cho, N. Harris McClamroch, Mahmut Reyhanoglu, “Feedback Control of a Space Vehicle with Unactuated Fuel Slosh Dynamics”, *AIAA Guidance, Navigation, and Control Conference and Exhibit*, August, 2000.
- [25] Kailash Krishnaswamy, Dan Bugajski, “Inversion Based Multibody Control - Launch Vehicle with Fuel Slosh”, *AIAA Guidance, Navigation, and Control Conference and Exhibit*, August, 2005.
- [26] Ioannou, P., Fidan, P., *Adaptive Control Tutorial*, SIAM, Advances in Design and Control, SIAM, PA, 2006.
- [27] Peterson, B.B., Narendra K.S., “Bounded error adaptive control”, *IEEE Transactions on Automatic Control*, 27, 1161-1168, 1982.
- [28] Pomet, J.B., Praly, L., “ Adaptive nonlinear regulation: Estimation from the Lyapunov equation”, *IEEE Transactions on Automatic Control*, 37, 729-740, 1992.

- [29] Kreisselmeier, G., Narendra, K.S., “Stable model reference adaptive control in the presence of bounded disturbances”, *IEEE Transactions on Automatic Control*, 27, 1169-1175 ,1982.
- [30] Keng Peng Tee, Shuzhi Sam Ge, "Control of Nonlinear Systems with full state constraint using a Barrier Lyapunov function, *IEEE conference on decision and control*, December ,2009.
- [31] Jacek Kabziński, Przemysław Mosiołek and Marcin Jastrzębski, "Adaptive Position Tracking with Hard Constraints-Barrier Lyapunov Functions Approach", *Studies in Systems, Decision and Control*, Vol. 75, 27-52,2017.
- [32] Andrea L'Afflito, "Barrier Lyapunov Functions and Constrained Model Reference Adaptive Control", *IEEE Control Systems Letters*, Vol 2, No.3, 2018.
- [33] Chaoyang Dong, Yang Liu, Qing Wang, "Barrier Lyapunov function based adaptive finite-time control for hypersonic flight vehicles with state constraints", *ISA Transactions*, Vol 96,163-176,2020.
- [34] Chen Liu, Chaoyang Dong, Zhijie Zhou, Zhaolei Wang, "Barrier Lyapunov function based reinforcement learning control for air-breathing hypersonic vehicle with variable geometry inlet", *Aerospace Science and Technology*, Vol 96,2020.
- [35] Yuhui Wang, Jun Zhang, “Analysis of a MIMO Dutch roll dynamic system and its adaptive non-affine flight control”, *Nonlinear Dynamics*, Issue 1, Vol 91, pp 565-576, 2018.
- [36] Qi Mao, Liqian Dou, Qun Zong , Zhengtao Ding, “Attitude controller design for reusable launch vehicles during reentry phase via compound adaptive fuzzy H-infinity control”, *Aerospace Science and Technology*, Vol 72, pp 36-48, 2018.

- [37] Zhen Wang, Zhong Wu, Yijiang Du, “Robust adaptive backstepping control for reentry reusable launch vehicles”, *Acta Astronautica*, Vol 126, pp 258-264, 2016.
- [38] Keum W. Lee, Sahjendra N. Singh, “Adaptive Control of Multi-Input Aeroelastic System with Constrained Inputs”, *Journal of Guidance, Control and Dynamics*, Vol 38, No. 12, December 2015.
- [39] Ming-Zhou Gao, Jian-Yong Yao, “Adaptive fault-tolerant attitude control for reentry vehicle involving actuator saturation”, *Proc IMechE Part G: Journal of Aerospace Engineering*, Vol. 233(11), 3968–3982, 2019.
- [40] Daniel P. Wiese, Anuradha M. Annaswamy, Jonathan A. Muse, Michael A. Bolender, Eugene Lavretsky,” Adaptive Output Feedback Based on Closed-Loop Reference Models for Hypersonic Vehicles”, *Journal of Guidance, Control and Dynamics*, Vol 38, No. 12, December 2015.
- [41] Maomao Li, Jun Hu, “An approach and landing guidance design for reusable launch vehicle based on adaptive predictor–corrector technique”, *Aerospace Science and Technology*, 75, 13-23, 2018.
- [42] Bailing Tian, Wenru Fan, Qun Zong, “Integrated guidance and control for reusable launch vehicle in reentry phase”, *Nonlinear Dynamics*, 80:397–412,2015.
- [43] Yao Zhang, Shengjing Tang, Jie Guo, “Adaptive-gain fast super- twisting sliding mode fault tolerant control for a reusable launch vehicle in re-entry phase”, *ISA Transactions*, 71, 380-390, 2017.
- [44] Chang Tan, Gang Tao, Ruiyun Qi, Hui Yang, “A direct MRAC based multivariable multiple-model switching control scheme”, *Automatica*, 84, 190-198, 2017.
- [45] Tanmay Rajpurohit, Wassim M. Haddad, Tansel Yucelen, “Output Feedback Adaptive Control with Low-Frequency Learning and Fast

Adaptation”, *Journal of Guidance, Control and Dynamics*, Vol. 39, No. 1, January 2016.

- [46] Arnab Maity, Leonhard Hocht, Florian Holzapfel, “Higher order direct model reference adaptive control with generic uniform ultimate boundedness”, *International Journal of Control*, Vol 88, No. 10, 2126-2142,2015.
- [47] Kangkang Zhang, Bin Jiang, Xing-Gang Yan, Zehui Mao, “Adaptive robust fault-tolerant control for linear MIMO systems with unmatched uncertainties”, *International Journal of Control*, Vol 90, No 10, 2253-2269, 2017.
- [48] Liyan Wen, Gang Tao, Hao Yang & Yanjun Zhang, “An adaptive disturbance rejection control scheme for multivariable nonlinear systems”, *International Journal of Control*, Vol 89, No 3, 594-610,2015.
- [49] Yan-Jun Liu, Shaocheng Tong, “Barrier Lyapunov Functions-based adaptive control for a class of nonlinear pure-feedback systems with full state constraints”, *Automatica*, Vol 64, 70-75, 2016.
- [50] Jianguo Guo, Zhenxin Feng, Jun Zhou, “Robust state-constrained control design for nonlinear systems with uncertainties using a new barrier Lyapunov function”, *Transactions of the Institute of Measurement and Control*, Vol 40 (12), 3489–3497, 2018.
- [51] Hao An, Hongwei Xia, Changhong Wang, “Barrier Lyapunov function-based adaptive control for hypersonic flight vehicles”, *Nonlinear Dynamics*, Vol 88 (3), 1833-1853, 2017.
- [52] Zhiyu Peng, Ruiyun Qi, Bin Jiang, “Adaptive Fault Tolerant Control of Hypersonic Flight Vehicle with State Constraints using Barrier Lyapunov Function”, *Chinese Control and Decision Conference (CCDC)*, 1474-1479, 2019.

- [53] Chen Liu, Chaoyang Dong, Zhijie Zhou, Zhaolei Wang, “Barrier Lyapunov function based reinforcement learning control for air-breathing hypersonic vehicle with variable geometry inlet”, *Aerospace Science and Technology*, Vol 96, 105537,2019.
- [54] Yongming Li, Yanjun Liu, Shaocheng Tong,” Observer-Based Neuro-Adaptive Optimized Control of Strict-Feedback Nonlinear Systems with State Constraints”, *IEEE Transactions on Neural Networks and Learning Systems*, January, 2021.
- [55] Yongming Li, Yanli Fan, Kewen Li, Wei Liu, Shaocheng Tong,” Adaptive Optimized Backstepping Control-Based RL Algorithm for Stochastic Nonlinear Systems with State Constraints and Its Application”, *IEEE Transactions On Cybernetics*, March, 2021.
- [56] Alireza Izadbakhsh, Payam Kheirkhahan, Saeed Khorashadizadeh, "FAT-based robust adaptive control of electrically driven robots in interaction with environment”, *Robotica*, volume 37, pp. 779–800, 2019.
- [57] Izadbakhsh A, Zamani I, Khorashadizadeh S. “Szász–Mirakyan-based adaptive controller design for chaotic synchronization”, *Int J Robust Nonlinear Control*, volume 31, pp. 1689-1703, 2021.
- [58] Hoelkner, R. F., “The Principle of Artificial Stabilization of Aerodynamically Unstable Missiles,” *ABMA DA-TR-64-59*, September 25, 1959.
- [59] Asha P.Nair., Selvaganesan, N., & Lalithambika, V. R. “Lyapunov based PD/PID in model reference adaptive control for satellite launch vehicle systems”. *Aerospace Science and Technology*, 51, 70–77,2016.
- [60] Hidehiko Mori, " Control system design of flexible-body launch vehicles", *Control Engineering Practice*, 7(9), 1163-1175, 1999.

- [61] Haeussermann, W., "Description and Performance of the Saturn Launch Vehicle's Navigation, Guidance, and Control System," *NASA Technical Reports Server*, NASA TN D-5869, July 1970.
- [62] Frosch, J. A. and Valley, D. P., "Saturn AS-501/S-IC Flight Control System Design," *Journal of Spacecraft*, Vol. 4, No. 8, 1967, pp. 1003-1009.
- [63] Wie, B. and Byun, K. W., "New Generalized Structural Filtering Concept for Active Vibration Control Synthesis," *Journal of Guidance, Control, and Dynamics*, Vol. 12, No. 2, 1989, pp. 147-154.
- [64] Byun, K. W., Wie, B. and Sunkel, J., "Robust Non-Minimum-Phase Compensation for a Class of Uncertain Dynamical Systems," *Journal of Guidance, Control, and Dynamics*, Vol. 14, No. 6, 1991, pp. 1191-1199.
- [65] Edited by H. Norman Abramson, *The dynamic behavior of Liquids in moving containers - with application to space vehicle technology*, NASA SP-106.
- [66] Chopra, A. K., *Dynamics of Structures*, Prentice Hall, New Jersey, 1995, pp. 585-600.
- [67] H.K. Khalil, *Nonlinear Systems*, 3rd Edition, Prentice Hall, 2002.
- [68] Slotine, J.J.E., Li, W., *Applied Nonlinear Control*, Prentice Hall, New Jersey, 1995.
- [69] Slotine, J.J.E., Coetsee, J.A.: "Adaptive sliding controller synthesis for nonlinear systems", *International journal of control*, 1986.
- [70] E. Lavretsky and N. Hovakimyan, "Positive μ – modification for stable adaptation in the presence of input constraints," *American Control Conference*, 2004.
- [71] Mohinder S. Grewal, Angus P. Andrews, *Kalman Filtering*, John Wiley & Sons, 2001.

- [72] Etkin, B., *Dynamics of Flight, Stability and Control*, 2nd edition, Wiley, New York, 1982.
- [73] McRuer, D., Ashkenas, I., Graham, D., *Aircraft Dynamics and Automatic Control*, Princeton University Press, Princeton, 1990.
- [74] Stevens, B.L., Frank L. Lewis, *Aircraft Control and Simulation*, Wiley, New York, 1992.
- [75] Michael V. Cook, *Flight Dynamics Principles-A Linear Systems Approach to Aircraft Stability and Control*, 2nd Edition, Elsevier Aerospace Engineering Series, 2007.
- [76] Daniel J Bugajski, Dale F.Enns,Gunter Stein “Dynamic Inversion: An Evolving Methodology for Flight Control Design,” *International Journal Of Control*, Volume 59, No. 1, 1994 pages 71 – 91.
- [77] Lane, S.H. and Stengel, R.F., “Flight Control Design using Non-Linear Inverse Dynamics,” *Automatica*, Vol.24, pp.471-483, 1988.
- [78] Snell, S.A., Enns, D.F., and Garrard, W., “Nonlinear Inversion Flight Control for a Super maneuverable Aircraft”, *Journal of Guidance, Control and Dynamics*, Vol.15, pp.976-984, July 1992.
- [79] Bugajski, D.J., Enns, D.F., and Elgersma, M., “A Dynamic Inversion based Control Law with Application to the High Angle of Attack Research Vehicle,” *Proceedings of the AIAA Guidance, Navigation, and Control Conference*, pp 826-836, August 1990.
- [80] R.Gifty, U.P. Rajeev, V.R. Lalithambika, M.V. Dhekane, “Entry guidance with smooth drag planning and non-linear tracking”, *Control Engineering Practice*, 63, pp 24-33, 2017.
- [81] George F. Simmons, *Introduction to Topology and Modern Analysis*, Tata McGraw-Hill Publishing Company Limited, New Delhi, 2006.

- [82] G.H. Hardy, J.E. Littlewood, G. Polya, *Inequalities*, Cambridge University Press, 1967.
- [83] Michael Stecher, *Linear Algebra*, Harper and Row Publishers, New York, 1988.

Appendix A

A.1 Mathematical Preliminaries Required to Derive the Control Laws in Chapter 3

Definitions given in this chapter are based on [81].

A.1.1 Metric Space

A metric space is a non-empty set equipped with the concept of distance. Let X be a non-empty set. A metric on X is a real function d of ordered pairs of elements of X which satisfies the following three conditions:

- a. $d(x, y) \geq 0$, and $d(x, y) = 0 \Leftrightarrow x = y$;
- b. $d(x, y) = d(y, x)$ (symmetry);
- c. $d(x, y) \leq d(x, z) + d(z, y)$ (the triangle inequality)

The function d assigns to each pair (x, y) of elements of X a non-negative real number $d(x, y)$, which by symmetry does not depend on the order of the elements. $d(x, y)$ is called the distance between x and y . A metric space consists of two objects, a non-empty set X and a metric d on X . Several different metrics can be defined on a single given non-empty set, giving different metric spaces.

A.1.2 Converging Sequences

A sequence $\{x_n\} = \{x_1, x_2, \dots, x_n, \dots\}$ of real numbers is said to be convergent if there exists a real number x (called the limit of the sequence) such that, given $\epsilon > 0$, a positive integer n_0 can be found with the property that $n \geq n_0 \Rightarrow |x_n - x| < \epsilon$. This condition means that x_n must be “close” to x for all “sufficiently large” n , and it is usually symbolized by $x_n \rightarrow x$ or $\lim x_n = x$ and expressed by saying that x_n *approaches* x or x_n *converges to* x .

A more general definition in metric space is as follows:

Let X be a metric space with metric d , and let $\{x_n\} = \{x_1, x_2, \dots, x_n, \dots\}$ be a sequence of points in X . We say that $\{x_n\}$ is convergent if there exists a point x in X such that either

- 1) For each $\epsilon > 0$, there exists a positive integer n_0 such that $n \geq n_0 \Rightarrow d(x_n, x) < \epsilon$; or equivalently,
- 2) For each open sphere $S_\epsilon(x)$ centered on x , there exists a positive integer n_0 such that x_n is in $S_\epsilon(x)$ for all $n \geq n_0$

Every convergent sequence is a Cauchy sequence

A.1.3 Complete Metric Space

It is a metric space in which every Cauchy sequence is convergent. Complex plane and real line are *complete*.

A.1.4 Continuous Function

A real function f defined on a non-empty subset X of the real line is said to be *continuous at x_0* in X if for each $\epsilon > 0$ there exists $\delta > 0$ such that x in X and $|x - x_0| < \delta \Rightarrow |f(x) - f(x_0)| < \epsilon$, and f is said to be continuous if it is continuous at each point of X . This can be defined in metric space as follows:

Let X and Y be metric spaces with metrics d_1 and d_2 , and let f be a mapping of X into Y . f is said to be continuous at a point x_0 in X if either of the following equivalent conditions is satisfied.

- 1) For each $\epsilon > 0$ there exists $\delta > 0$ such that $d_1(x, x_0) < \delta \Rightarrow d_2(f(x), f(x_0)) < \epsilon$;
- 2) For each open sphere $S_\epsilon(f(x_0))$ centred on $f(x_0)$ there exists an open sphere $S_\delta(x_0)$ centred on x_0 such that $f(S_\delta(x_0)) \subseteq S_\epsilon(f(x_0))$.

A.1.5 Compactness

Let X be a topological space. A class $\{G_i\}$ of open subsets of X is said to be an open cover of X if each point in X belongs to at least one G_i , that is $\cup_i G_i = X$. A compact space is a topological space in which every open cover has a finite subcover. A compact subspace of a topological space is a subspace which is compact as a topological space in its own right.

A.1.6 Compactness for Metric Spaces

- 1) Bolzano-Weirstrass theorem: if X is a closed and bounded subset of the real line, then every infinite subset of X has a limit point in X . A metric space is said to have the *Bolzano-Weirstrass* property if every infinite subset has a limit point. A metric space is said to be sequentially compact if every sequence in it has a convergent subsequence.
- 2) A metric space is compact implies that it is complete and totally bounded.
- 3) A closed subspace of a complete metric space is compact implies that it is totally bounded.

A.1.7 Connectedness

A connected space is a topological space X which cannot be represented as the union of two disjoint non-empty open sets. Connectedness of X amounts to the condition that \emptyset and X are its only subsets which are both open and closed.

A.2 Uniform Ultimate Stability

Definition 1: Stability of Equilibrium in the Sense of Lyapunov

A nonautonomous unforced dynamical system can be defined as

$$\dot{x} = f(t, x) \quad (\text{A.1})$$

with $f: [0, \infty) \times D \rightarrow R^n$ which is piece-wise continuous in t and locally Lipschitz in x and with a domain $D \subset R^n$ that contains the origin $x = 0$.

A nonzero vector $x^* \in R^n$ can be defined as an equilibrium point of (A.1) at a nonzero initial time $t_0: f(t, x^*) = 0, \forall t \geq t_0$. The equilibrium point $x^* = 0$ of the nonautonomous unforced dynamics (A.1) is stable if for any $\varepsilon > 0$ and $t_0 \geq 0$ there exists $\delta(\varepsilon, t_0) > 0$ such that for all initial conditions $\|x(t_0)\| < \delta$ and for all $t \geq t_0 \geq 0$, the corresponding system trajectories are bounded, as in $\|x(t)\| < \varepsilon$. The equilibrium is uniformly stable if it is stable and δ does not depend on t_0 . Finally, the equilibrium is unstable if it is not stable.

Definition 2: Global Stability

The origin is globally stable if it is stable and $\lim_{\varepsilon \rightarrow \infty} \delta(\varepsilon, t_0) = \infty$.

Uniform Ultimate Boundedness

Uniform Ultimate Boundedness (UUB) is considered as a milder form of stability in the sense of Lyapunov. Consider the nonautonomous system

$$\dot{x} = f(t, x) + \xi(t), x(t_0) = x_0 \quad (\text{A.2})$$

The solutions of this equation are uniformly ultimately bounded with ultimate bound b if there exists positive constants b and c , independent of $t_0 \geq 0$, and every $a \in (0, c)$, there is $T = T(a, b)$, independent of t_0 , such that

$$\|x(t_0)\| \leq a \Rightarrow \|x(t)\| \leq b, \quad \forall t \geq t_0 + T \quad (\text{A.3})$$

These solutions are said to be globally uniformly ultimately bounded if (A.3) holds for arbitrarily large a . In the definition above, the term “uniform” indicates that the bound b does not depend on t_0 . The term “ultimate” means that boundedness holds after the lapse of a finite time T . The constant c defines a neighborhood of the origin, independent of t_0 , such that all trajectories starting in the neighbourhood will remain bounded in time. If c can be chosen arbitrarily large, then the local UUB property becomes global.

A.3 Projection Operator

A Lipschitz-continuous version of the projection operator as described in [3][26][27][29] is explained here.

Definition 1: A subset $\Omega \subset R^n$ is convex if

$$[\forall x, y \in \Omega \subset R^n] \Rightarrow [\lambda x + (1 - \lambda)y = z \in \Omega], \forall 0 \leq \lambda \leq 1 \quad (\text{A.4})$$

This shows that if two points belong to a convex subset Ω then all the points on the connecting line also belong to Ω .

Definition 2: A function $f: R^n \rightarrow R$ is convex on R^n if

$$f(\lambda x + (1 - \lambda)y) \leq \lambda f(x) + (1 - \lambda)f(y), \forall 0 \leq \lambda \leq 1, \forall x, y \in R^n \quad (\text{A.5})$$

The graph of a convex function must be located below the straight line, which connects the two corresponding function values.

Lemma 1: Let $f(x): R^n \rightarrow R$ be convex. Then for any constant $\delta > 0$, the subset $\Omega_\delta = \{\theta \in R^n | f(\theta) \leq \delta\}$ is convex.

Proof of Lemma 1: Let $\theta_1, \theta_2 \in \Omega_\delta$. Then $f(\theta_1) \leq \delta, f(\theta_2) \leq \delta$. Since $f(x)$ is convex, then for any $0 \leq \lambda \leq 1$, $f\left(\frac{\lambda\theta_1 + (1 - \lambda)\theta_2}{\theta}\right) \leq \lambda \underbrace{f(\theta_1)}_{\leq \delta} + (1 - \lambda) \underbrace{f(\theta_2)}_{\leq \delta} \leq \lambda\delta + (1 - \lambda)\delta = \delta$. Therefore, $f(\theta) \leq \delta$ and consequently, $\theta \in \Omega_\delta$.

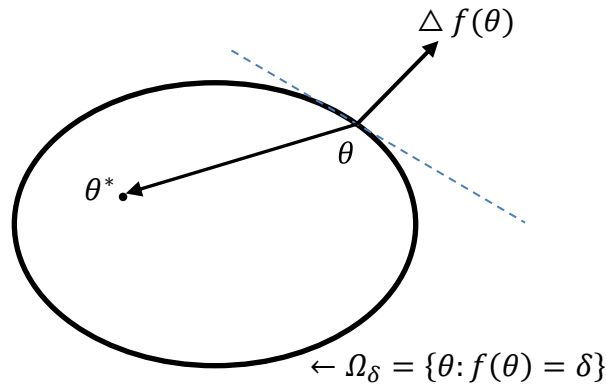


Figure A.3. 1 Gradient Vector on the Boundary of a Convex Set

Lemma 2: Let $f(x): R^n \rightarrow R$ be a differentiable convex function. Choose a constant $\delta > 0$ and consider the subset $\Omega_\delta = \{\theta \in R^n | f(\theta) \leq \delta\} \subset R^n$. Let $\theta^* \in \Omega_\delta$ and assume that $f(\theta^*) < \delta$, that is θ^* is an interior point (not on the boundary) of Ω_δ . Also let $\theta \in \Omega_\delta$ and assume that $f(\theta) = \delta$, that is θ is on the boundary of Ω_δ . Then the following inequality holds

$$(\theta^* - \theta)^T \nabla f(\theta) \leq 0, \text{ where } \nabla f(\theta) = \left(\frac{\partial f(\theta)}{\partial \theta_1} \dots \frac{\partial f(\theta)}{\partial \theta_n} \right)^T \in R^n \quad (\text{A.6})$$

is the gradient vector of f evaluated at θ .

Figure A.3.1 shows that the gradient vector of a function, evaluated at the boundary of a convex level set generated by this function, always points away from the set.

Proof of Lemma 2:

Since $f(x)$ is convex, then

$$f(\lambda\theta^* + (1 - \lambda)\theta) \leq \lambda f(\theta^*) + (1 - \lambda)f(\theta) \quad (\text{A.7})$$

Re-writing the above equation

$$f(\theta + \lambda(\theta^* - \theta)) \leq f(\theta) + \lambda(f(\theta^*) - f(\theta)) \quad (\text{A.8})$$

For any nonzero $0 < \lambda \leq 1$

$$\frac{f(\theta + \lambda(\theta^* - \theta)) - f(\theta)}{\lambda} \leq \underbrace{f(\theta^*)}_{< \delta} - \underbrace{f(\theta)}_{\delta} < \delta - \delta = 0 \quad (\text{A.9})$$

Taking the limit as $\lambda \rightarrow 0$ gives $(\theta^* - \theta)^T \nabla f(\theta) \leq 0$. This completes the proof.

Continuous Projection Operator

Suppose that a parameter vector θ belongs to a convex set

$$\Omega_0 = \{\theta \in R^n | f(\theta) \leq 0\} \quad (\text{A.10})$$

Another convex set is defined such that $\Omega_0 \subseteq \Omega_1$

$$\Omega_1 = \{\theta \in R^n | f(\theta) \leq 1\} \quad (\text{A.11})$$

Projection operator is defined as in [3]

$$\begin{aligned} & Proj(\theta, y) \quad (\text{A.12}) \\ & = \begin{cases} y - \frac{\Gamma \nabla f(\theta) (\nabla f(\theta))^T}{\|\nabla f(\theta)\|_\Gamma^2} y f(\theta), & \text{if } f(\theta) \geq 0 \wedge y^T \nabla f(\theta) > 0 \\ y, & \text{if not} \end{cases} \end{aligned}$$

where, $\Gamma \in R^{n \times n}$ is any constant symmetric positive definite matrix and $\|\nabla f(\theta)\|_\Gamma^2 = \nabla f^T \Gamma \nabla f$ is the weighted Euclidean squared norm of ∇f . This concept is given Figure A.3.2.

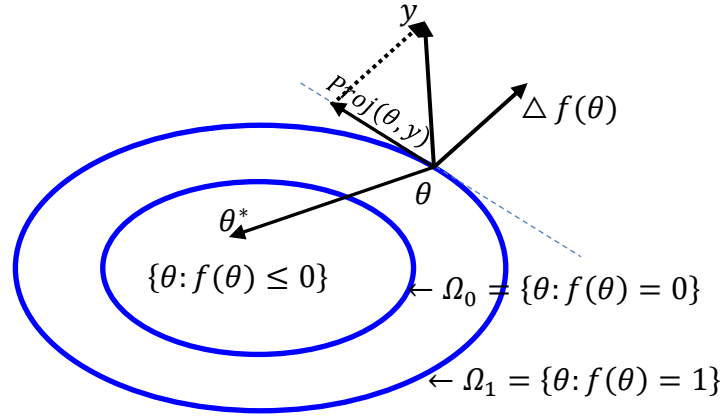


Figure A.3. 2 The Projection Operator

For an identity matrix Γ , $Proj(\theta, y)$ will not alter the vector y if θ belongs to the convex set Ω_0 . In the annulus between $0 \leq f(\theta) \leq 1$, the projection operator subtracts a vector normal to the boundary $f(\theta) = \lambda$ from y . As a result, we get a smooth transformation from the original vector field y for $\lambda = 0$ to the tangent to the boundary vector for $\lambda = 1$.

Lemma 3: Convex Property of Projection Operator

For any symmetric positive-definite matrix $\Gamma \in R^{n \times n}$,

$$(\theta - \theta^*)^T (\Gamma^{-1} Proj(\theta, \Gamma y) - y) \leq 0 \quad (\text{A.13})$$

Proof: Using (A.6) and (A.12)

$$\begin{aligned}
& (\theta - \theta^*)^T (\Gamma^{-1} \text{Proj}(\theta, \Gamma y) - y) \tag{A.14} \\
& = \left\{ \begin{array}{l} \frac{\overbrace{-(\theta - \theta^*)^T \nabla f}^{>0}}{\|\nabla f(\theta)\|_F^2} \left[\overbrace{\nabla f^T \Gamma y}^{>0} \right] \overbrace{\tilde{f}}^{>0}, \text{ if } f(\theta) > 0 \wedge y^T \Gamma \nabla f(\theta) > 0 \\ 0, \text{ if not} \end{array} \right\} < 0
\end{aligned}$$

Lemma 4: Let $f(\theta)$ be a convex continuously differentiable map from $R^n \rightarrow R$. Using the projection operator (A.12), consider the n -dimensional dynamics

$$\dot{\theta} = \text{Proj}(\theta, y) \tag{A.15}$$

where, $\theta \in R^n$ is the system state and $y \in R^n$ is a time-varying piecewise continuous vector. Then starting from any initial condition $\theta(0) = \theta_0$ within the set

$$\Omega_0 = \{\theta \in R^n \mid f(\theta) \leq 0\} \tag{A.16}$$

the system trajectory $\theta(t)$ will remain in the set

$$\Omega_1 = \{\theta \in R^n \mid f(\theta) \leq 1\} \tag{A.17}$$

for all $t \geq 0$.

Proof: To get the solution of the system (A.15), following facts are used: (i) the projection operator is locally Lipchitz in θ and (ii) the system external input y is piecewise continuous in time. To prove the lemma, we need to show that the following relation holds

$$\underbrace{f(\theta_0) \leq 0}_{\theta_0 \in \Omega_0} \Rightarrow \underbrace{f(\theta(t)) \leq 1}_{\theta(t) \in \Omega_1}, \forall t \geq 0 \tag{A.18}$$

The time derivative of $f(\theta(t))$ along the trajectories of the system dynamics (A.15) is derived as

$$\begin{aligned}
\dot{f}(\theta) &= (\nabla f(\theta))^T \text{Proj}(\theta, y) \tag{A.19} \\
&= \left\{ \begin{array}{l} ((\nabla f(\theta))^T y (1 - f(\theta)), \text{ if } [f(\theta) > 0 \wedge y^T \nabla f(\theta) > 0] \\ (\nabla f(\theta))^T y, \text{ if not} \end{array} \right\}
\end{aligned}$$

Hence,

$$\begin{aligned}
 \dot{f}(\theta) &> 0, & \text{if } 0 < f(\theta) < 1 \wedge y^T \nabla f(\theta) > 0 & \quad (\text{A.20}) \\
 &= 0 & \text{if } f(\theta) = 1 \wedge y^T \nabla f(\theta) > 0 \\
 &\leq 0, & \text{if } f(\theta) \leq 0 \wedge y^T \nabla f(\theta) \leq 0
 \end{aligned}$$

The first and second relations in (A.20) imply that if $f(\theta_0) > 0$, then $f(\theta(t))$ monotonically increases in time for all $t \geq 0$, but will never exceed 1. The third condition indicates that if $\dot{f}(\theta) \leq 0$, then $f(\theta(t))$ will monotonically decrease for all $t \geq 0$. Therefore, irrespective of initial values (as long as they are negative) $f(\theta(t)) \leq 1$ for all $t \geq 0$. Hence, Lemma 4 is proved.

A.4 Barrier Lyapunov Based Control Design

Consider a compact, connected constraint set

$C \triangleq \{(e, \Delta K) \in \mathbb{R}^n \times \mathbb{R}^{m \times (n+m+N)} : f(e^T M e, \Delta K \Gamma^{-1} \Delta K^T) \geq 0\}$, where M and Γ are symmetric and positive-definite. This set captures the user defined constraints on the trajectory tracking error and the estimated adaptive gains' error. The Lyapunov function can be selected as

$$V(e, \Delta K) = \frac{e^T P e + \text{tr}(\Delta K \Gamma^{-1} \Delta K^T)}{f(e^T M e, \Delta K \Gamma^{-1} \Delta K^T)}, \quad (e, \Delta K) \text{ inside } C \quad (\text{A.21})$$

Derivative of the Lyapunov function is

$$\begin{aligned} \dot{V}(e, \Delta K) &= f^{-2} \{ f \cdot (e^T P \dot{e} + \dot{e}^T P e + \text{tr}(\Delta K^T \Gamma^{-1} \dot{\Delta K} + \dot{\Delta K}^T \Gamma^{-1} \Delta K)) \\ &\quad - (e^T P e + \text{trace}(\Delta K \Gamma^{-1} \Delta K^T)) \cdot f_e (e^T M \dot{e} + \dot{e}^T M e) \\ &\quad + f_k (\Delta K^T \Gamma^{-1} \dot{\Delta K} + \dot{\Delta K}^T \Gamma^{-1} \Delta K) \} \\ &= f^{-1} \{ (e^T P \dot{e} + \dot{e}^T P e + \text{tr}(\Delta K^T \Gamma^{-1} \dot{\Delta K} + \dot{\Delta K}^T \Gamma^{-1} \Delta K)) \\ &\quad - V \cdot (f_e (e^T M \dot{e} + \dot{e}^T M e) \\ &\quad + f_k (\Delta K^T \Gamma^{-1} \dot{\Delta K} + \dot{\Delta K}^T \Gamma^{-1} \Delta K)) \} \\ \dot{V}(e, \Delta K) &= f^{-1} \\ &\quad * \{ (e^T (P - V f_e M) \dot{e} + \dot{e}^T (P - V f_e M) e \\ &\quad + \text{tr}(\Delta K^T \Gamma^{-1} \dot{\Delta K} + \dot{\Delta K}^T \Gamma^{-1} \Delta K) - V f_k (\Delta K^T \Gamma^{-1} \dot{\Delta K} \\ &\quad + \dot{\Delta K}^T \Gamma^{-1} \Delta K) \} \\ &= f^{-1} \{ e^T (P - V f_e M) \dot{e} + \dot{e}^T (P - V f_e M) e \\ &\quad + (I - V f_k) (\dot{\Delta K} \Gamma^{-1} \Delta K^T + \Delta K \Gamma^{-1} \dot{\Delta K}^T) \} \\ &= f^{-1} \{ e^T (P - V f_e M) (A_m e + B \widetilde{\Delta K} \pi) \\ &\quad + (A_m e + B \widetilde{\Delta K} \pi)^T (P - V f_e M) e \\ &\quad + (I - V f_k) (\dot{\Delta K} \Gamma^{-1} \Delta K^T + \Delta K \Gamma^{-1} \dot{\Delta K}^T) \} \\ &= f^{-1} \{ e^T (P - V f_e M) A_m e + e^T (P - V f_e M) B \widetilde{\Delta K} \pi \\ &\quad + e^T A_m^T (P - V f_e M) e + \pi^T \widetilde{\Delta K}^T B^T (P - V f_e M) e \\ &\quad + (I - V f_k) (\dot{\Delta K} \Gamma^{-1} \Delta K^T + \Delta K \Gamma^{-1} \dot{\Delta K}^T) \} \end{aligned} \quad (\text{A.22})$$

Assuming that there exists a $Q \geq \alpha I_n$ where $\alpha > 0$ such that

$$-Q(e^T M e, \Delta K \Gamma^{-1} \Delta K^T) = A_m^T [P - V f_e M] + [P - V f_e M] A_m \quad (\text{A.23})$$

$$\begin{aligned} \dot{V}(e, \Delta K) = f^{-1} \{ & e^T (-Q) e + e^T (P - V f_e M) B \widetilde{\Delta K} \pi + \pi^T \widetilde{\Delta K}^T B^T (P \\ & - V f_e M) e + (I - V f_k) (\Delta K \Gamma^{-1} \Delta K^T + \Delta K \Gamma^{-1} \dot{\Delta K}^T) \} \end{aligned} \quad (\text{A.24})$$

Using the property of trace $\text{trace}(AB) = \text{trace}(BA)$; $\text{trace}(yx^T) = x^T y$

$$\begin{aligned} \dot{V}(e, \Delta K) = & -\alpha f^{-1} e^T e \\ & + 2f^{-1} \text{tr} \{ \widetilde{\Delta K} \pi e^T (P - V f_e M) B + \Delta K \Gamma^{-1} \dot{\Delta K}^T (I \\ & - V f_k) \} \end{aligned} \quad (\text{A.25})$$

Control parameter update law is

$$\dot{\widehat{K}}^T = -\Gamma \pi(t) e^T(t) [P - V f_e M] B \times [I_m - V f_k]^{-1} \quad (\text{A.26})$$

By assumption $\|\widetilde{\Delta K}(t) = \widehat{K}(t)\| \leq \varepsilon, \varepsilon > 0$. Using (A.25) and Cauchy–Schwarz inequality

$$\dot{V}(e, \Delta K) \leq f^{-1} [-\alpha e^T e + 2\varepsilon \text{tr}(\pi e^T (P - V f_e M) B)] \quad (\text{A.27})$$

Another set is defined as

$$\begin{aligned} G_{\alpha, \pi} = \{ & -\alpha e^T e \\ & + 2\varepsilon \text{tr}((\pi e^T [P - V f_e M] B) \\ & * (\pi e^T [P - V f_e M] B))^T)^{1/2} \} \end{aligned} \quad (\text{A.28})$$

Inside C , $\pi^* = \text{argmax}[-\alpha e^T e + 2\varepsilon \text{tr}((\pi e^T [P - V f_e M] B)(\pi e^T [P - V f_e M] B))^T)^{1/2}]$. Hence $\dot{V}(e, \Delta K) < 0 \forall (e, \Delta K) \in C \setminus G_{\alpha, \pi^*}$. G_{α, π^*} gives the inability of finding K which will limit the tracking error within the bounds and \dot{V} becomes positive in G_{α, π^*} . By choosing sufficiently large α , M and Γ we can enforce that G_{α, π^*} is a proper subset of C and hence the trajectories of $(e, \Delta K)$ will not leave C . To prove this, let us assume that $(e(t_0), \Delta K(t_0)) \in \text{interior of } C \setminus \{0\}$ and suppose that there exists a $T^* > 0$ such that $\lim_{t \rightarrow T^*} \text{dist}((e(t), \Delta K(t)), \partial C) = 0$

where ∂C is the boundary of the set C and $dist$ gives the distance of a point in the set. As per definition $\lim_{t \rightarrow T^*} f(e^T(t)Me(t), \Delta K(t)\Gamma^{-1}\Delta K^T(t)) = 0$ along the trajectory of e and ΔK . Since $f(e^T(t)Me(t), \Delta K(t)\Gamma^{-1}\Delta K^T(t)) > 0$ for all $(e, \Delta K) \in \text{interior of } C$ and $(0,0) \in C$ by assumption.

$$\begin{aligned} \lim_{t \rightarrow T^*} f(e^T(t)Me(t), \Delta K(t)\Gamma^{-1}\Delta K^T(t)) & \quad (A.29) \\ &= f(e^T(T^*)Me(T^*), \Delta K(T^*)\Gamma^{-1}\Delta K^T(T^*)) \\ &\Rightarrow (e^T(T^*), \Delta K(T^*)) \neq 0 \end{aligned}$$

Since $e^T P e + tr(\Delta K \Gamma^{-1} \Delta K^T) > 0 \forall (e, \Delta K)$ inside C ,

$$e^T(T^*)Pe(T^*) + tr(\Delta K(T^*)\Gamma^{-1}\Delta K^T(T^*)) \neq 0 \quad (A.30)$$

$$\begin{aligned} \lim_{t \rightarrow T^*} V(e(t), \Delta K(t)) &= \frac{e^T(T^*)Pe(T^*) + tr(\Delta K(T^*)\Gamma^{-1}\Delta K^T(T^*))}{f(e^T(T^*)Me(T^*), \Delta K(T^*)\Gamma^{-1}\Delta K^T(T^*))} \quad (A.31) \\ &= \infty \end{aligned}$$

If the initial points of $e(t_0), \Delta K(t_0) \in G_{\alpha, \pi^*}$, then $\forall T^{**} > t_0$ such that $e(T^{**}), \Delta K(T^{**}) \in \partial G_{\alpha, \pi^*}$ where $\partial G_{\alpha, \pi^*}$ is the boundary of G_{α, π^*} . Since $G_{\alpha, \pi^*} \subset C$ by assumption, $T^{**} < T^*$. As per (A.26), $\forall t_1, t_2$, and $t_2 \geq t_1$, $V(e(t_2), \Delta K(t_2)) \leq V(e(t_1), \Delta K(t_1)) < \infty$ along the trajectories of e and K . This contradicts (A.30). Similarly, for $e(t_0), \Delta K(t_0) \in C \setminus G_{\alpha, \pi^*}$ also we can prove that (A.31) is contradicted. Therefore for $e(t_0), \Delta K(t_0) \in C \setminus \{0\}$, the trajectories of e and ΔK will remain inside the connected constraint compact set C with the control update law given in (A.26).

A.5 Derivation of the Adaptive PID Control Law for the Simplified SLV Plant

The state-space representation of the simplified transfer function model of the rigid body dynamics of the SLV can be written as

$$\begin{aligned} \dot{x}_p &= A_p x + B_p u \\ y_p &= C_p x + D_p u \end{aligned} \quad (\text{A.32})$$

where, $A_p = \begin{bmatrix} 0 & 1 \\ \mu_\alpha & 0 \end{bmatrix}$, $B_p = \begin{pmatrix} 0 \\ \mu_c \end{pmatrix}$, $C_p = \begin{bmatrix} 1 & 0 \\ 0 & 1 \end{bmatrix}$, $D_p = \begin{pmatrix} 0 \\ 0 \end{pmatrix}$

Assuming a full state feedback control law

$$u = K_1^T x \quad (\text{A.33})$$

Let the reference model be

$$\dot{x}_m = A_m x_m + B_m u_c \quad (\text{A.34})$$

where, $A_m = \begin{bmatrix} 0 & 1 \\ -\omega_m^2 & -2\xi_m\omega_m \end{bmatrix}$, $B_m = \begin{bmatrix} 0 \\ \omega_m^2 \end{bmatrix}$. Using the matching condition

$$A_p - A_m = B_p * K^T \quad (\text{A.35})$$

The integrator state (x_I) is augmented to the original plant defined in Equation (A.32). Integrator dynamics can be written as

$$\dot{x}_I = x(1) - u_c \quad (\text{A.36})$$

The augmented plant with integral state is

$$\begin{bmatrix} \dot{x} \\ \dot{x}_I \end{bmatrix} = \begin{bmatrix} A_p & 0 \\ 1 & 0 \end{bmatrix} \begin{bmatrix} x \\ x_I \end{bmatrix} + \begin{bmatrix} B_p \\ 0 \end{bmatrix} u + \begin{bmatrix} 0 \\ -1 \end{bmatrix} u_c \quad (\text{A.37})$$

The control law with integrator can be written as

$$u = K_1^T x_p + K_I x_I \quad (\text{A.38})$$

Hence the closed loop system is

$$\begin{bmatrix} \dot{x} \\ \dot{x}_I \end{bmatrix} = \begin{bmatrix} A_p + B_p K^T & B_p K_I \\ 1 & 0 \end{bmatrix} \begin{bmatrix} x \\ x_I \end{bmatrix} + \begin{bmatrix} 0 \\ -1 \end{bmatrix} u_c \quad (\text{A.39})$$

Applying additional matching condition, we get

$$\begin{bmatrix} A_p + B_p K^T & B_p K_I \\ 1 & 0 \end{bmatrix} = \overline{A_m} \quad (\text{A.40})$$

where $\overline{A_m} = \begin{bmatrix} 0 & 1 & 0 \\ a1 & a2 & a3 \\ 1 & 0 & 0 \end{bmatrix}$

A standard quadratic Lyapunov function in terms of tracking error and gains is chosen.

$$V(e, \tilde{K}) = e^T P e + tr(\tilde{K}^T \Gamma^{-1} \tilde{K}) \quad (\text{A.41})$$

The parameter update law can be obtained using the Lyapunov function based approach and is given by

$$\begin{bmatrix} \dot{K} \\ \dot{K}_I \end{bmatrix} = -\Gamma \begin{bmatrix} x \\ x_I \end{bmatrix} e^T P B \quad (\text{A.42})$$

A.6 Derivation of the Inequalities Given in Chapters 3 and 4

First derivative of the Lyapunov function is

$$\begin{aligned}\dot{V}(e, \Delta\theta) = & -e^T Q e + 2 \text{trace}(\Delta\theta^T \{\Gamma^{-1} \dot{\hat{\theta}} - \Phi(x) e^T P B\} \Lambda) \\ & + 2e^T P \xi(t)\end{aligned}\quad (\text{A.43})$$

The adaptive law chosen was to make $\dot{V}(e, \Delta\theta)$ negative semi-definite, that is

$$\dot{\hat{\theta}} = \Gamma \Phi(x) e^T P B \quad (\text{A.44})$$

Next, we will try to use Lyapunov's direct method to prove the Uniform Ultimate boundedness (UUB) of the closed loop system. It is a milder form of Stability in the Sense of Lyapunov (SISL).

This adaptation law will make the first derivative of the Lyapunov function

$$\begin{aligned}\dot{V}(e, \Delta\theta) = & -e^T Q e + 2e^T P \xi(t) \\ = & -e^T (Q e - 2P \xi(t))\end{aligned}\quad (\text{A.45})$$

The upper bound of $\dot{V}(e, \Delta\theta)$ can be found out from (A.45)

$$\begin{aligned}\dot{V}(e, \Delta\theta) = & -e^T (Q e - 2P \xi(t)) \\ \leq & -\|e\| (\lambda_{\min}(Q) \|e\| - 2\lambda_{\max}(P) \xi_{\max})\end{aligned}\quad (\text{A.46})$$

where $\lambda_{\min}(Q)$ is the minimum eigen value of Q and $\lambda_{\max}(P)$ is the maximum eigen value of P . Proof of this is given below.

Proof: [82][83]

Let us take the first term on the R.H.S of (A.45) ie. $e^T Q e$. This is in quadratic form. Here Q is chosen as a real symmetric positive definite matrix. Hence the solution (P) of the algebraic Lyapunov equation $P A_m + A_m^T P = -Q$ also will be real symmetric positive definite.

We have to prove that $e^T Q e > \lambda_{\min}(Q) \|e\|^2$. Since Q is a real symmetric positive definite matrix, all its eigen values will be real and positive and $\exists U$ such that $D = UQU^T$ and $U^T = U^{-1}$ where D is the diagonal matrix. We can write Q in terms of D and U .

$$Q = U^T D U \quad (\text{A.47})$$

$$e^T Q e = e^T U^T D U e \quad (\text{A.48})$$

Let $Ue = y$. Then

$$\begin{aligned} e^T Q e &= y^T D y \\ &= \sum_{i=1}^n y_i^2 \lambda_i, \lambda_i > 0 \forall i \in [1, n] \\ &\geq \sum_{i=1}^n y_i^2 \lambda_{\min} \\ &= \lambda_{\min} \sum_{i=1}^n y_i^2 \\ &= \lambda_{\min} \|y\|_2 \end{aligned} \quad (\text{A.49})$$

Since transformation by unitary matrix is norm preserving, $\|y\|_2 = \|e\|_2$ the lower bound of $e^T Q e \geq \lambda_{\min} \|e\|_2$

The second term ($2e^T P \xi(t)$) in the R.H.S of (3.27) is in the bilinear form. Here the matrix P is a real symmetric positive definite matrix. Since the eigenvalues λ_i are positive for a positive definite matrix $\lambda_i = |\lambda_i|$. We have to show that $e^T P \xi \leq \lambda_{\max}(P) \|e\| \|\xi\|$. Following the arguments given in the first part of the proof

$$\begin{aligned} e^T P \xi &= e^T U^T D U \xi, \quad \text{Let } Ue = f \text{ and } U\xi = g \\ &= f^T D g \\ &= \sum_{i=1}^n f_i g_i \lambda_i \end{aligned} \quad (\text{A.50})$$

Since $e^T P \xi \leq |e^T P \xi|$

$$\begin{aligned}
e^T P \xi &\leq |e^T P \xi| \\
&= \left| \sum_{i=1}^n f_i g_i \lambda_i \right| \\
&\leq \sum_{i=1}^n |f_i g_i \lambda_i| \\
&= \sum_{i=1}^n |f_i g_i| \lambda_i \\
&\leq \sum_{i=1}^n |f_i g_i| \lambda_{max} \\
&\leq \|f\|_2 \|g\|_2 \lambda_{max} \\
&= \|e\| \|\xi\| \lambda_{max}(P)
\end{aligned} \tag{A.51}$$

(Since transformation by unitary matrix is norm preserving, $\|f\|_2 = \|e\|_2$ and $\|g\|_2 = \|\xi\|_2$)

The upper bound of $\dot{V}(e, \Delta\theta)$ can be found out from (A.45)

$$\begin{aligned}
\dot{V}(e, \Delta\theta) &= -e^T (Qe - 2P\xi(t)) \\
&\leq -\|e\| (\lambda_{min}(Q)\|e\| - 2\lambda_{max}(P)\xi_{max})
\end{aligned} \tag{A.52}$$

$(\lambda_{min}(Q)\|e\| - 2\lambda_{max}(P)\xi_{max}) > 0$ to make $\dot{V}(e, \Delta\theta)$ negative definite

$$\|e\| > \frac{2\lambda_{max}(P)\xi_{max}}{\lambda_{min}(Q)} \tag{A.53}$$

Hence, $\dot{V}(e, \Delta\theta) < 0$ outside of the set E_0 which is defined as

$$E_0 = \{(e, \Delta\theta): \|e\| \leq 2 \frac{\lambda_{max}(P)}{\lambda_{min}(Q)} \xi_{max} = e_0\} \tag{A.54}$$

List of Publications Based on Thesis

Papers in Refereed International Journals

1. Asha P. Nair, N.Selvaganesan, and V. R. Lalithambika, *Lyapunov based PD/PID in Model Reference Adaptive Control for Satellite Launch Vehicle Systems*, Journal Aerospace Science and Technology, Elsevier, 51(2016) 70-77. (Impact Factor – 5.107)
2. Asha P. Nair, N.Selvaganesan, and V. R. Lalithambika, *Robust Adaptive Control Laws for a Winged Re-entry Vehicle*, IETE Journal of Research, 1-13, March 2022, (Impact Factor – 2.333)
3. Asha P. Nair, N.Selvaganesan, and V. R. Lalithambika, *Projection and Barrier Lyapunov based Controller Update Laws in MRAC Structure for Flexible Satellite Launch Vehicles*, IETE Journal of Research, 1-13, January 2023, (Impact Factor – 2.333)